SCIENTIFIC RESEARCHES-2

EDITORS
Prof. Dr. Sevi ÖZ

AUTHORS
Prof. Dr. Yağmur UYSAL
Assoc. Prof. Dr. Dimitrios KALDERIS
Assoc. Prof. Dr. Güzide PEKCAN ERTOKUŞ
Assoc. Prof. Hilal ACAY
Assist. Prof. Dr. Ayfer YILDIRIM
Assist. Prof. Dr. Mine SULAK
Assist. Prof. Dr. Murat KIRANŞAN
Assist. Prof. Dr. Ümit TOKEŞER
Assist. Prof. Dr. Tamer GÜZEL
Assist. Prof. Dr. Zeynep Görkem DOĞAROĞLU
Dr. Handan ENGİN KIRIMLI
Ceyhun BAKAN

İKSAD
Publishing House

SCIENTIFIC RESEARCHES 2

EDITORS
Prof. Dr. Sevi ÖZ

AUTHORS
Prof. Dr. Yağmur UYSAL
Assoc. Prof. Dr. Dimitrios KALDERIS
Assoc. Prof. Dr. Güzide PEKCAN ERTOKUŞ
Assoc. Prof. Hilal ACAY
Assist. Prof. Dr. Ayfer YILDIRIM
Assist. Prof. Dr. Mine SULAK
Assist. Prof. Dr. Murat KIRANŞAN
Assist. Prof. Dr. Ümit TOKEŞER
Assist. Prof. Dr. Tamer GÜZEL
Assist. Prof. Dr. Zeynep Görkem DOĞAROĞLU
Dr. Handan ENGİN KIRIMLI
Ceyhun BAKAN

İKSAD
Publishing House

(The Licence Number of Publicator: 2014/31220)
TURKEY TR: +90 342 606 06 75
USA: +1 631 685 0 853
E mail: iksadyayinevi@gmail.com
www.iksadyayinevi.com

It is responsibility of the author to abide by the publishing ethics rules.
Iksad Publications – 2022©

ISBN: 978-625-8405-70-5
Cover Design: İbrahim KAYA
March / 2022
Ankara / Turkey
Size = 16x24 cm

CONTENTS

FOREWORD

I am delighted to write the foreword for this scientific book. This book contains eight chapters. In the first chapter of this book, selective and sensitive fluorescent sensor for lead ion, in the second chapter the viability of biochar-doped hydrogels in the fight against drought, in the third chapter simultaneous determination cholesterol-reducing combinatıon using principal components regression method, in the fourth chapter the effect of high electrical power on the physical structure of graphene nanosheets produced by anodic electrochemical exfoliation process, in the fifth chapter dynamic nuclear polarization parameters of nitroxide radical with 4-fluorobenzylamine, in the sixth chapter vajda theorems of jacobsthal and jacobsthal-lucas octonions, in the seventh chapter physicochemical properties of zeolite and modified zeolite clay, nanocatalyst and nanoadsorbent supported applications and in the eighth chapter bionanocomposites as fungicide against phytopathogenic fungi is examined.

I want to say thanks to all IKSAD publication team and the authors who have contributed to this book. It is my hope and expectation that this book will provide an effective learning experience and referenced resource for all science professionals.

Editor
Prof. Dr. Sevi ÖZ
Ankara Hacı Bayram Veli University

CHAPTER 1

SYNTHESIS OF *p*-tert-BUTYLCALIX[4]ARENE WITH BODIPY BY CLICK REACTION TO BECOME SELECTIVE AND SENSITIVE FLUORESCENT SENSOR FOR LEAD ION

Assist. Prof. Dr. Mine SULAK[1]

[1]Pamukkale University, Department of Mathematics and Science Education, Faculty of Education, Science Education, Denizli, Turkey, msulak@pau.edu.tr, ORCİD: ID/0000-0003-1300-8661

INTRODUCTION

Heavy metals are naturally occurring compounds in the earth's crust. Some of these metals are essential for human metabolism and are taken into our body in very small amounts by food, drinking water, and air. However, high levels of heavy metals ingested can cause acute or chronic poisoning. Heavy metals can cause chronic health problems because they cause bioaccumulation if taken into the body even at low doses for a long time. Lead is a soft metal that has been used for many years (Leita, 1991). Lead was widely used in BC. From 5000 onwards it has been used in the fields of metal products, cables and pipelines, and even paints and pesticides. The important usage areas of lead are; tin can lids, lead-tin alloy containers, ceramic glazes, pesticides, batteries, etc. are fields. Food and water can also be a source of lead, as well as lead gasoline and dyes (Kurniawan et al., 2019; Ozdemir et al., 2009; Okcu et al., 2009; Kafadar et al., 2010).

When a molecule in the ground state absorbs light at the appropriate energy, electrons rise from the fundamental energy level to the excited energy level and this process is called absorption (Craznik et al., 2002; Wu et al., 2017). There are different ways for the excited electron to return to the ground level. If the excited electron is rotating from the excited level to the base level by emitting light, this event is called fluorescence.

Fluorescent sensors, which can detect, measure, and display certain molecules or ions, are used in a wide variety of fields such as modern medicine, clinical diagnostics, biotechnology, molecular biology and biochemistry, materials science, analytical chemistry, and environmental chemistry, and contribute greatly to the understanding of chemical and biological systems (Simsir et al., 2021; Ali et al., 2016; Quiraga-Campano et al., 2021).

A typical fluorescence sensor consists of an analyte recognition group (receptor) and a fluorophore that converts the relationship between analyte and receptor into a fluorescence output signal, and this fluorophore group converts the information it receives into an optical signal in terms of changes in photophysical properties (Guliyev et al., 2009).

The receptor in the structure and the fluorophore group are conjugated to each other, or some fluorescent sensors have a linking group between the receptor and the fluorophore. The receptor is important because of its effect

on binding and selectivity. The receptor must have a strong affinity for the target ion. A fluorophore can be described as a signal transformer that converts information into an optical signal. Depending on the nature or concentration of the analyte when connected to the sensor, there will be a shift in fluorescence wavelength or a change in fluorescence intensity.

Among fluorescent sensors, 4,4-Difluoro-4-bora-3a, 4a-diaza-s-indacene (BODIPY) fluorophore, which was discovered in 1968, has high quantum efficiency, easy synthesis, the functionality of spectrum range adjustment, sharp emission peak good photostability property. It has been the center of attention for most researchers for many reasons (Banuelos et al., 2016; Boens et al., 2012).

BODIPY dye stuff thanks to its properties; As a very good photosensitizer in photodynamic therapy in molecular sensing systems. It has shown its applicability in optoelectronic devices as a chemical sensor, in light collecting systems, ion detection systems, biological imaging, and solar cells (Uppal et al., 2013; Atılgan et al., 2008).

Calixarenes, which have a three-dimensional space and can be derivatized from both phenolic oxygen and para position with suitable reagents, are suitable compounds used in the synthesis of fluorescent receptors (Gutsche et al., 1998; Baldini et al., 2012; Kim et al., 2007; Kumar et al., 2019).

The click reaction is used to regulate the fluorescent sensor between fluorescent portions and calixarene (Kolb et al., 2001; Sharpless et al., 2006). To construct a new fluorescent ionophore, characterize and investigate the fluorescence properties of boradiazaindacene (BODIPY) building blocks are our goal in this study, we have designed compound **6** (**Fig. 1**) in which BODIPY is connected to the symmetrical OH groups of the *p-tert*-butylcalix[4]arene. Meanwhile, the triazole group in the structure plays an important role in recognizing the lead (II) ion.

1. MATERIALS AND METHODS

All reagents used for the synthesis were purchased from Merck (Germany) and Sigma-Aldrich (USA), which were used without purification due to high purity. Commercially available solvents were purified by distillation. ^{1}H-NMR spectra were obtained using a Varian 400 MHz

spectrometer operating at 400 MHz, while attenuated total reflection-Fourier transform infrared (ATR-FTIR) measurements of synthesized compounds were made with 4 cm^{-1} resolution and 50 scans (PerkinElmer Inc., Norwalk)., CT, USA).

Measurements of the emission (fluorescence and phosphorescence) of the fluorescence-specific compound calixarene were performed at room temperature with a Perkin Elmer LS 55 spectrofluorimeter fluorimeter with a 1 cm quartz cuvette.

The excitation and emission slits were set to 5 nm. Pre-characterization of the obtained compounds was performed using UV-visible spectroscopy (UV/Vis-1601, Shimadzu, Kanagawa, Japan) in quartz cuvettes with 1 mm optical path length in the wavelength range of 200-400 nm with dichloromethane as the reference solution.

1.1Synthesis of sensor molecule (6):

p-tert-butylcalix[4]arene (**1**), 1,4-dibrombutan-*p-tert*-butylcalix[4]arene (**2**) and BODIPY compound functionalized with alkyl group (**5**) has been synthesized according to previously reported studies (Gutsche et al., 1989; Kolemen et al., 2018; Sayin et al. 2010; Yilmaz et al., 2010; Sulak et al. 2017).

1.2. Synthesis of 25,27-Bis[4-azidobutoxy]-26,28-dihyydroxy-5,11,17,23-tetra-*p*-[*tert*-butyl]calix[4]arene (3)

25,27-Bis[4-bromobutoxy]-26,28-dihydroxy-5,11,17,23-tetra[*tert*-butyl]calix[4]arene (**2**) (3.79 g, 5 mmol) and sodium azide (0.97 g, 150 mmol) was stirred in DMF at 80 ^{o}C for 2h. Reaction mixture was then poured in ice-cold water. The pale yellow solid, azidocalixarene (**3**) that separated out was filtered and recrystallised from ethanol, yield 73%.

ATR-FTIR: 2098 (azide), 1608 (CN).

^{1}H- NMR ($CDCl_3$): 7.31 (s, 2H, OH), 7.04 (s, 4H), 6.71 (s, 4H), 3.93 (d, *J*: 11,5 Hz, 4H, $ArCH_2Ar$), 3.83(t, 4H, $N_3CH_2CH_2CH_2$), 3.09(d, 4H, $ArCH_2Ar$), 2.21 (m, 4H, $OCH_2CH_2CH_2$)

1.3. Synthesis of 6

Azidocalixarene (**3**) (1.0 eq.) was dissolved with dry dichloromethane under an atmosphere of N_2 gas for 10 minutes. After adding the BODIPY

derivative (**5**) (1.5 eq.), it was stirred for half an hour, then 6 mol% sodium ascorbate was added. 1 mole of powdered $CuSO_4$ was added and stirring was continued for 40 minutes under a nitrogen atmosphere. The reaction was followed by TLC to room temperature. When it was clear that the starting azide compound was finished, the solvent was evaporated. The resulting solid compound was first washed with water and then dried over Na_2SO_4. Triazolyl compounds were purified by column chromatography

^{1}H- NMR ($CDCl_3$, 400 MHz): 8.0 (s, 2H, OH), 7.19 (s, 2H, CCHN), 7.09 (d, *J* = 8.67 Hz, 2H, Ph-H), 6.99 (d, *J* = 8.71 Hz, 2H, Ph-H), 5.16 (s, 4H, OCH_2), 4.47 (t, 2H, CH_2CH_2), 4.13 (d, *J* = 13.00 Hz, 2H, OCH_2), 3.89 (t, 2H, CH_2CH_2), 3.26 (d, J = 13.12 Hz, 1H, Ph- CH_2-Ph), 2.46 (s, 6H, CH_3), 2.22 (q, 4H, CH_2CH_3), 1.18 (s, 18H, t-Bu) 0.90 (t,12H CH_3CH_2-), 0.84 (s, 18H, t-Bu)

CONCLUCSION

In this study, firstly, the fluorophore group was synthesized by Williamson ether synthesis in the presence of 1,4-dibromobutane *p-tert*-butylcalix[4] arene (**1**) and potassium carbonate. Compound **2** was heated under reflux with sodium azide to obtain the azide compound. The formation of the azide compound was confirmed by ATR-FTIR spectroscopy with the characteristic peak at 2098 cm $^{-1}$. *p-tert*-butylcalix[4]arene azide compound and BODIPY derivative (**4**) were reacted with boron trifluoride diethyl etherate in the presence of TFA, DDQ and triethylamine, and ether- bound fluoride **6** was obtained with 28% yield by column chromatography using DCM as a solvent **(Figure 1).**

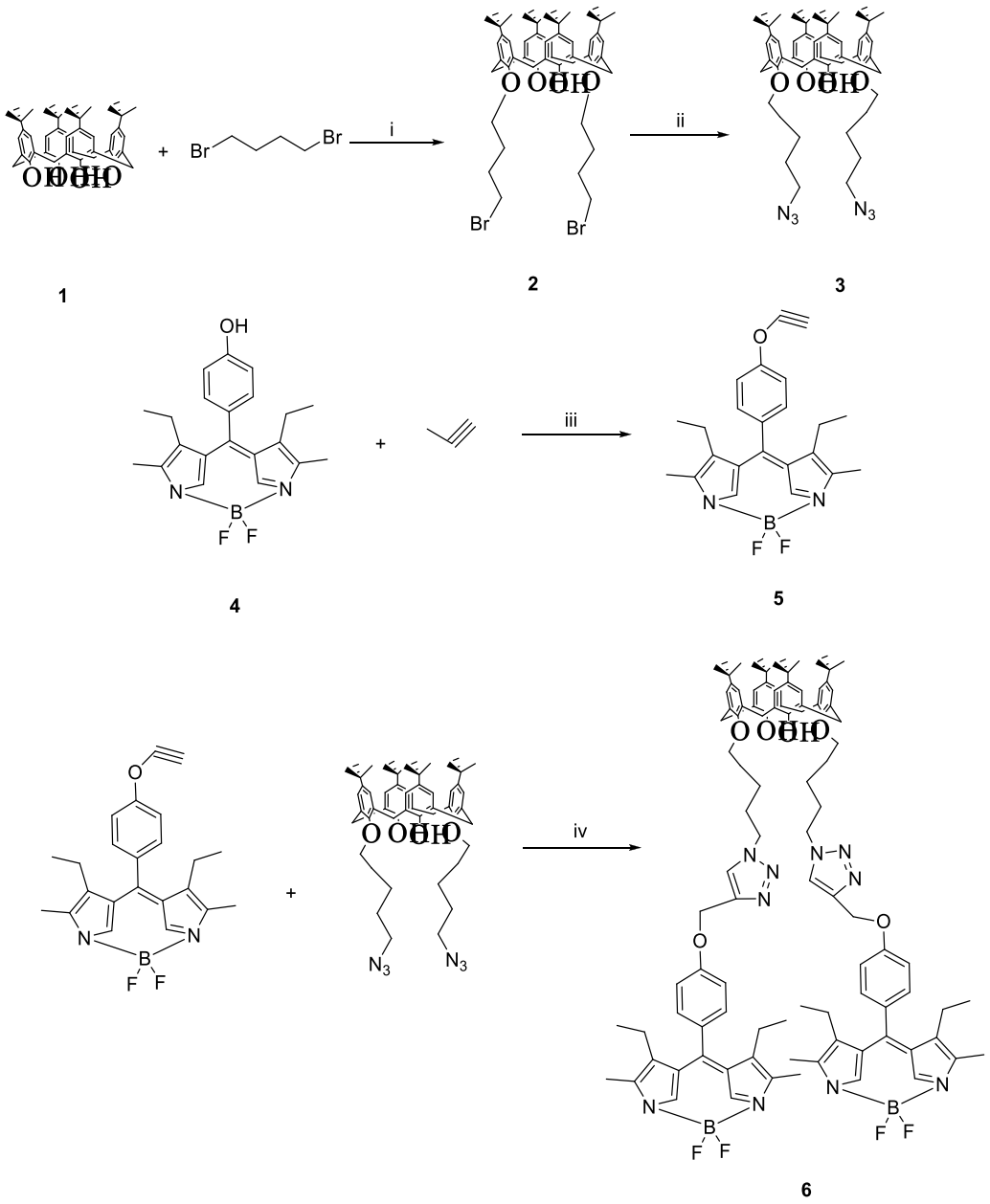

Figure 1. Synthesis of sensor *p-tert*-butylcalix[4]arene (**6**). Reagents and conditions (i) K_2CO_3, MeCN, (ii) sodium azide/H_2O, rt, 15 min. (iii) propargyl bromide, sodium hydride, DMF, 70 ˚C, 2 h;
(iv) 1-Azidocalixarene, sodium ascorbate, $CuSO_4$, CH_2Cl_2

The ^{1}H-NMR spectrum of compound **6 (Figure 2)** showed two pairs of signals at 4.13 and 4.26. These signals can be attributed to the methylene bridge protons of calixarene due to their C_{2v} symmetries. These signals indicate a cone conformation for the *p-tert*-butylcalix[4]arene as shown in **Figure 2**. The proof that compound 6 is present is the single peak observed at 5.16 ppm of hydrogen ether (OCH_2). Also, the disappearance of the C-CH hydrogen belonging to compound **3** in the ^{1}H-NMR spectrum of compound **6**, the emergence of a new single peak at 7.19 ppm is the proof of the formation of the triazole ring. Bridging aromatic hydrogen at the *meso* position of the BODIPY core resonates at 7.03 and 7.04 ppm. Aromatic hydrogens of the compound **6** resonate at 6.99 as doublet (J = 8.71 Hz) and at 7.09 ppm as doublet (J = 8.67 Hz)

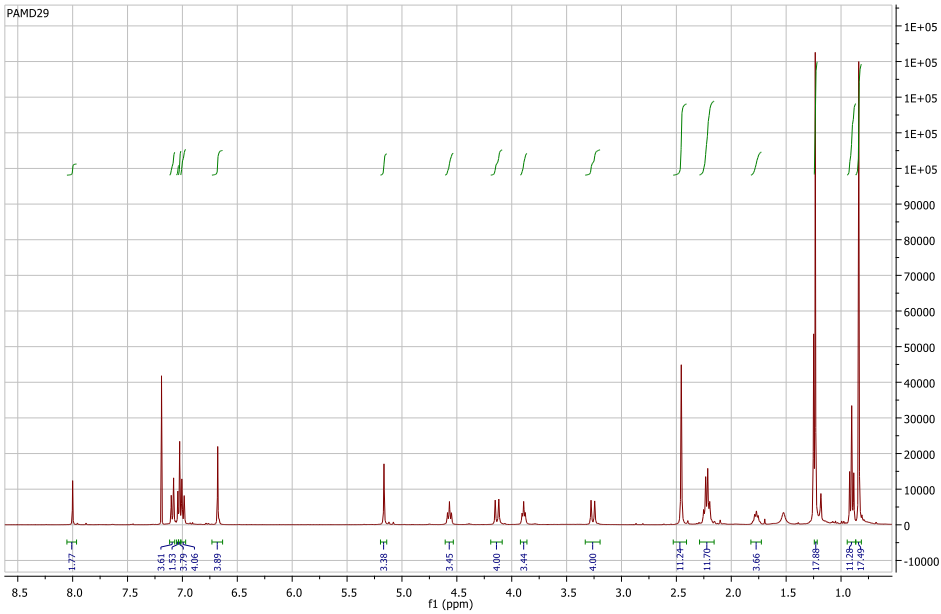

Figure 2. ^{1}H- NMR (400 MHz) spectrum of **6** in $CDCl_3$.

For absorption studies, 1.10^{-5} M ligand solutions and perchlorate solutions of 1.10^{-4} M metals were prepared in EtOH 2 mL of 1.10^{-4} M metal perchlorate solution was added to 2 mL of 1.10^{-5} M ligand solution, and it was shaken for 3-4 minutes at room temperature and the absorption spectra of the resulting solutions were taken.

We scanned the ion-binding abilities of nine metals (Fe^{3+}, Cu^{2+}, Hg^{2+}, Pb^{2+}, Co^{2+}, Ag^{+}, Ni^{2+}, Al^{3+} and Zn^{2+}) using fluorescence spectroscopy and analyzed the fluorescence intensities of the solutions before and after adding nine metal ions as perchlorate salts. The increase or decrease in fluorescence observed with the help of fluorophore **3** is caused by the binding of the analyte to the chemosensor. Calixarene-based fluorescence sensors are designed on the photo-induced mechanism that induces photophysical changes upon cation binding: PET (photo-induced electron transfer), PCT (photo-induced charge transfer), excimer / exciplex formation, and extinction or energy transfer. We gave information about the fluorescence resulting from the complexation of nitrogen (N) groups in azide groups linked to two *p-tert*-butylcalix[4]arene with Pb^{2+} ion.

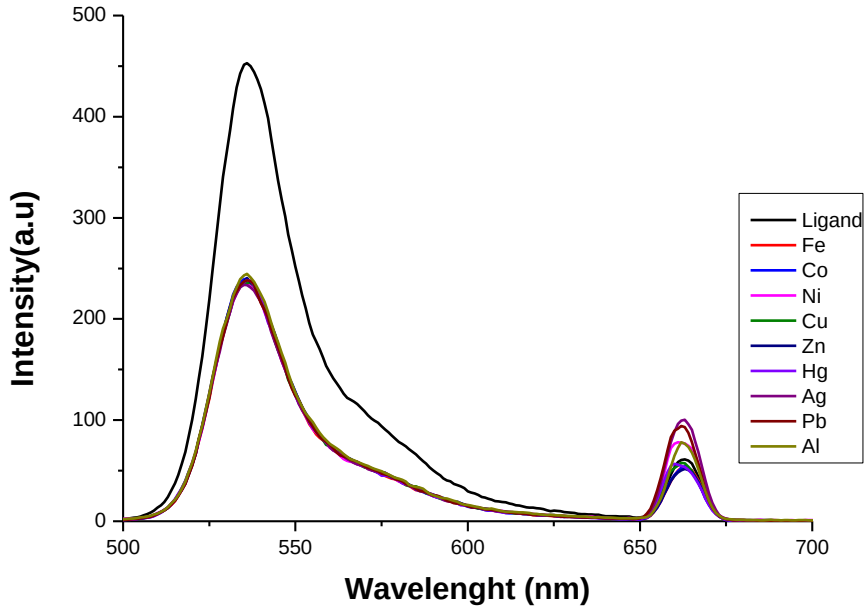

Figure 3. Fluorescence response of **6 (**5×10^{-6} mol.L^{-1}) upon addition of different metal ions (5×10^{-6} mol.L^{-1}) in EtOH.

According to the hard acid-base theorem, d orbitals are full or nearly full ions that tend to have soft acid properties. Heavy metal ions with large

radii and small charges are expected to behave as a soft acid. One of the reasons affecting the hardness and softness properties is the presence of π bonds. As their π bonds help the electron to diffuse, it increases the softness property. The reason why the CN ion is soft is that there are π bonds in its structure. We used triazole unit in which was bound to BODIPY unit by Click reaction can easily and strongly coordinate with Pb^{2+}. BODIPY units probably behave as PET acceptors whereas the triazole groups behave as electron donor when the Pb^{2+} ion is bound by the two triazole nitrogen atoms. In the absorption spectrum, we can interpret that emission range of BODIPY dyes is very wide from 500 nm to 900 nm. Compound **6** shows emission peak *λ max* at 545 nm the extinction maximum at 660 nm (**Figure 3**). Fluorescence intensity of 6 has special selectivity and sensitivity to Pb^{2+} ion. The solvents used can change the intensity of the fluorescence or the wavelength at which it is seen. Of course, the polarity of the solution also affects the system, but this situation affects the wavelength rather than the intensity of the fluorescence. In general, with increasing polarity, the maximum fluorescence emission shifts to longer wavelengths.

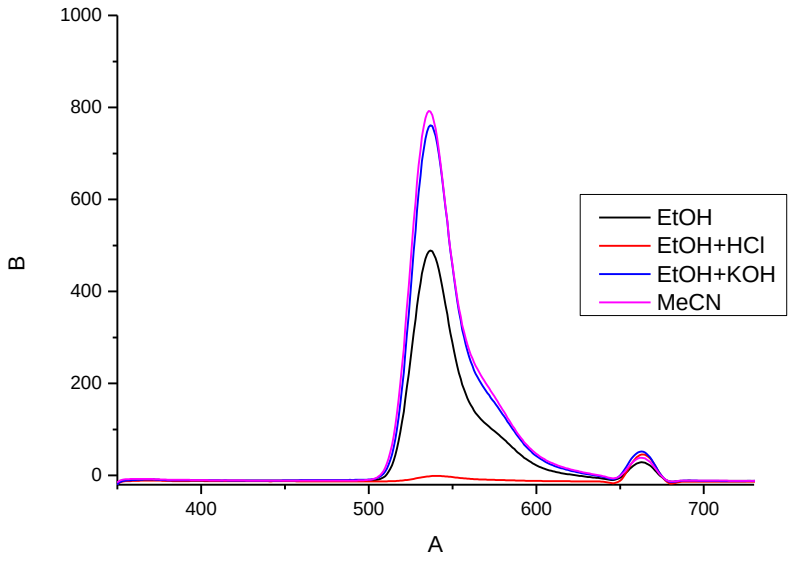

Figure 4. Fluorescence response of 6 in different solvent and pH (1-10)

We observed that fluorescence bands increased in MeCN because of solvent polarity. The effect of the solvent acidity affects mainly the emission band. Fluorescence of **6** was a larger intensity in fluorescence emission due to protonation of the nitrogen in the triazole in a very acidic solution (pH :1). The deprotonation of nitrogen in the triazole occurred in a very basic solution (pH:10) fluorescence emission not much changed (**Figure 4**).

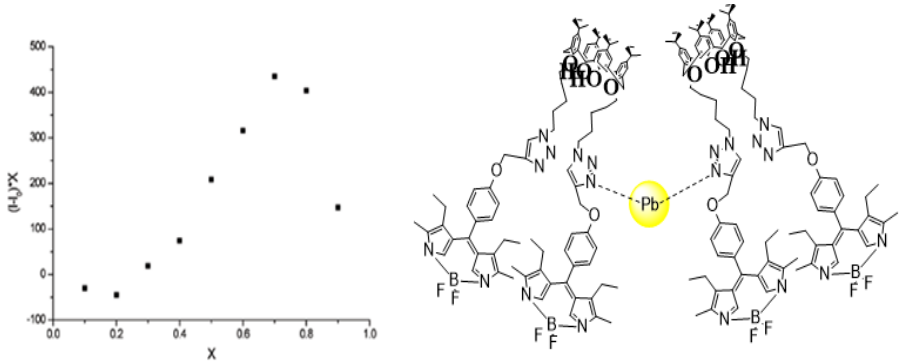

Figüre 5. Job's plot for ***6*** ($5.0x10^{-7}$ M) and Pb (II) complexation in a mixture of $EtOH/H_2O$ (9:1, v/v)

In the job stoichiometry of such complexation was studied, the maximum point appears at the mole fraction of 0.7, which indicates 6 and Pb^{2+} from a 2:1 complex (**Fig. 5**). Although the job study was repeated several times, the same results were obtained. The ratio of lead, calixarene derivative compound was observed as 1:2. The complex of lead with calixarene with BODIP was thought to be as in Figure 5. In future studies, experimental studies will be supported by theoretical studies.

REFERENCES

Ali, R., Razi, S.S., Shahid, M., Srivastava, P., and Misra. A. (2016). Off – On – Off Fluorescence Behavior of an Intramolecular Charge Transfer Probe Toward Anions and CO_2, Spectrochimica Acta Part A: Molecular and Biomolecular Spectroscopy. Vol 168, pp 21– 28

Atilgan, S., Ozdemir, T., Akkaya, E. U. (2008). A sensitive and selective ratiometric near IR fluorescent probe for zinc ions based on the distyryl-bodipy fluorophore, Organic Letters, Vol 10, pp 4065–4067

Baldini, L., Sansone, F., Casnati, A., Ungaro, R. (2012). Calixarenes in molecular recognition, Supramolecular Chemistry: From Molecules to Nanomaterials , Vol 3, pp 863

Banuelos, J. (2016). BODIPY Dye, the Most Versatile Fluorophore Ever? Chem. Rec., Vol 16, pp 335–348

Boens, N., Leen, V., Dehaen, W. (2012). Fluorescent indicators based on BODIPY, Chemical Society Reviews, Vol 41, pp 1130-1172

Czarnik, W. (2002). In: J. R. Lakowicz (ed). Topics in Fluorescence Spectroscopy, Vol 4. Springer, Boston, MA

Guliyev, R., Coskun, A., Akkaya, E. U. (2009). Design Strategies for Ratiometric Chemosensors: Modlulation of Excitation Energy Transfer at the Energy Donör Site, Journal of the American Chemical Society, Vol 131, pp 9007-9013

Gutsche C. D. and Stoddart, J. (1989). Royal Society of Chemistry, Cambridge, Vol 1

Gutsche C. D. and Nam, K. C. (1988). Calixarenes. 22. Synthesis, properties, and metal complexation of aminocalixarenes, J. Am. Chem. Soc., Vol 110, pp 6153

Gutsche., C. D. (1998). Calixarene Revisited, The Royal Society of Chemistry. Cambridge. United Kingdom

Kafadar, F., Saygıdeğer, S. (2010). Gaziantep İlinde Organize Sanayi Bölgesi Atık Suları İle Sulanan Bazı Tarım Bitkilerinde Kurşun Miktarlarının Belirlenmesi, Ekoloji, Vol 75 pp 41-48

Kim, J.S., Quang, D.T. (2007). Calixarene-derived fluorescent probes, Chemical Reviews, Vol 12 No 107(9) pp 3780-99.

Kolb, H.C., Finn, M.G., Sharpless, K.B. (2001). Click chemistry: diverse chemical function from a few good reactions, Angew. Chem. Int. Ed. Eng., Vol 40 pp 2004–2021

Kolemen, S., Akkaya, E.U. (2018). Reaction-based BODIPY probes for selective bio-imaging, Coordin. Chem. Rev., Vol 354, pp 121–134

Kumar, R., Sharma, A., Singh, H., Suating,P., Seok, H., Sunwoo, K., Shim ,I., Bruce C. Jong, G., Ki, S. (2019). Revisiting Fluorescent Calixarenes: From Molecular Sensors to Smart Materials. Chemical Reviews, Vol 119 (16), pp 9657-9721

Kumar, R., Sharma, A., Singh, H., Suating, P., Kim, H.S., Sunwoo, K., Shim, I., Gibb, B.C., Kim, J.S. (2019). Revisiting Fluorescent Calixarenes: From Molecular Sensors to Smart Materials, Chem. Rev, Vol 119, pp 9657–9721

Kurniawan, Y.S., Ryu , M., Sathuluri, R.R., Iwasaki W., Morisada, S., Kawakita, H., Ohto, K., Maeki, M., Miyazaki, M. and Jumina, V. (2019). Separation of Pb(II) Ion with Tetraacetic Acid Derivative of Calix[4]arene by Using Droplet-based Microreactor System, Indonesian Journal of Chemistry, Vol 19, pp 368–375

Leita, L. (1991). Heavy metal bioaccumulauon in lamp and sheep bred in smelting and mining areas of Sardinia, SW Enviromental Contamination Toxicology, Vol 46, pp 887-893

Li, Z.T., Ji, G.Z., Zhao, C. X., Yuan, S. D., Ding, H., Huang, C., Du, A. L. and Wei, M. (1999). Self-Assembling Calix[4]arene [2]Catenanes., Preorganization, Conformation, Selectivity, and Efficienc, .J. Org. Chem, Vol 64, pp 3572

Okcu, M., Tozlu, E., Kumlay, A.M., Pehluvan. (2009). M. Ağır Metallerin Bitkiler Üzerine Etkileri, Alınteri Zirai Bilimler Dergisi Vol 17(2), pp 14-26

Ozdemir, T., Atilgan, S., Kutuk, I., Yildirim, L T., Tulek, A., Bayindir, M., Akkaya, E. U. (2009). Solid-state emissive BODIPY dyes with bulky substituents as spacers, Organic letters, Vol 11, pp 2105-2107

Quiroga-Campano, C., Gómez-Machuca, H., Moris, S., Pessoa-Mahana, H., Jullian, C., Sait, C. (2021). Synthesis of calix[4]arenes bearing thiosemicarbazone moieties with naphthalene groups: Highly

selective turn off/on fluorescent sensor for Cu(II) recognition, Journal of Molecular Structure, Vol 1225, pp 125-129

Sayin, S., Ozcan, F., Memon, S., Yilmaz, M. (2010). Synthesis and oxoanions (dichromate/arsenate) sorption study of N-methylglucamine derivative of calix[4]arene immobilized onto poly[(phenyl glycidyl ether)-co-formaldehyde], Journal of Inclusion Phenomena and Macrocyclic Chemistry, Vol 67, pp 385–391

Sharpless , K.B., Manetsch ,R. (2006). In situ click chemistry: a powerful means for lead discovery, Exp. Opin. Drug Discov, Vol 1 pp 525–538

Simsir, A.E., Erdemir, S., Tabakci, M., Tabakci. B. (2021). Nano-scale selective and sensitive optical sensor for metronidazole based on fluorescence quenching: 1H-Phenanthro[9,10-d]imidazolyl-calix[4]arene fluorescent probe, Analytica Chimica Acta, Vol 1162 , pp 338494

Sulak M., Kurşunlu A.N., Girgin B., Karakuş Ö.Ö., Güler E. (2017). A highly selective fluorescent sensor for mercury (II) ion based on Bodipy and Calix [4] arene bearing triazolenaphthylene groups; synthesis and photophysical investigations, Journal of Photochemistry and Photobiology A: Chemistry, Vol 349, pp 129-137

Treibs, A., Kreuzer, F.H. (1968). Difluorboryl-Komplexe von Di- und Tripyrrylmethene, Justus Liebigs Annalen der Chemie, Vol 7, No 18(1), pp 208-223

Uppal, T., Bhupathiraju, N.V.S.D.K., Vicente, M.G.H. (2013). Synthesis and cellular properties of near-IR BODIPY–PEG and carbohydrate conjugates, Tetrahedron, Vol 69, pp 4687–4693

Wu, D., Sedgwick, A. C., Gunnlaugsson, T., Akkaya, E.U., Yoon, J. and James, T.D. (2017). Fluorescent Chemosensors: The Past, Present and Future, Chemical Society Reviews, Vol 46 pp 7105–7123

Yilmaz, E., Memon, S., Yilmaz, M. (2010). Removal of direct azo dyes and aromatic amines from aqueous solutions using two β-cyclodextrin-based polymers, Journal of Hazardous Materials, Vol 174, pp 592–597

CHAPTER 2

INVESTIGATION OF THE VIABILITY OF BIOCHAR-DOPED HYDROGELS IN THE FIGHT AGAINST DROUGHT

Asst. Prof. Zeynep Görkem DOĞAROĞLU[1],

Prof. Dr. Yağmur UYSAL[1] and Assoc. Prof. Dimitrios KALDERIS[2]

[1] Mersin University, Engineering Faculty, Environmental Engineering Department, Mersin, TURKEY, gorkemdogaroglu@gmail.com (ORCID: 0002-6566-5244) (+90 538 8486164), yuysal@mersin.edu.tr (ORCID: 0002-7217-8217) (+90 532 6448308)

[2] Department of Electronic Engineering, Hellenic Mediterranean University, Crete, GREECE, kalderis@hmu.gr (ORCID: 0000-0002-4983-065X)

INTRODUCTION

The application of the sustainable agriculture approach, it has become the focus of research, against climate change due to global warming and environmental risks. The preservation of natural resources in the basic targets of sustainable agriculture, is closely related to the correct management of a basic component such as water (Nassaj-Bokharaei et al. 2021). Climate change also significantly affects the agricultural sector. The deterioration of agricultural soils due to improper irrigation and fertilization prevents access to healthy and adequate food. In order to make the most efficient use of water and fertilizers, research has become widespread today and the biggest share in this regard is the use of hydrogels in agricultural production (Gholamhoseini et al. 2018; Tomadoni et al. 2020).

Hydrogels are hydrophilic gels that can make physical and chemical three-dimensional cross-links between polymer chains, thereby absorbing, storing and releasing water molecules (Chen et al. 2009; Abdellaoui et al. 2020; Nassaj-Bokharaei et al. 2021). These materials are natural or synthetic structures that can absorb hundreds of times water of their dry weight (Tomadoni et al. 2020). The content of many commercial hydrogels used as soil conditioners consists of petroleum-based synthetic polymers. These hydrogels have environmental hazards because they have low biodegradability and water absorption capacity, high production cost or toxic byproduct formation (Mazloom et al. 2019). In order to eliminate all these environmental risks and produce more resistant hydrogels, the researchers have focused on to produce new generation of bio-compatible, environmentally friendly and hydrogels with high water absorption capacity and strength.

Natural polymers such as gelatin, cellulose, chitin, chitosan, alginate, and also synthetic polymers such as poly(vinyl alcohol) (PVA), poly(ethylene glycol), polyacrylamide is used in hydrogel production (Bayraktar, 2013). In this study, sodium alginates and PVA was used in hydrogel synthesis. Sodium alginates, which is one of the most studied biopolymers today, has features such as hydrophilic structure, biocompatibility, biodegradability, non-toxicity and antimicrobial activity, which makes it a valuable raw material in water and fertilizer management (Feng et al. 2017; Tomadoni et al. 2020). In cross-linked polymers, chains are connected to each other in three dimensions by

covalent or ionic bonds, thus forming networked polymers and these polymers have a good swelling capacity in solvents but they do not dissolve. In order for a polymer to have hydrogel properties, some hydrophile functional groups (such as hydroxyl, carboxyl, carbonyl, amine and amid) must be present in the main or minor chain (Bayraktar, 2013).

Water and fertilizer applications are the main factors affecting agricultural production (Du et al. 2015). Therefore, reducing the consumption of water required for optimal use of plant nutrients and agriculture are considered priorities in the development of sustainable agriculture (Aouada et al. 2008; Nassaj-Bokharaei et al. 2021). Biochar from agricultural waste is an important recycling step that shows great potential in carbon emissions, greenhouse gas emission reduction, soil improvement and crop yield growth. These environmentally friendly bio-stimulants are potentially valuable applications in agriculture to increase soil fertility, to assist sustainable agricultural production and to mitigate the negative effects of different biotic/abiotic stresses on the plant (Semida et al. 2019). Biochar is a new term used to describe porous charcoal (fine pulverized charcoal) made from various biomass. Biochar is obtained as a result of incomplete combustion of wood, pruning wastes, leaves, grass or agricultural biomass in an environment with limited or no oxygen. At the same time, biochar production is a fast process that is economically profitable due to the value of the final product obtained from the process, but it can also be used as an energy source and carbon storage.

In this study, it is aimed to obtain biochar from olive tree wastes and to synthesize biochar-based hydrogels. After the synthesis of different ratios of biochar-based hydrogels, lettuce seeds were planted in vials containing turf and turf + hydrogels. To determine the effectiveness of biochar-based hydrogels on plant height, fresh and dry biomass and chlorophyll content, plants were subjected to 2, 4, and 7 days of drought stress after the germination in turf.

1. MATERIAL AND METHOD

1.1. Synthesis of biochar

Dry pruning of the olive tree (*Olea Europaea* L.) were obtained free of charge from the local municipal waste management company of Greece and used as the raw material for biochar production. A purpose-made flame curtain pyrolysis kiln was constructed and used for the preparation of biochar. The pruning was randomly separated into 3 batches and flame-curtain pyrolysis was carried out in triplicate. Each batch was pyrolyzed for 1 h at 600 °C, as measured by thermocouples attached to the kiln. No external source of heating was required, and the process was self-sustained after the first pruning started to pyrolyze. After quenching with water, the biochar was air-dried for 96 h. The dried biochar was crushed and the 125-250 μm fraction was sieved and stored for further analyses.

1.2. Synthesis of biochar-based hydrogel

Sodium alginate/polyvinyl alcohol (SA/PVA) hydrogels were synthesized using the method by Feng et al. (2017). For the preparation of SA/PVA hydrogels, they were mixed in a magnetic stirrer at 25°C for 2 hours to obtain a homogeneous solution of 5% (w/v) SA and 2.5% (w/v) PVA. A certain amount of biochar (1%, 2%, 3% and 4%) were added to the obtained polymer solution to ensure a homogeneous distribution. To obtain the hydrogels, this homogeneous solution was dropped into a 5% (w/v) $CaCl_2$ solution, which is continuously stirred (100 rpm) in a magnetic stirrer. Next, the encapsulated hydrogels spheres were washed with distilled water to remove residual $CaCl_2$ solution on their surface.

1.3. Characterization of biochar and biochar-based hydrogel

The chemical and physical properties of olive tree biochar were determined using analytical methods and also the Scanning Electron Microscopy (SEM) images of the biochar samples were taken. The chemical structure of synthesized BCH/SA/PVA hydrogels and biochar to be obtained from olive tree wastes will be examined by Fourier Transform Infrared (FTIR) Spectroscopy in the wavelength range of 4000-400 cm^{-1}. Samples will be polished with analytical KBr prior to FTIR analyzes. SEM images of the synthesized hydrogel samples were taken.

1.4. Swelling Capacity of Biochar-Based Hydrogel

The swelling capacity of the synthesized BCH/SA/PVA hydrogels were determined by the classical gravimetric method (Liu and Huang, 2016). For this purpose, the synthesized BCH/SA/PVA hydrogels were left to dry for 2 days at room temperature to dehydrate. 0.2 g of the dried hydrogels were weighed and left in distilled water at room temperature for 4 days until equilibrium is reached. Swelling hydrogels were removed from the water and lightly dried with wet filter paper and weighed immediately. The equilibrium swelling ratio of the hydrogels were determined using the below formulation.

$$ESR(\%) = \frac{W_s - W_d}{W_d} * 100$$

Where; W_s and W_d are mass of the swollen and dry samples (g), respectively.

The swelling-drying cycle of synthesized pure and biochar-based hydrogels were determined in three cycle. In the experiments the synthesized hydrogels were dried at room temperature for 2 days. Then, 0.2 g hydrogels were weighed and left in distilled water for 80 min, after that they were slightly dried with wet filter paper and weighed immediately. The weighed hydrogels were dried at 80 ^{o}C for 60 min. Thus, the first cycle was completed. These steps were realized for three times to complete the swelling-dried cycles.

1.5. Plant Treatments

1.5.1. Phytotoxicity Tests

Phytotoxicity tests of synthesized BCH/SA/PVA hydrogels were performed on lettuce seeds. The germination test of lettuce was carried out according to Doğaroğlu (2019). Ten lettuce seeds were placed in petri dishes filled with 10 mL of distilled water (control) or water-saturated BCH/SA/PVA hydrogels. Petri dishes were incubated in the dark at 25°C for 14 days and then the number of germinated seeds were counted.

1.5.2. Pot Experiments

The lettuce seeds were sown in pots which included 8 g turf (control), and 8 g turf + 0.5 g BCH/SA/PVA hydrogels which included different olive tree biochar (OTB) concentrations. The pots were irrigated every two days for the germination period (14 days). After this period, the plants were irrigated every 2, 4, and 7 days for 28 days to determine the effectiveness of hydrogels against to drought stress in plants. Plants height, dry and fresh weight, and chlorophyll content of 28 days old plants were determined. The chlorophyll content of plants was measured using Konica-Minolta SPAD-502 chlorophyll meter, and then plant root and shoot lengths were measured by removing the plants from the pots. Removed plants were weighed to determine the fresh weight and they were dried in an oven at 65 ^{o}C for 48h to determine dry weights. All treatments and measurements were conducted three replications.

2. RESULTS AND DISCUSSIONS

2.1. Characterization of Biochar and Biochar-Based Hydrogel

Chemical and physical properties of olive tree biochar samples were determined and shown in Table 1. The pH and the electrical conductivity (EC) of the OTB samples were measured as 8.52 and 525 µS/cm, respectively. The OTB had ash content as 7.9 % and C content as 76.67 % (Table 1). These results similar with Sánchez-García et al. (2019). The authors characterized 22 biochar samples and found that the pH changes in the range of 9.3-12.4, depending on the pyrolysis temperature. They indicated that when the pyrolysis temperature increases, the amount of C content and the relative ash content increases. Biochar has a high and constant C content, when the ash and volatile organic content are below 30% and 40%, respectively, according to the triangle diagram (volatile content (%)-constant C (%)-ash (%)). It is stated in the literature that it is possible to obtain high C content with pyrolysis at high temperatures (Sánchez-García et al. 2019). In this study, the C, H, N and O contents of the biochar obtained from olive tree pruning wastes were determined to be 75.67%, 1.65%, 0.80% and 12.98%, respectively. In addition, according to the results of BET surface area analysis, it was determined that the biochar samples had a surface area of 292 m^2/g.

Table 1. Physical and Chemical Properties of Olive Tree Biochar

	Olive tree biochar
Yield after pyrolysis (%)	19
pH	8.52
EC (µS/cm)	525
C (wt. %)	76.67
H (wt. %)	1.65
N (wt. %)	0.80
O (wt. %)	12.98
Ash content (wt. %)	7.9
BET surface area (m^2/g)	292

The SEM images showed that the biochar particles were in different sizes and shapes, also had pores (Figure 1). It was observed that in the hydrogel images, biochar-based hydrogel had more wrinkles than pure hydrogel after dried in the oven. The biochar-based hydrogel had irregular protrusions, while the pure hydrogel had uniform and neat folds. The biochar-based hydrogel can absorb more water than pure hydrogel because of irregular surface morphology (Feng et al. 2017).

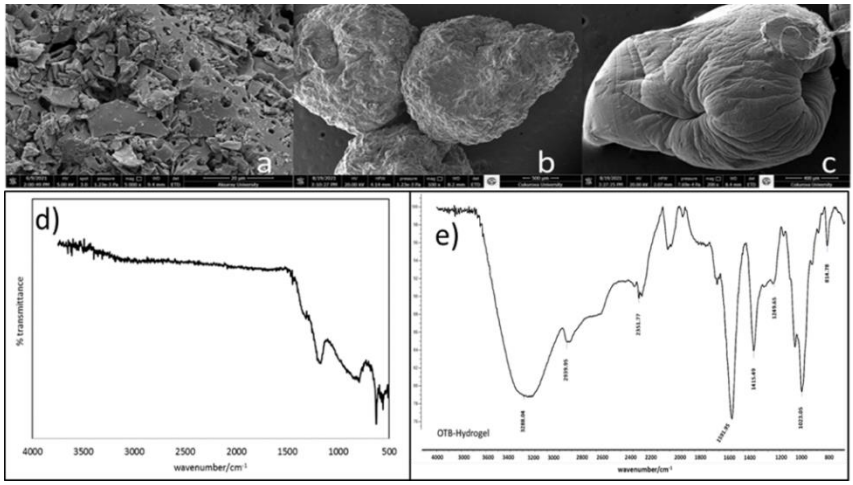

Figure 1. SEM Images of a) Olive Tree Pruning Biochar, b) Biochar-Based Hydrogel, and c) Pure Hydrogel and FTIR Spectra of d) Olive Tree Pruning Biochar and e) Biochar-Based Hydrogel

In the single-bond region (2500-4000 cm^{-1}) no bands were observed, specifically the O–H bond stretching vibration is completely absent. The same applies in the double- and triple-bond region, 2000-2500 and 1500-2000 cm^{-1}, respectively. This phenomenon is probably due to the effect of washing the biochar with distilled water after its preparation. In the fingerprint region (500-1500 cm^{-1}), a strong band at 1168 cm^{-1} can be observed. This may be attributed to the stretching vibrations of hydrogen-bonding C-OH group. The broad band at 790 cm^{-1} is probably due to the aromatic C-H out-of-plane bend, whereas the sharp band at 624 cm^{-1} corresponds to C-H bending of alkyne (Figure 1d) (Coates, 2000). In addition, the FTIR spectra of BCH/PVA/SA crosslinked with $CaCl_2$ beads were analyzed (Figure 1e). FTIR spectrum of BCH/PVA/SA hydrogels showed the bands around 3288, 1591, 1415, 1023, and 2939 cm^{-1} which are correspond to the stretching of −OH, −COO− (asymmetric), −COO− (symmetric), C−O−C, –CH stretching, respectively. By the way, the band at 814 cm^{-1} correspond to C-H bending which given by Sali et al. (2016). These results were similar in the report of Sali et al. (2016) and Shivakumara and Demappa (2019).

2.2. Swelling Capacity of Biochar-Based Hydrogel

The most important property of hydrogels is that they can absorbed in hundreds of times more water than their own weight. Water management can be planned in agriculture by determining the water holding capacity. It was determined that the addition of biochar in hydrogel improved the water holding capacity (Figure 2). The maximum and the minimum swelling rate of hydrogel was observed in the 0.1 % OTB based hydrogel as 115.6 %, and pure hydrogel as 32.4 %, respectively. The water holding capacities of hydrogels vary according to the synthesis method, chemical composition, and polymer structure used. Besides that, the water absorption mechanism is similar in all hydrogels and is realized by taking water into the 3D network of hydrogels and loosening the polymer chains (Chen et al. 2009; Tomadoni et al. 2020)

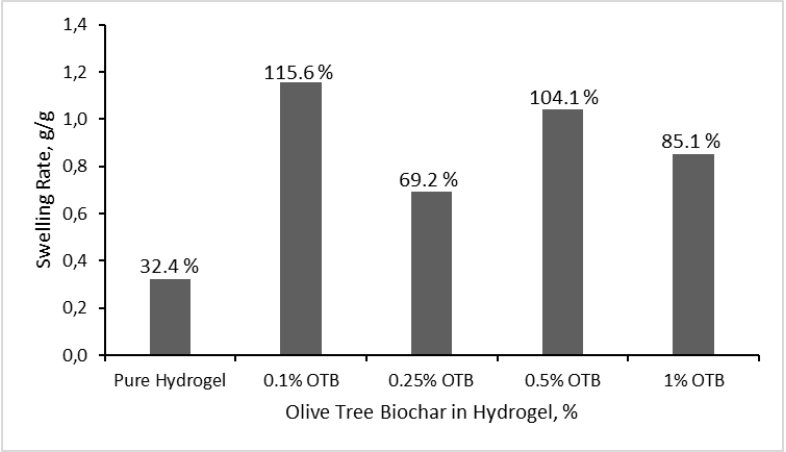

Figure 2. Swelling Rate of Pure and Olive Tree Biochar-Based (OTB) Hydrogels

In addition to the swelling rates in the use of hydrogels in agriculture, the swelling-drying cycle is also important (Durpekova et al. 2020). Therefore, in this study, the swelling-drying cycle of pure and biochar-based hydrogels was also evaluated. Accordingly, pure and bichar based hydrogels are swolled and dried 3 times (Figure 2). The swelling rate of pure hydrogels decreased by 37.3% after 3 cycles. Although, the maximum decrease among biochar-based hydrogel was 11.11% at a concentration of 0.5 % OTB, none of the biochar hydrogels suffered more swelling loss than pure hydrogels. Also, it was observed that all the hydrogels have 50% swelling ratio after third cycles. Lv et al. (2019) realized ten times of swelling/deswelling cycles and indicated that the PVA based hydrogels did not show any significantly decreases in pure water after at the end of cycles. Also, Durpekova et al. (2020) stated that the synthesized cellulose-based hydrogels have sustainable water holding capacity after the 5 drying and swelling cycle.

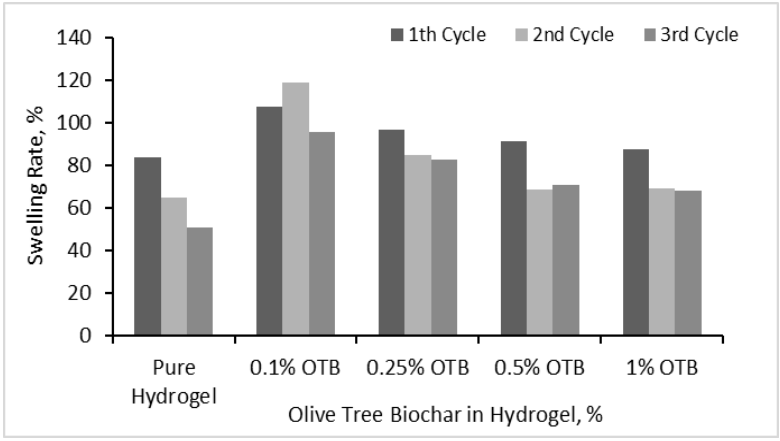

Figure 2. Swelling Rate of Biochar-Based Hydrogel at Different Concentrations in The First, Second and Third Cycle

2.3. Plant Treatments

2.3.1. Germination Tests

In order to determine whether synthesized hydrogels have a phytotoxic effect on lettuce seeds, germination experiments were first carried out in petri dishes. It was determined that the lettuce seeds were not germinated 14 days after planting, except the control. Although, it was observed that the seeds were germinated late in the petri which include pure and biochar-based hydrogels compared to control (absence of hydrogels). However, germinated seeds in the presence of hydrogel, especially 0.1 % OTB-based hydrogels, even survived the 42 days after start of experiments (Figure 3). The germinated seeds in petri which include the control, 0.5%, and 1% OTB-based hydrogels were died, while they were alive in the 0.25%, 0.1% and pure hydrogels. It is thought that this is since the water release rate of pure, 0.1%, and 0.25% OTB-based hydrogels was slower than the other OTB-based hydrogels. Although 0.5% and 1% OTB-based hydrogels, which do not have any toxic effect on the plant, have an over water retention capacity, it was observed that they dry out faster, also Alburquerque et al. (2013) showed that the germination indices of lettuce treated with olive tree biochar in soil were above 60%. Thus, it was determined that the biochar application in soil or in hydrogel were not toxic for lettuce, however biochar in hydrogel caused late germination.

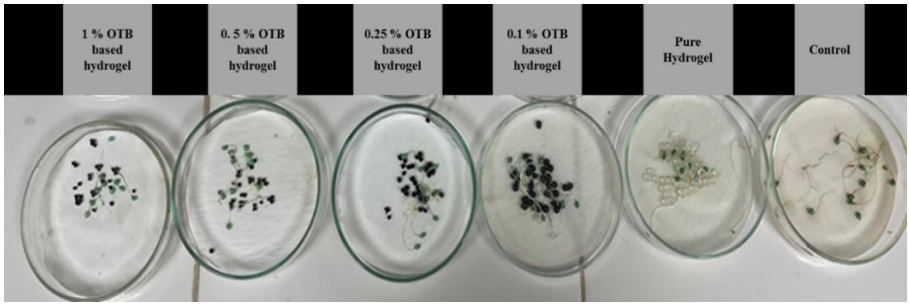

Figure 3. Germinated Seeds in Petri Dishes at The End of 42 Days After Start of Germination Experiments

2.3.2. Pot experiments

In the pot experiments, lettuce seeds were sown in 8 g turf at the absence or presence of hydrogels, in tree replicates. Seeds were germinated in the turf and the seedlings were irrigated with tap water every two days until the plants have 2-3 leaves. After the germination period, first set was irrigated every two days, second set was irrigated every four days, and third set was irrigated every seven days. Thus, the stress of drought in lettuce could be observed. Plants were grown in turf for 28 days after germination in turf, and the chlorophyll content, plant height, fresh and dry biomass were determined. Before the harvesting, chlorophyll content of plants was measured and given as SPAD Units in the Figure 4a. It is important to determine the factors that cause the change of the chlorophyll content to provide information in many different areas from plant health to stress factors. There was not any significantly change in the chlorophyll content of 2 days irrigated plants, so it was observed that the hydrogels did not effective in this watering set. On the other hand, the chlorophyll content of 4 days irrigated plants was decreased with the increasing OTB concentration in hydrogels. It is thought that the high biochar concentrations in hydrogels caused fast water release rate, so they dried earlier than lower biochar concentrations in hydrogels, as mentioned before in the 3.3.1 section. According to Kırnak and Demirtaş, (2002), the decrease in the amount of leaf water slows down the rate of chlorophyll synthesis as well as accelerates the breakdown of chlorophyll, but as in this study, there is not any significantly difference in short-term stresses.

To determine the effectiveness of pure and OTB-based hydrogels on plant growth, the shoot and root lengths were measured. It was observed that

there were not any significantly changes in the shoot length of 2- and 4-days irrigated plants applied with pure and OTB-based hydrogels, compared to control. However, it was seemed that in Figure 4b, the shoot lengths of lettuce, irrigated 7 days, increased at the application of 0.1%- and 0.25%-OTB-based hydrogels, compared to control. Although the frequency of irrigation has been reduced, it has been determined that the shoot lengths of these plants exposed to 7 days of irrigating are almost same to those of plants exposed to 2 and 4 days of irrigating.

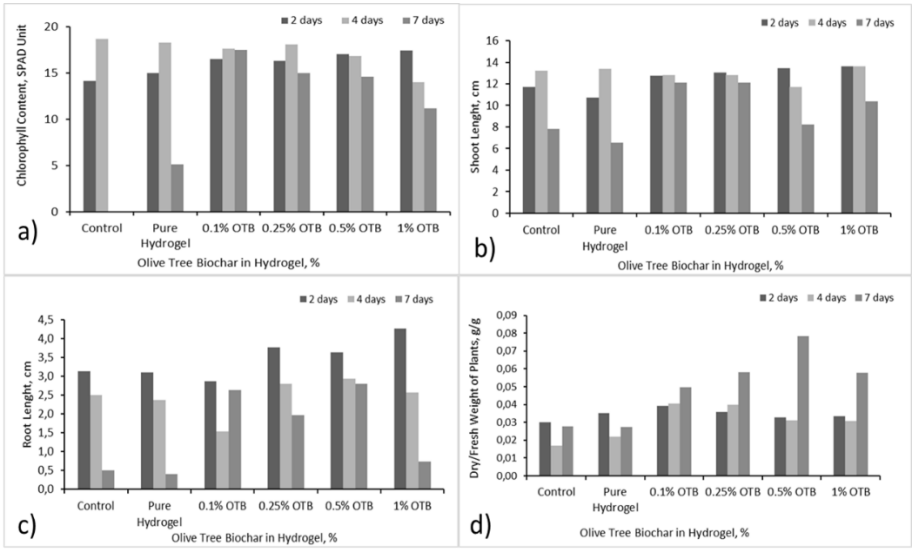

Figure 4. a) Chlorophyll Content, b) Shoot Length, c) Root Length, d) Dry Weight/Fresh Weight of Lettuce Treated With Pure and Different OTB-Based Hydrogel

The root length of lettuce seedlings which irrigated 2 days increased with increasing amount of OTB in hydrogels, while there were no changes at 4 days of irrigating (Figure 4c). It was observed that the plants which irrigated 7 days, the root lengths increased with application of OTB-based hydrogels compared to control and pure hydrogels. The important differences in root length was determined at the 0.1%-, 0.25%-, and 0.5%-OTB-based hydrogels. It was determined that according to both root and shoot length measurements 0.1% and 0.25% OTB-based hydrogels applications were more effective than pure and 1% OTB-biochar hydrogels. Akhter et al. (2004) used

acrylamide and acrylic acid to synthesize of hydrogel and the authors stated that the addition of hydrogel in soil did not change the growth of chickpea seedlings while wheat and barley growth increased. Besides that, Nassaj-Bokharaei et al. (2021) determined that the natural char nanocomposite-based hydrogel application increased root length and plant height of tomato plants under drought stress, but the authors indicated that if hydrogels are used correctly in the agriculture, the plant growth parameters can be improved. Drought stress causes deficient nutrient uptake by plants or reduce transportation of nutrients from soil to plants, so that carbon and dry matter stores are reduced in the plant exposed to drought stress. In these changes in the plant, plant type, soil type and stress level are the most important factors (Nassaj-Bokharaei et al. 2021). Therefore, in order to determine the stress effect on plants, fresh and dry biomass of plants was evaluated (Figure 4d). It was observed that the dry weight (D) and fresh weight (F) rate were positively affected from the presence of OTB-based hydrogels. The D/F rate has the highest value in the plants of 7 days irrigated. This can be explained as the plants in drought stress may be stored the nutrients, supported by water and carbon from OTB-based hydrogel.

CONCLUSION

In this study, sodium alginate and polyvinyl alcohol are the main polymers in the synthesized hydrogels. In this study, which evaluates agricultural wastes, it was determined that these polymers are non-toxic and should be added 0.1% olive tree biochar in order to provide a good swelling capacity in distilled water to synthesized hydrogels. Our results also showed that OTB-based hydrogel treatments delay lettuce seed germination, but for long periods of time germinated seeds can survive and have positive effects on seedling growth and the survival of seedlings under drought stress. These results confirm that the hydrogels which include at low concentrations of olive tree biochar can be used for water management in the agricultural irrigation.

REFERENCES

Abdellaoui, H., Qaiss, A., Bouhfid, R. (2020). Review of nanocellulose and nanohydrogel matrices for the development of sustainable future materials, In: Sustainable Nanocellulose and Nanohydrogels from Natural Sources, Mohammad F., Al-Lohedan H.A. and Jawaid M. (Ed.), Elsevier, pp. 155-176

Akhter, J., Mahmood, K., Malik, K.A., Mardan, A., Ahmad, M., Iqbal, M.M. (2004). Effects of hydrogel amendment on water storage of sandy loam and loam soils and seedling growth of barley, wheat and chickpea. Plant Soil Environment, 50:(10), 463–469

Alburquerque, J.A., Salazar, P., Barrón, V., Torrent, J., Campillo, M.C., Gallardo, A., Villar, R. (2013). Enhanced wheat yield by biochar addition under different mineral fertilization levels. Agronomy for Sustainable Development, 33:475–484

Aouada, F.A., Moura, M.R., Menezes, E.A., Nogueira, A.R.A., Mattoso, L.H.C. (2008). Hydrogel synthesis and kinetics of ammonium and potassium release. Rev. Bras. De. Ciˆencia Solo, 32, 1643–1649

Bayraktar, İ. (2013). Synthesis, characterization and investigation of adsorption properties of magnetic hydrogels. Adnan Menderes Üniversitesi Fen Bilimleri Enstitüsü, Yüksek Lisans Tezi

Chen, J., Liu, M., Liu, H., Ma, L. (2009). Synthesis, swelling and drug release behavior of poly(N,N-diethylacrylamide-co-N-hydroxymethyl acrylamide) hydrogel. Materials Science and Engineering C, 29, 2116–2123

Coates, J. (2000). Interpretation of infrared spectra, a practical approach. Encyclopedia of analytical chemistry, 12, 10815-10837

Doğaroğlu, Z.G. (2019). Role of EDDS and ZnO-nanoparticles in wheat exposed to TiO_2Ag-nanoparticles. Archives of Environmental Protection, 45:(4), 78–83

Du, T., Kang, S., Zhang, J., Davies, W.J. (2015). Deficit irrigation and sustainable water resource strategies in agriculture for China's food security. Journal of Experimental Botany. 66, 2253–2269.

Durpekova, S., Filatova, K., Cisar, J., Ronzova, A., Kutalkova, E., Sedlarik, V. (2020). A novel hydrogel based on renewable materials for

agricultural application. International Journal of Polymer Science vol.2020, Article ID 8363418, 1-13

Feng, D., Bai, B., Wang, H., Suo, Y. (2017). Novel fabrication of biodegradable superabsorbent microspheres with diffusion barrier through thermo-chemical modification and their potential agriculture applications for water holding and sustained release of fertilizer. Journal of Agricultural and Food Chemistry, 65, 5896−5907

Gholamhoseini, M., Habibzadeh, F., Ataei, R., Hemmati, P., Ebrahimian, E. (2018). Zeolite and hydrogel improve yield of greenhouse cucumber in soil-less medium under water limitation. Rhizosphere, 6, 7–10

Kırnak, H., Demirtaş, M.N. (2002). Determination of physiologic and morphologic changes in sweet cherry seedlings under water stress. Atatürk Üniv. Ziraat Fak. Derg. 33 (3), 265-270

Liu, Z., Huang, H. (2016). Preparation and characterization of cellulose composite hydrogels from tea residue and carbohydrate additives. Carbohydrate Polymers, 147, 226–233

Lv, Q., Wu, M., Shen, Y. (2019). Enhanced swelling ratio and water retention capacity for novel super-absorbent hydrogel. Colloids and Surfaces A: Physicochemical and Engineering Aspects, doi: https://doi.org/10.1016/j.colsurfa.2019.123972

Mazloom, N., Khorassani, R., Zohuri, G. H., Emami, H., Whalen, J. (2019). Development and characterization of lignin-based hydrogel for use in agricultural soils: preliminary evidence. Clean – Soil, Air, Water, 47, 1900101

Nassaj-Bokharaei, S., Motesharezedeh, B., Etesami, H., Motamedi, E. (2021). Effect of hydrogel composite reinforced with natural char nanoparticles on improvement of soil biological properties and the growth of water deficit-stressed tomato plant. Ecotoxicology and Environmental Safety, 223, 112576

Sali, R., Naik, L.R., Mohan, S. (2016). Optical and microstructural changes in 5(6)-carboxyfluorescein doped PVA. Journal of Polymer & Composites, 4(3), 45–51

Shivakumara, L.R., Demappa, T. (2019). Synthesis and swelling behavior of sodium alginate/poly(vinyl alcohol) hydrogels. Turkish Journal of Pharmaceutical Sciences, 16(3), 252-260

Sánchez-García, M., Cayuela, M.L., Rasse, D.P., Sánchez-Monedero, M.A. (2019). Biochars from Mediterranean agro-industry residues: physico-chemical properties relevant for C sequestration and soil water retention. ACS Sustainable Chem. Eng., 7:5, 4724–4733

Semida, W.M., Beheiry, H.R., Sétamou, M., Simpson, C.R., Abd El-Mageed, T.A., Rady, M.M., Nelson, S.D. (2019). Biochar implications for sustainable agriculture and environment: A review. South African Journal of Botany, 127, 333-347.

Tomadoni, B., Salcedo, M.F., Mansilla, A.Y., Casalongué, C.A., Alvarez V.A. (2020). Macroporous alginate-based hydrogels to control soil substrate moisture: Effect on lettuce plants under drought stress. European Polymer Journal, 137, 109953

CHAPTER 3

SIMULTANEOUS DETERMINATION CHOLESTEROL-REDUCING COMBINATION USING PRINCIPAL COMPONENTS REGRESSION METHOD

Assoc. Prof. Güzide PEKCAN ERTOKUŞ[1*], Ceyhun BAKAN[2]

[1] Department of Chemistry, Faculty of Science&Art, Süleyman Demirel University, 32260 Isparta-Turkey guzideertokus@sdu.edu.tr, ORCID ID.0000-0001-9230-5634.
[2] Department of Chemistry, Faculty of Science&Art, Süleyman Demirel University, 32260 Isparta-Turkey ORCID ID. 0000-0003-1398-0290

INTRODUCTION

Cardiovascular (heart and vascular) diseases are today's and developing leading causes of mortality (death) and morbidity (incapacity) in countries for a number of reasons. In addition, due to its direct or indirect costs, health plays a major role in spending. In many European countries in recent years, cardiovascular disease mortality rates are significantly lower. is doing. Although it has decreased, it still remains the most important cause of premature death in Europe. More than 80% of cardiovascular disease deaths occur in developing countries. It is estimated to occur (Narla et al. 2009, Uyar 2009, Perk et al. 2012). In the decreasing trend of cardiovascular disease in developed countries, the behavior of society's conservation programs aimed at change has had an impact. Studies have shown that an unhealthy lifestyle and social environment are the basis of cardiovascular diseases. (Arıkan et al. 2009).

Cholesterol is divided into two types: Our health depends on the presence of benign cholesterol (HDL), which is important in the body and should have high levels. HDL helps excess cholesterol in our bodies reach the liver, where it is processed and excreted through the digestive system. HDL is known as "good cholesterol" because it slows blood circulation and eliminates cholesterol from the body that causes vascular blockage. On the other hand, malignant cholesterol (LDL) is a protein that is generated in the liver and carried through the bloodstream. LDL has various positive qualities in addition to being well-known. When LDL (Güven A., 2005), which transports antioxidants and amino acids to other cells, is detected in excess in the human body, it has a deleterious impact on the body. As a result, diagnosis and therapy are critical. Drugs like ezetimibe and simvastatin are used to treat the condition. As a result, atorvastatin and ezetimibe concentrations must be determined. UV spectroscopy data was used to make chemometric measurements of cholesterol medications in this research.

1. MATERIALS AND METHODS

The treatment for cholesterol was applied and assessed in terms of UV/VIS spectrometry and chemometry in this study. Chemometric analysis was used to assess the results. The spectra of the ones that are generated individually (Figure 1.) were first taken, and then in varying proportions.

Finally, measurements of commercially purchased medication tablets were taken. The Minitab 17 program was used to perform the calculation (İnova Danışmanlık).

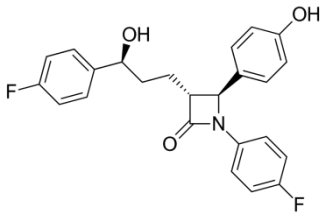

Ezetimibe

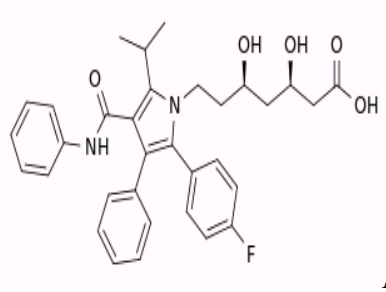

Atorvastatin

Figure 1: Chemical structures of the drugs.

The chemometric approach was used to evaluate the amount of ezetimibe and atorvastatin in cholesterol-lowering medications, with the spectrum values determined using the UV 1700 PHARMASPEC SHIMADZU spectrophotometer with a 1 cm long cell controlled by a computer. For spectrophotometric studies, stock solutions of ezetimibe and atorvastatin were produced at 25 mg/250 mL of 0.1 M HCl. A 0.1 M HCl solution was employed as the solvent in this experiment. To begin, spectrophotometric measurements were used to produce spectra of single taekva communities at various ratios at ezimibe and statin periods. Measurements were done on commercially obtained tablet samples as a final step. The results were analyzed using several chemometrics. The UV spectrophotometer instrument was initially calibrated (reset) in the first step. The calibration procedure was started by leaving two cells blank, which were made up of two light samples. The blind are always prepared in this manner in all readings. When choosing blind, it is preferable to be blind. The commercial tablet (Liptruzet) is assessed in the final step. When crushing

medicine samples, the agate air thins all of the pills in the package, allowing them to be screened. For use, a tablet is weighed, dissolved, and made fit for use. The chemometric approach was used to evaluate the amount of ezetimibe and atorvastatin in cholesterol-lowering medications, with the spectrum values determined using the UV 1700 PHARMASPEC SHIMADZU spectrophotometer with a 1 cm long cell controlled by a computer.

2. RESULTS AND DISCUSSIONS

Using methanol as a 25 mg/250 mL solvent, 100 g/mL (ppm) solutions of the active components of Atorvasatin and Ezetimibe were produced. The solutions for analyzing the spectroscopic characteristics of each individual substance were produced in the range of 5–25 g/mL for each substance in the next step. The wavelength (atorvastatin: 247nm; ezetimibe: 231nm) at which the active components of atorvasatin and ezetimibe produce the most spectrum was determined. The link between absorbance and concentration was investigated, and the correlation coefficients (R^2) values for atorvastatin and ezetimibe were determined to be 0.9998 and 0.9994, respectively. The regression coefficient (Miao, 2018) was close to one, confirming the linear connection between absorbance and concentration (Sharma, 2017). In the case of atorvastatin and ezetimibe, the absorbance value rises as the concentration was increased. In the range of 4–25 mg/mL, 15 synthetic combination solutions were created from Atorvasatin and Ezetimibe (Table 1).

Table 1: Calibration set containing ezetimibe and atorvastatin.

No	**Ezetimibe mg/mL**	**Atorvastatin mg/mL**	**No**	**Ezetimibe mg/mL**	**Atorvastatin mg/mL**
1	5	5	9	25	10
2	10	5	10	15	15
3	15	5	11	20	15
4	20	5	12	25	15

5	25	5	13	25	20
6	10	10	14	25	20
7	15	10	15	25	25
8	20	10			

UV spectroscopy was used to get the absorbance values of these combination solutions, and then the chemometry method was used to these results. Chemometric calculations are the most popular, rapid, and reliable methods for quantifying each component in multicomponent mixtures in recent years. When the relationship between absorbance and concentration is studied by the principal component regression approach, it is based on the premise of creating orthogonal lines by decomposition of the measured absorbance values for the concentration set. These resulting lines represent the calibration's coordinate order, and the computations are based on this precision (Dinç, 2009).

2.1. Calculated Values by Principal Component Regression (PCR)

Table 2: Results calculated by principal component regression for each substance in the mixture containing ezetimibe and atorvastatin.

	Ezetimibe			**Atorvastatin**		
Mix Number	**Added**	**Founded**	**% Recovery**	**Added**	**Founded**	**% Recovery**
1	5	4.98	99.6	5	4.56	91.2
2	10	9.89	98.9	5	4.98	99.6
3	15	14.56	97.07	5	4.85	97
4	20	19.87	99.35	5	4.75	95
5	25	23.99	95.96	10	9.96	99.6

6	10	9.98	99.8	10	9.97	99.7
7	15	14.96	99.73	10	10.01	100.1
8	20	20	100	10	9.97	99.7
9	25	24.87	99.48	15	14.55	97
10	15	14.98	99.87	15	14.42	96.13
11	20	19.97	99.85	15	14.87	99.13
12	25	25.03	100.12	20	19.96	99.8
13	25	24.96	99.84	20	19.87	99.35
14	25	24.97	99.88	25	24.63	98.52
15	25	24.89	99.56	25	24.62	98.48
			Mean= 99.27 **RSD**=0.012			**Mean**=98.02 **RSD**=0.03

The criterion value F is greater than the calculated value of F is one of the characteristics used to assess the method's appropriateness. The P value for Pearson's correlation coefficient should likewise be greater than 0.05. These steps were used to examine the ANOVA data that had been calculated. To check the compatibility of principal component regression, the ANOVA test (Bajpai, 2017) was performed to the derived findings. For ezetimibe, the F criteria value was 4.20, whereas the F calculated value was 0.0033, with a P value of 0.95. For Atorvastatin, the F criteria value was 4.20, whereas the F calculated value was 0.0063; the P value was 0.94.

Data with the Fewest Predicted Resudial Errors Some of the Squares PRESS were achieved by the use of PCR calibration for the measurement of chemicals in mixes containing the active compounds Atorvasatin and Ezetimibe. The closeness of the PRESS value to zero improves accuracy (Uyank, 2012). The PRESS values found are small enough. The standard error of calibration (SEC) and the square root of the mean squares of the estimation (RMSEC) were used to represent other parameters in the validation (Bilgili, 2014). The parameters of limit of detection (LOD) and limit of detection

(LOQ) are related but have various definitions (Shrivasta, 2015). LOQ > LOD and LOQ = LOD were considered while evaluating the derived LOD values (Armbruster, 2008) (Table3.).

Table 3: Principal Component Regression Validation Parameters

PARAMETRER	METHOD	EZETIMIBE	ATORVASTATIN
SEC	PCR	0.048	0.068
PRESS	PCR	0.085	0.076
RMSEC	PCR	0.075	0.071
LOD	PCR	0.639	0.326
LOQ	PCR	2.130	1.09

2.2. Application of the Principal Ingredient Regression Method to Commercial Pharmaceutical Tablets

The chemometric methods employed in this study were applied to commercial medicine tablets in the last phase after verifying the applicability of the methods and the analytical control of the generated data (Table 4.).

Table 4: Results in the drug sample

	Ezetimibe (gram)	**Atorvastatin (gram)**
NO	**PCR**	**PCR**
1	0.0096	0.011
2	0.0089	0.009
3	0.011	0.0088

4	0.0095	0.01
5	0.0094	0.0095
Mean	0.0097	0.0097
Relative Standard Deviation	0.0008	0.0009

It has been studied with a drug called Liptruzet. It contains 10 mg of ezetimibe and 10 mg of atorvastatin.

3. CONCLUSIONS

The measurement of the active components of atorvasatin and ezetimibe in mixtures containing these medications was achieved by combining UV spectroscopy data with chemometric programs. Both ingredients were used to make mixtures. Both approaches were evaluated, and the data's dependability was examined, before going on to commercial medicine tablets with these mixes. The recovery values were relatively high and the relative standard deviation values were achieved as adequately small values using both the principle component regression (PCR) approach. When the press, sec, rmsec, lod, and loq values calculated for the validity of the method were examined, it was observed that the lod values were smaller than the loq values. Other calculated parameters should be close to zero. Values close to zero were also observed in the data we calculated. The suitability of the methods applied before switching to commercial drug tablets was also checked. An ANOVA test was performed for this process. The F calculated values must be lower than the criteria or F theoretical values. The Pearson correlation coefficient, which is a P value, should also be greater than 0.05. It was decided that the calculated values and the methods were appropriate. The methods applied in this study can be applied to complex two-component drug mixtures.In the mixtures containing the active ingredients of atorvasatin and ezetimibe, the quantification of these substances was achieved by supporting the data obtained from UV spectroscopy with chemometric programs. Mixtures containing both substances were prepared. Before moving on to

commercial drug tablets with these mixtures, both methods were tested, and the reliability of the data was examined. When looking at the values calculated by the principal component regression (PCR), the recovery values were quite high and the relative standard deviation values were obtained as sufficiently small values.

ACKNOWLEDGMENT

This research work has been supported by research grants from the Süleyman Demirel University Scientific Research Project: FYL-2019-7351.

REFERENCES

Arıkan, İ., Metintaş, S., Kalyoncu, C., Yıldız, Z. (2009). The Cardiovascular Disease Risk Factors Knowledge Level (CARRF-KL) Scale: a validity and reliability study. Arch. Turk. Soc. Cardiol. (37), 35-40.

Armbruster D.A., Pty, T. (2008), Limit of blank, limit of detection and limit of quantitation, Clin Biochem Rev, (29), 49-52.

Bajpai V., Kumar S., Singh A., Singh J., Negi M.P.S., Bag S.K., Kumar N., Konwar R., Kumar V. (2017), Chemometric base did entification and validation of specific chemical markers for go egraphical, seasonal and gender variations in tinospora cordifolia stemusing HPLC-ESI-QTOF-MS Analysis, Photochemical Analysis, (28-4), 277-288.

Bilgili A.V., Çullu M.A., Aydemir S. (2014), Tuzdan etkilenmiş toprakların yakın kızılötesi yansıma spektroradyometre ve elektromanyetik indüksiyon tekniği yardımıyla karakterize edilebilme potansiyelinin araştırılması, Harran Tarım ve Gıda Bilimleri Dergisi, (18-1), 32-45.

Dinç E. (2009), Kemometrik İşlem ve Yöntemlerin Analitik Kimyadaki Tipik Uygulamaları, Uygulamalı Kemometri Yaz Okulu Notları, 13-17.

Güven A. (2005). Hiperkolesterolemi oluşturulmuş tavşanlarda kefirin total kolesterol, trigliserit, HDL-kolesterol, LDL-kolesterol ve lipit peroksidasyonu üzerine etkisi, Kafkas Üniversitesi Veteriner Fakültesi Dergisi, (11:2), 127-131.

Miao J., Forget B., Smith K. (2018). Predicting Correlation Coefficients for Monte Carlo Eigen value Simulations With Multitype Branching Process, Annals of Nuclear Energy, (112), 307-321, 2018.

Minitab 17 Statistical Programme: http://www.inovadanismanlik.com.tr (19.01.2022).

Narla, V., Blaha, M.J., Blumenthal, R.S., Mıchos, E.D. (2009). The JUPITER and AURORA clinical trials for rosuvastatin in special primary prevention populations: perspectives, outcomes, and consequences. Vasc. Health Risk Manag. (5), 1033-1042.

Perk, J., Backer, G.D. (2012). Avrupa Klinik Uygulamada Kardiyovasküler Hastalıklardan Korunma Kılavuzu, Türk Kardiyol. Dern. Arş. (40), 1-76.

Sharma D., Singh, R., Garg V. (2017). Development and validation of stabilityindicating UV spectro-photometric method for the estimation of benzydamine hydrochloride in bulkand in pharmaceutical dosage form: a novel analytical technique for conducting in-vitroquality control tests, International Journal Of Pharma ceutical Sciences And Research, vol. (9(2)), 678-686.

Shrivastava A., Gupta V.B. (2011), Methods for the determination of limit of detectionand limit of quantitation of tha analytical methods , Chronicles of Young Scientist, (2 (1)), 21-25.

Uyanık A. (2012), Analitik Kimyacılar İçin İstatistik ve Kemometri, Pegem Akademi Yayıncılık, 6. Baskı, 254-259.

Uyar, B. (2009). Rosuvastatin kalsiyumun elektrokimyasal Davranışlarının incelenmesi ve farmasötik Preparatlardan miktar tayini, Yüksek Lisans. Hacettepe Üniversitesi Sağlık Bilimleri Enstitüsü, Ankara.

CHAPTER 4

THE EFFECT OF HIGH ELECTRICAL POWER ON THE PHYSICAL STRUCTURE OF GRAPHENE NANOSHEETS PRODUCED BY ANODIC ELECTROCHEMICAL EXFOLIATION PROCESS

Assist. Prof. Dr. Tamer GÜZEL[1]

[1] Niğde Ömer Halisdemir University, Mechatronics Department, NİĞDE
Email: tamerguzel7840@gmail.com, Orcid: **0000-0003-3870-7223**

1.INTRODUCTION

The current century has witnessed unprecedented developments in many fields. One of these areas is the developments in the electronics industry. Especially with the development of nanotechnology, a unique miniaturization process has begun to be experienced in electronic applications. It is also quite clear that when compared to the technological innovations of human beings in other fields, electronics have made much more progress than these fields. From this point of view, this century can be called an electronic century. On the basis of this development, it can be said that the developed electronic materials have a great impact. One of them is the synthesis of materials with atomic-scale thickness, called 2D materials, and their use in applications. The most striking of these materials is graphene. Graphene is an electronic material that has found its place in many fields from energy to electronics with its unique electronic properties (Geim & Novoselov, 2007). Graphene is basically each of the vertically positioned and stacked layers of graphite connected by weak van der Waals forces. Many graphene production methods have been proposed since it was first synthesized (Akbar, Kolahdouz, Larimian, Radfar, & Radamson, 2015). Each of these methods has its own advantages and disadvantages. One of these methods is the production of graphene by electrochemical method, which is environmentally friendly, does not contain toxic gases and is a galvanic application (Fang, Lin, & Hu, 2019). Although this method is low in cost, it has specific usage areas such as supercapacitor, fuel cells, and quantum dots depending on the characteristics of the product produced (Danial et al., 2021). In this method, many inputs of the system determine the quality of graphene. Among them, there are parameters such as the characteristics of the carbon source used in the anode and cathode, the type of ionic solution used as the electrolyte, and the voltage/current applied to the system. Therefore, investigating the effects of these inputs in graphene synthesis still remains a hot topic.

According to the literature, there are many studies on the effect of system parameters on graphene synthesis by electrochemical method. However, very few of these studies include investigating the effect of application inputs such as high voltage/power. When the literature is examined, it has been reported that a voltage of around 10 volts is applied to

produce graphene by electrochemical method. Few of these are on high voltage and power application. Gurzeda et al. designed an experiment for the synthesis of graphene oxide by electrochemical method with a two-stage study. They first investigated the oxidation level of different electrical powers. They reported that high electrical power plays a role in the oxidation of graphene (Gurzęda et al., 2020). Zhou et al. investigated the production of graphene by novel electrochemical exfoliation at the Air-electrolyte interface. For this they applied 30V to the experimental system. As a result, they showed that it is possible to produce high-quality graphene with this method (Zhou, Lu, & Xu, 2019). Ejigu et al. reported that a study was conducted to investigate the antioxidant function of some transition metal salts and to determine their effect on graphene production by electrochemical method. For this, they applied a voltage of 20 volts to the system in which various transition metal salts were present in the electrolyte. They explained that they synthesized high-quality, oxygen-free graphene by inhibiting the oxidation of transition metal ions in graphene (Ejigu et al., 2018). Najafabadi et al. presented a new electrochemical method for making ultrathin graphene from graphite electrodes. For this, they applied a voltage of 20 volts to the experimental system containing an electrolyte containing acetonitrile. They explained that as a result, ultrathin-layer graphene was produced (Najafabadi & Gyenge, 2015).

In this study, graphene nanosheets have been obtained by the electrochemical exfoliation method by applying high electrical power. X-ray diffractometer and Raman spectroscopy were used for the structural investigations of these produced materials. The obtained results were discussed and compared with the literature.

2. EXPERIMENTAL STUDIES

The Experimental setup in Figure 1 was used for the production of graphene by the electrochemical method. A pure graphite rod was used as the anode and a pure platinum was used as the cathode. The anode and the cathode were placed in the liquid electrolyte in such a way that they are 6 cm opposite each other.

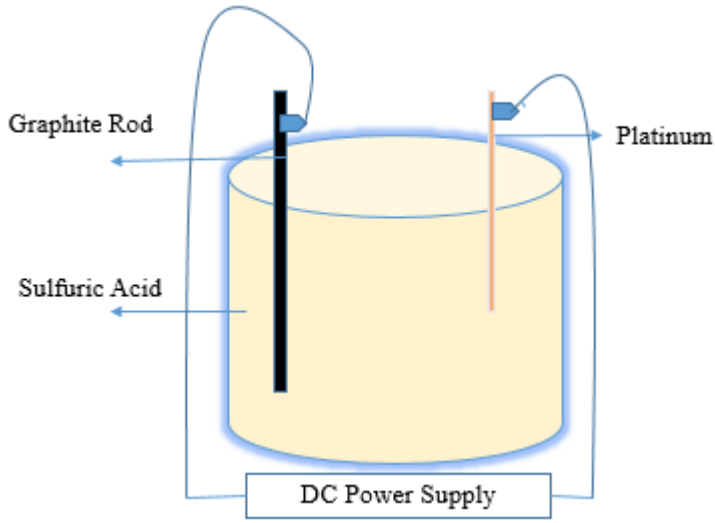

Figure 1. Experimental setup

0,5M H2SO4 solution was used as the liquid electrolyte for the electrochemical process. Then, a current of 20 volts and 1.2 ampere (24 W) was applied to the polars with DC Power Supply. The color of the liquid began to take on a dark color due to the graphene/graphite particles that were exfoliated with the applied voltage. It was determined that some graphitic pieces collapsed to the bottom. The part floating in the electrolyte was collected by the filter and dried in the drying oven at 75° for 6 hours and was ready for characterization. X-ray diffraction patterns of graphite and graphene nano parts were made using a Panalitic empirical X-Ray diffraction device with a monochromatic CuKα laser source (X-ray tube power: 4 kW, tube voltage: 15-60 kV, tube current: 5 - 60 mA). The structural analysis scan was performed at a 5°-60° (2θ) angle with an increase of 0.013°. Raman spectra were obtained with a CCD camera as well as a Reinshow Invia device equipped with a Leica microscope furnished with various lenses, monochromators and filters. A silicon standard sample (520 cm^{-1}) was used as a reference for calibration. Spectra were obtained by stimulating with green laser light (532 nm) with 150 to 3500 cm^{-1}.

3. RESULTS AND DISCUSSION

The X-ray diffractometer (XRD) is used to characterize and investigate the arrangement of atoms in the unit cell, the position of the atoms, and the atom spacing angles due to the comparative wavelength of the x-ray with respect to the atomic size (Pappas, 2006).

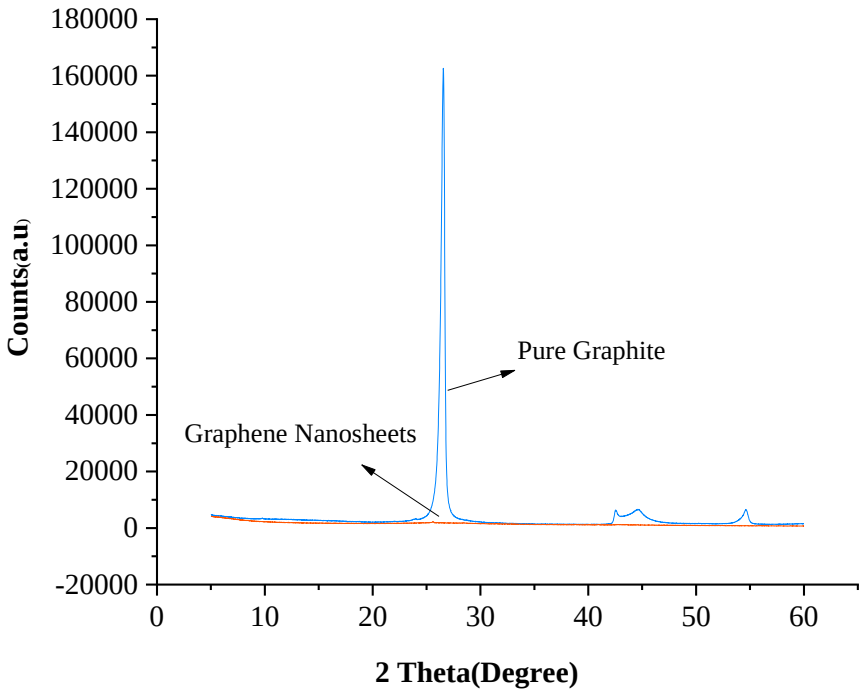

Figure 2. XRD diffraction pattern of graphite and graphene nanosheets

As a non-destructive technique, x-ray diffraction has a wide spectrum of material analysis, from minerals to ceramics, plastics, semiconductors, and solar cells (Guma, Madakson, Yawas, & Aku, 2012). The XRD patterns of the pure graphite used as the anode in the electrochemical process and the material produced are shown in Figure 2. Accordingly, a very sharp and intense peak can be seen at 26.52 degrees in Graphite. This peak corresponds to the 0 0 2 reflection plane corresponding to the characteristic peak of graphite. This indicates that graphite's crystal structure is due to an ordered group of atoms arranged very tightly in a particular direction (Gurzęda et al.,

2020). However, it can be seen that the 0 0 2 reflection plane peak of the material produced together with the 24 W power applied to the anode is considerably reduced relative to the same plane of graphite. This may indicate the effective reduction in the number of layers stacked in a particular direction. To explain this, it is necessary to look at the basis of the XRD technique. According to Figure 2, the Y-axis shows the energy of the photons that the x-ray hits the crystal lattice of the sample and is re-emitted. Therefore, an intense backscattering is measured in the direction of the 0 0 2 plane due to the dense regular atomic structure of the graphite lattice, while it can be seen that this density is considerably reduced in the produced material.

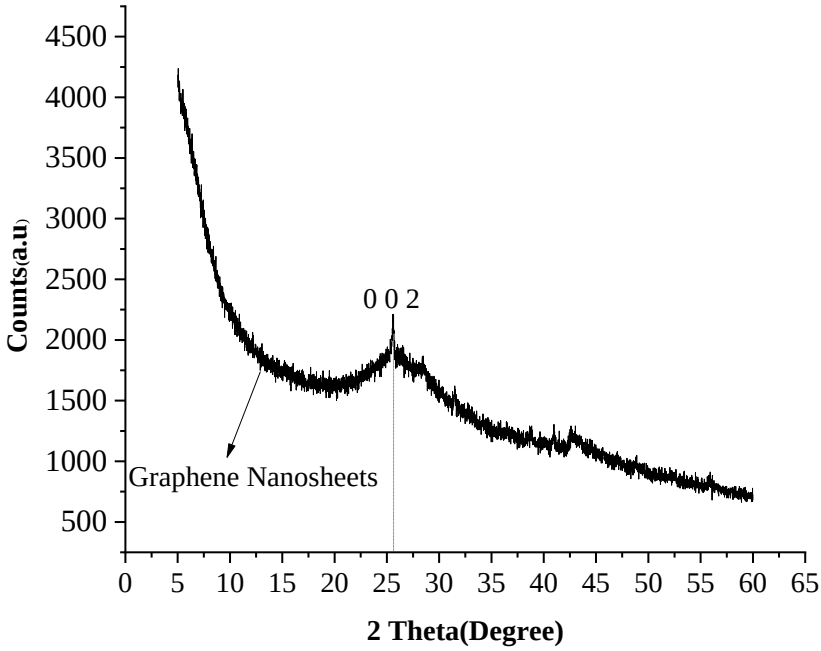

Figure 3. XRD diffraction pattern of graphene nanosheets

It could be said that this indicates a very low layer thickness due to the reduction of regular atomic groups in that direction. However, the presence of the 0 0 2 peaks still indicates the crystalline structure of the material that was broken down as a result of exfoliation. With these two interpretations, it could be said that the produced material turns into graphene

nanosheets. This peak can be seen better in Figure 3. Again, if Figure 3 is examined carefully; It can be observed that the 0 0 2 plane reflection angle of the produced material shifts to lower angles than the graphite reflection angle. This situation can be seen better in Figure 4. Accordingly, the 0 02 plane reflection angle of graphite has shifted from 26.52º to 25.20º. This means that the interlayer spacing, which was calculated as 0.334 nm depending on Bragg's law ($n\lambda = 2dSin\theta$), increased to 0.353 nm in the produced material. The increase in the spacing between the layers is accepted as one of the most important signs of the conversion from graphite to graphene in the literature (Sumari, Roesyadi, & Sumarno, 2013).

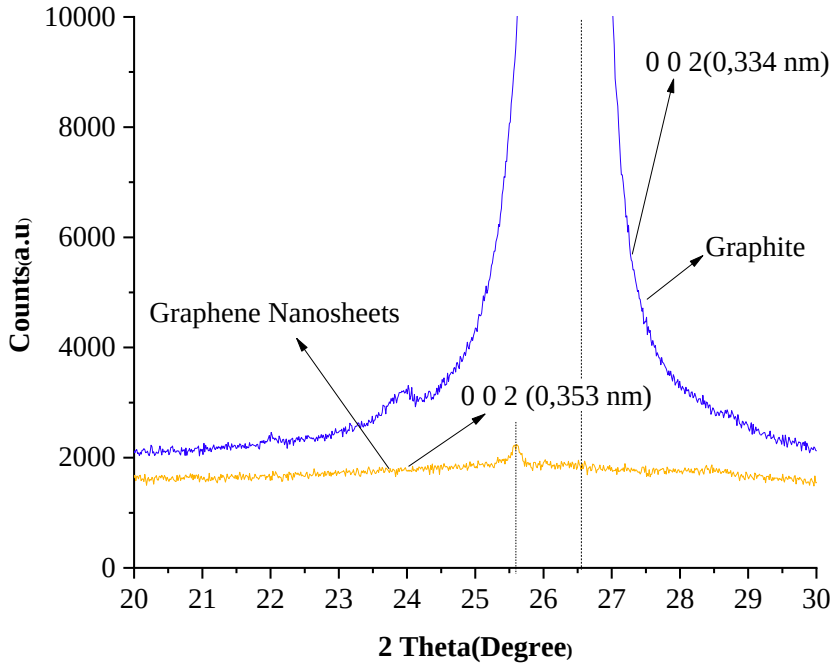

Figure 4. 0 0 2 plane Peaks of graphite and graphene nanosheets

In the literature, Sahoo et al. reported that the 0 0 2 plane peak of the graphene nanosheets was obtained as a result of applying a lower 10 volts to a graphite rod by using 0.5M sulfuric acid electrolytic, shifted by 25.39º (Sahoo & Mallik, 2015). In fact, there are reports in the literature stating that graphene nanosheets are obtained as a result of much lower voltage

applications (Sahoo, Ratha, Rout, & Mallik, 2016). On the other hand, the reason for the increase in the interlayer spacing value may be the decrease in the stress created by the dense atomic structure in the graphite crystal due to the decrease in the number of layers during the exfoliation process. Raman Spectroscopy has a very important place in the structural research of materials consisting of carbon atoms. Carbon-based materials usually have three basic peaks. The peak, which appears around 1350 cm^{-1} and is called the D peak, is sensitive to structural defects. The peak that appears around 1580 cm^{-1} and called the G peak indicates regular atomic structure, while the 2D peak around 2700 cm^{-1} is sensitive only to the layer thickness (Ferrari et al., 2006).

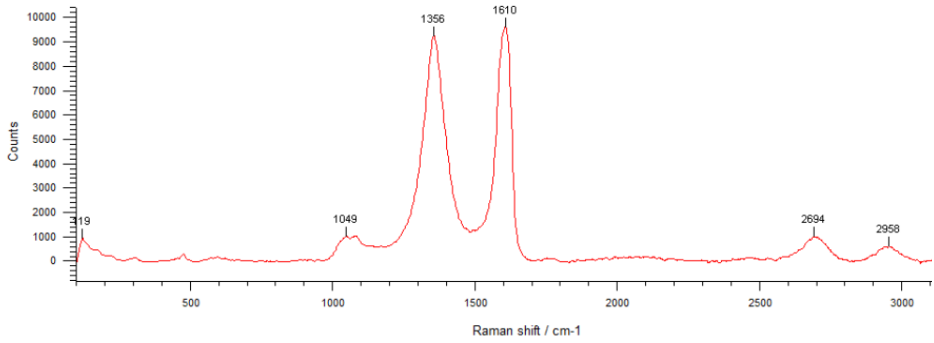

Figure 5. Raman spectrum of graphene nanosheets

The Raman spectrum of the produced material is shown in Figure 5. Accordingly, the peak observed at 1356 cm^{-1} indicates that there is a serious structural defect in the structure. This may be due to the high electrical power applied to the system to produce the graphene nanosheets. This may have caused strong oxidation of the anode. This may have damaged the structure of graphene by molecules containing oxygen entering the structure or leaving the structure for a certain period of time. Sahoo et al., on the other hand, reported that graphene produced at lower voltages (10V) was less damaged in their study under experimental conditions similar to the scope of this study (Sahoo & Mallik, 2015). On the other hand, the G peak observed at 1610 cm^{-1} shows that the productions are still in crystalline form. The 2D peak seen at 2694 cm^{-1} shows a symmetrical appearance, although its intensity is low. In the literature, the number of layers of graphene has been tried to be determined by

many methods, from the location of the 2D peak to its appearance, its density, and its separation into its constituent components. However, although the symmetrical appearance of the 2D peak indicates around 2 or 3 layers, it is necessary to use different characterizations to determine the graphene layer (Ferrari, 2007). Unfortunately, it is very difficult to separate graphite and graphene in the Raman technique (Abdelkader, Cooper, Dryfe, & Kinloch, 2015). The peak at 1049 cm^{-1} is active due to the amorphous structure of the part in graphene, while the peak at 2958cm^{-1} is known as the D+G peak and is active in severe structural disorders (Bico, Tordeux, & Quéré, 2001; Wang, Alsmeyer, & McCreery, 1990**)**. The Raman results show that despite the successful production of graphene, there is too much damage to its structure.

4. CONCLUSION

With the anodic electrochemical exfoliation method, a power such as 24W, which can be considered high according to the literature, was applied to the pure carbon rod placed in the anode, and the structural characterization of the produced material was carried out using x-ray diffraction diffractometer and Raman spectroscopy. While XRD results indicate a crystalline structure and low-layered of material, Raman results confirmed the crystalline structure and showed that the structure was seriously damaged during processing. When both results are evaluated together, it was determined that although high power was successful in opening the layers, it caused structural damage to the product. In addition, it was understood that the produced material was graphene nanosheets containing a serious amount of damaged structure. This shows that a serious optimization (for quality graphene with a lower layer and much less defects) should be carried out, especially for the productions made with this method. Graphene nanosheets produced by these techniques are important electronic materials and are promising in applications such as supercapacitor and fuel cells.

REFERENCES

Abdelkader, A., Cooper, A., Dryfe, R. A., & Kinloch, I. (2015). How to get between the sheets: a review of recent works on the electrochemical exfoliation of graphene materials from bulk graphite. *Nanoscale, 7*(16), 6944-6956.

Akbar, F., Kolahdouz, M., Larimian, S., Radfar, B., & Radamson, H. (2015). Graphene synthesis, characterization and its applications in nanophotonics, nanoelectronics, and nanosensing. *Journal of Materials Science: Materials in Electronics, 26*(7), 4347-4379.

Bico, J., Tordeux, C., & Quéré, D. (2001). Rough wetting. *EPL (Europhysics Letters), 55*(2), 214.

Danial, W. H., Norhisham, N. A., Noorden, A. F. A., Majid, Z. A., Matsumura, K., & Iqbal, A. (2021). A short review on electrochemical exfoliation of graphene and graphene quantum dots. *Carbon Letters*, 1-18.

Ejigu, A., Fujisawa, K., Spencer, B. F., Wang, B., Terrones, M., Kinloch, I. A., & Dryfe, R. A. (2018). On the role of transition metal salts during electrochemical exfoliation of graphite: antioxidants or metal oxide decorators for energy storage applications. *Advanced Functional Materials, 28*(48), 1804357.

Fang, S., Lin, Y., & Hu, Y. H. (2019). Recent advances in green, safe, and fast production of graphene oxide via electrochemical approaches. *ACS Sustainable Chemistry & Engineering, 7*(15), 12671-12681.

Ferrari, A. C. (2007). Raman spectroscopy of graphene and graphite: disorder, electron–phonon coupling, doping and nonadiabatic effects. *Solid State Communications, 143*(1-2), 47-57.

Ferrari, A. C., Meyer, J., Scardaci, V., Casiraghi, C., Lazzeri, M., Mauri, F., . . . Roth, S. (2006). Raman spectrum of graphene and graphene layers. *Physical review letters, 97*(18), 187401.

Geim, A. K., & Novoselov, K. S. (2007). The rise of graphene. *Nat Mater, 6*(3), 183-191. doi:10.1038/nmat1849

Guma, T., Madakson, P., Yawas, D., & Aku, S. (2012). X-ray diffraction analysis of the microscopies of some corrosion-protective bitumen coatings. *Int. J. Mod. Eng. Res, 2*, 4387-4395.

Gurzęda, B., Subrati, A., Florczak, P., Kabacińska, Z., Buchwald, T., Smardz, L., . . . Krawczyk, P. (2020). Two-step synthesis of well-ordered layered graphite oxide with high oxidation degree. *Applied Surface Science, 507*, 145049.

Najafabadi, A. T., & Gyenge, E. (2015). Synergistic production of graphene microsheets by simultaneous anodic and cathodic electro-exfoliation of graphitic electrodes in aprotic ionic liquids. *Carbon, 84*, 449-459.

Pappas, N. (2006). Calculating retained austenite in steel post magnetic processing using X-ray diffraction.

Sahoo, S. K., & Mallik, A. (2015). Simple, fast and cost-effective electrochemical synthesis of few layer graphene nanosheets. *Nano, 10*(02), 1550019.

Sahoo, S. K., Ratha, S., Rout, C. S., & Mallik, A. (2016). Physicochemical properties and supercapacitor behavior of electrochemically synthesized few layered graphene nanosheets. *Journal of Solid State Electrochemistry, 20*(12), 3415-3428.

Sumari, S., Roesyadi, A., & Sumarno, S. (2013). Effects of ultrasound on the morphology, particle size, crystallinity, and crystallite size of cellulose. *Scientific Study & Research. Chemistry & Chemical Engineering, Biotechnology, Food Industry, 14*(4), 229.

Wang, Y., Alsmeyer, D. C., & McCreery, R. L. (1990). Raman spectroscopy of carbon materials: structural basis of observed spectra. *Chemistry of Materials, 2*(5), 557-563.

Zhou, Q., Lu, Y., & Xu, H. (2019). High-yield production of high-quality graphene by novel electrochemical exfoliation at air-electrolyte interface. *Materials Letters, 235*, 153-156.

CHAPTER 5

DYNAMIC NUCLEAR POLARIZATION PARAMETERS OF NITROXIDE RADICAL WITH 4-FLUOROBENZYLAMINE

Dr. Handan ENGİN KIRIMLI[1]

[1] Bursa Uludag University, Faculty of Arts and Sciences, Physics Department, Bursa/Turkey. hengin@uludag.edu.tr ORCID NO: 0000-0003-0300-3381

INTRODUCTION

The Hyperpolarization techniques enable the enhancement of Nuclear Magnetic Resonance NMR signals up to a few orders of magnitude, which will allow the investigation of many processes by NMR that are not currently possible. One of the most important hyperpolarization techniques is Dynamic Nuclear Polarization (DNP). Both the liquid state DNP and solid-state DNP are in a stage of rapid development. DNP is an effective method to obtain great nuclear spin polarization and enhancing the polarization of nuclear spins in the vicinity of unpaired electrons. (Biller, Stupic, & Moreland, 2018; Wenckebach, 2021). During DNP, NMR signals are enhanced by way of a microwave (MW) irradiation induced polarization transfer from the electron spins to the nuclear spins in a specimen (Banerjee, Shimon, Feintuch, Vega & Goldfarb, 2013; Corzilius, 2020).

In 1953, Overhauser was the first to propose this method, using the DNP method for the first time to polarize nuclear spins in metals (Overhauser, 1953; Steiner, Hautle & Wenckebach, 2021; Wenckebach, 2021). It was first developed to study the role of spin in high-energy physics (Niinikoski, 2020) and dipolar ordering of nuclear spins more recently. It later activated enhancements of sensitivity in NMR (Atsarkin & Kockenberger, 2012).

The liquid state Overhauser DNP (ODNP) operation permit target molecules to be hyperpolarized straight in solution (Dai et al., 2021; Overhauser, 1953; Hausser & Stehlik, 1968). While early studies used the conduction electrons of metals, modern studies use stable free radicals such as nitroxide (Ardenkjaer-Larsen et al., 2019).

Lately, DNP has been experiencing steady icrease, including current experimental technique. Therefore, DNP technique may enable new implementations of DNP spanning across materials science, chemistry, medicine and, significantly, structural biology fields (Doll et al., 2012; Biller, Barnes & Hanb, 2018; Franck &Han, 2019; Jaudzems et al., 2019; Keller & Maly, 2021; Nevzorov, Marek, Milikisiyants & Smirnov, 2021; Wenckebach, 2021). Especially it can be used in clinical imaging (Nelson et al., 2008), hyperpolarization (Johansson et al., 2004; Ardenkjaer-Larsen et al., 2019) and particle physics (Goertz, Meyer & Reicherz, 2002; Bunyatova, 2004;).

In many DNP applications, the unpaired electron spins are presented such as paramagnetic radicals (Dai et al., 2021). Nitroxide radicals can be used as a polarizing agent for DNP to enhance NMR signals (Marko, Sojka, Laguta & Neugebauer, 2021; McCoy, Rogawski, Stovicek & McDermott, 2019).

1. MATERIALS AND EQUIPMENT

The stable nitroxide radical as 2,2,6,6-tetramethyl-1-piperidinyloxy (TEMPO) and solvent were purchased from Aldrich Chemical Co. (USA). The CAS number of the TEMPO 2564-83-2. The solvent was 4-fluorobenzylamine (4FBA). The main properties of 4FBA are given in Table 1 and of structural view in Figure 1. The molecular structure of the selected free radical is shown in Figure 2.

Table 1: CAS number of 4-fluorobenzylamine (4FBA) and basic constants.

Solvent	**CAS Number**	**Purity ≥**	**Molecular Weight (g mol^{-1})**	**Boiling Point (°C)**	**Density (g cm^{-3})**	**NMR Sensitivity (x10^{22} spin/cm^{3})**
4-fluorobenzylamine (4FBA) (C_7H_8FN)	140-75-0	% 97	125.15	183	1.095	4.23

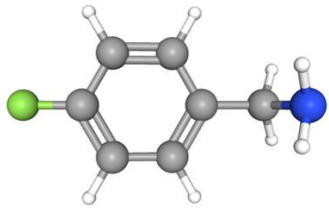

Figure 1: Structural View of 4-fluorobenzylamine (C_7H_8FN) (green color "fluorine"; blue color "nitrogen"; white color "hydrogen" and grey color "carbon").

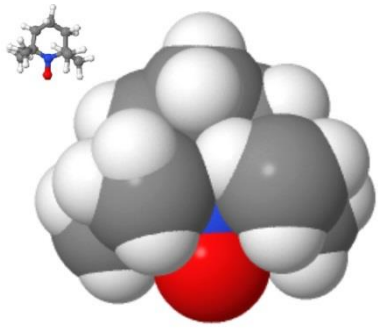

Figure 2: 2,2,6,6-tetramethyl-1-piperidinyloxy (TEMPO) (van der Waals spheres) with nearby structural view of molecule (balls and sticks). Here, red represents oxygen, blue nitrogen, white hydrogen, and grey represents carbon.

TEMPO, fundamental radical, present a well known class of stable nitroxide applied in different areas. A piperidine-based molecule is a commonly used type of nitroxide ring structure (Armstrong, Soto, Shea & Han, 2009). Nitroxides are stable organic radicals with an unpaired electron delocalised between the nitrogen and oxygen atom and they can attached to large macromolecules (Ionita, Madalan, Andrei, Medvedovici & Ionita, 2015).

DNP theory and applications for liquid states are existing in the literature (Kirimli, 2017; Hausser & Stehlik, 1968). DNP measurements were done at 1.53 mT fixed magnetic field NMR spectrometer. The spectrometer is hand-built and has a resonance frequency of 61.2 kHz for protons and 43 MHz for electrons. Details of weak-field double resonance NMR spectrometry have been given in previous articles (Akay & Yalciner, 1995; Kirimli & Peksoz, 2011).

The solutions were prepared as 15, 30 and 60 mM. For each concentration, TEMPO radical was first weighted and dissolved in 4-fluorobenzylamine. The sample volumes were 6.5 cm^3. Then the prepared samples were placed in Pyrex tubes of 18 mm diameter.

The presence of oxygen affects the enhancement factor. Degassing treatment should be performed in order to minimize the interactions with air molecules, to saturate the EPR line easily and to ensure the long life of the sample. Degassing process was performed in Leybold-Heraeus vacuum system at 7.0×10^{-4} Pa pressure value.

2. RESULTS

2.1. EPR spectrum

The EPR spectrum of radical is required to calculate the DNP parameters in a given magnetic field. The EPR spectrum of the TEMPO/4FBA was sighted as a single Gaussian which is created by the superposition of several Lorentzians.

In order to performed DNP measurements and determine DNP parameters, saturation experiments were carried out at 43 MHz, the peak value of a single Gaussian. Figure 3 presents the EPR spectrum of TEMPO in 4FBA solvent at 15 mM concentrations at room temperature. The Gaussian fit function was applied to the empirical points (Figure 3). The fitted Gaussian equation is as follows:

$$y = A\, e^{-(x-\bar{x})^2/2\sigma^2} \quad . \qquad (1)$$

where $y = -(P_{DNP}-P_{TP})/P_{TP}$ is the enhancement factor, x = f (MHz) is the EPR frequency, $\bar{x}$ is the EPR frequency equaled to the peak point of the Gaussian, and σ is the standard deviation. Thermal equilibrium and dynamic polarizations for P_{DNP} and P_{TP} nuclear spins, respectively. The peak value of y is A at $x = \bar{x}$. For all the specimens, the obtained Gaussian parameters for 15 mM concentration the sample are tabulated in Table 2.

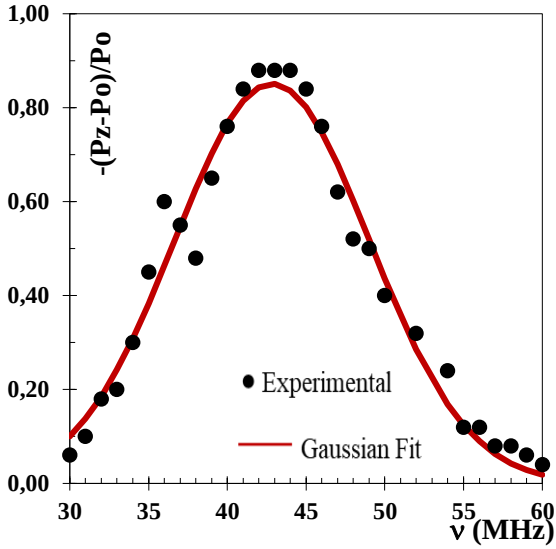

Figure 3: EPR spectrum of the 4-fluorobenzylamine solvent with the nitroxide free radical for 15 mM concentrations at room temperature. It is a single Gaussian curve with a peak frequency of 43 MHz fitted curve.

Table 2: Gaussian parameters obtained for 15 mM concentration of TEMPO/4FBA sample at room temperature.

Samples	***A***	$\bar{x}$	σ	R^2
TEMPO/4-fluorobenzylamine	0.851	42.837	6.202	0.964

2.2 DNP parameters (E_∞, E_{end}, U_∞, ξ, s and K)

The DNP enhancement by OE is given by (Hausser & Stehlik, 1968; Müller-Warmuth & Meise-Gresch, 1983; Franck et al., 2013; Ravera, Luchinat & Parigi, 2016; Gizatullin, Mattea & Stapf, 2019)

$$E = \frac{P_{DNP}}{P_{TP}} = 1 - \xi f s \left|\frac{\gamma_e}{\gamma_n}\right| \qquad (2)$$

where, γ_e and γ_n, are the gyromagnetic ratios of the electron and nuclear spins (for ^1H; $|\gamma_e/\gamma_n| = 658$), respectively. The three parameters ξ, f and s in the right-hand side of Equation (2) are the coupling, leakage and saturation factors, respectively. When saturation of electron levels is at full the leakage factor f, saturation factor s, becomes equal to 1. That is, the saturation factor s defines the efficiency of MW radiation. A positive

enhancement is referred to the scalar interaction displacement with a maximum value of ξ = -1, while the dipolar coupling limit approaches ξ = 0.5 with a corresponding negative net increase. The ξ values obtained vary between the limit values of +0.5 and -1. However, in real systems both additives may be present (Gizatullin, Mattea & Stapf, 2019).

The enhancement factor for infinite EPR power when saturation is performed is present as:

$$\left(\frac{P_{DNP}-P_{TP}}{P_{TP}}\right)_{s\to 1}^{-1} = -\left(\xi f \left|\frac{\gamma_e}{\gamma_n}\right|\right)^{-1} = E_\infty^{-1}, \qquad (3)$$

and thus the ultimate enhancement factor for infinite concentration

$$(E_\infty^{-1})_{f\to 1, c\to\infty} \to \left(-\xi \left|\frac{\gamma_e}{\gamma_n}\right|\right)^{-1} = U_\infty^{-1} \qquad (4)$$

is obtained. As $|\gamma_S/\gamma_I|$=+658 for proton, ξ determines the nuclear-electron interaction and given as

$$\xi = -\frac{U_\infty}{658}. \qquad (5)$$

K is the parameter for the relative importance of scalar coupling. Since ξ is an experimentally obtainable, the parameter K can be easily calculated.

$$K = \frac{1-2\,\xi}{1+\,\xi} \qquad (6)$$

DNP studies are based on pure and double resonance NMR signal intensities (P_{TP} and P_{DNP}). As seen in Figure 4, the signals are taken as the derivative of the central band. P_{TP} was measured four times for each sample and P_{DNP} values were obtained from six various EPR powers to saturate the ESR. P_{TP} and P_{DNP} values are calculated by taking the peak-to-peak values of the derivative curve of the central band of each signal. Figure 4 shows an example of DNP experiment performed on 4FBA. A concentration of 60 mM was created by doping 4FBA with the stable radical TEMPO. The spectra were obtained in a field of 1.53 mT, with and without DNP. The irradiation EPR voltage has 90 V amplitude and 43 MHz frequency. P_{TP}, pure ^{1}H-DNP signal (Figure 4a) and P_{DNP} double resonance ^{1}H-DNP sinyal (Figure 4b) were

holded at the room temperature. A signal enhancement of approximately four times was observed.

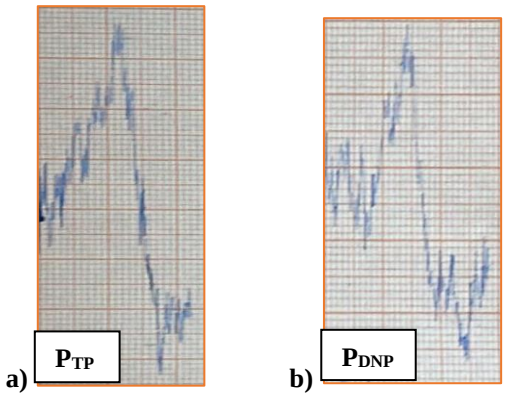

Figure 4: ^{1}H NMR signal of TEMPO/4FBA solution (a) P_{TP}, Pure NMR signal (without DNP); EPR voltage: 0 (EPR power is off.) (b) P_{DNP}, enhanced NMR signal (with DNP); EPR voltage: 90 V (EPR power is on)

For each sample, E_{∞} values were determined by extrapolating from the optimal fit lines drawn by obtaining the inverse of the enhancement factors. As well inverse of the enhancement factors are as a function of the inverse of the square of the high frequency voltage, which is scaled to the inverse of the ESR power.

E_{∞}^{-1} values correspond to the crossing points of the extrapolated fit lines passing through the experimentally obtained points with the $V_{eff}^{-2}=0$ line (Figure 5). When the ESR power is taken to infinity, it is in a state of full saturation. Here V_{eff} represents the high frequency voltage across the ESR coil.

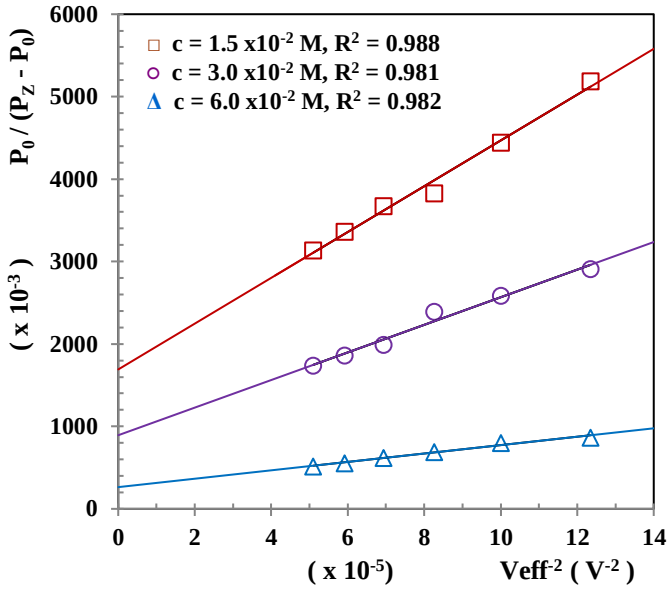

Figure 5: Obtaining E_∞ in solutions of TEMPO with a concentration of 15, 30 and 60 mM in 4-fluorobenzylamine solvent medium. R^2 values show the degree of agreement of the linear fit line and the experiment points.

The U_∞^{-1} value correspond to the crossing points of the $c^{-1} = 0$ line and the extrapolated best-fit lines (Figure 6). After the determination U_∞, ξ value calculated from Equation (5) and K value can be found by Equation (6). The DNP parameters obtained for the TEMPO/4FBA sample, E_∞, E_{end}, ξ, s (E_{end}/ E_∞), K are presented in Table 3. As seen in Table 3, the E_∞ values vary between 0.59 and 3.79. ESR saturation experiments were performed at an average value of 52 %. We calculated the ξ value of our sample as 0.012, which shows us that the interaction is dipolar.

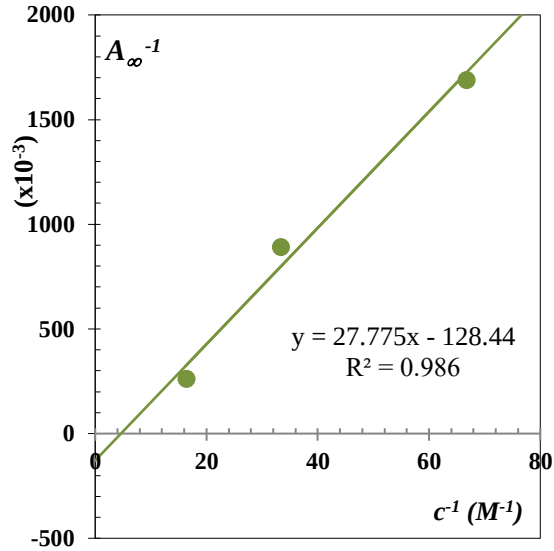

Figure 6: For TEMPO/4-Fluorobenzylamine, it is seen that the U_∞, the ultimate enhancement factor for infinite concentration.

Table 3. DNP parameters for TEMPO/4-fluorobenzylamine solutions.

	c (mM)	E_∞	E_{end}	$-U_\infty$	ξ	s	K
TEMPO/ 4-fluorobenzylamine	15	0.59	0.32			0.542	
	30	1.12	0.57	7.79	0.012	0.509	0.965
	60	3.79	1.94			0.512	

In the literature, we see that ^{1}H-DNP studies for nitroxides and protons in liquids such as acetone (Küçük, Neugebauer, Prisner & Sezer, 2015), toluene (Sezer, 2013) and water (Nicholson, Lurie & Robb, 1994) are also the dipolar interaction dominates (Keller, Laut, Sirigiri & Maly, 2020; Prisner, Denysenkov & Sezer, 2016). ξ values were positive in the DNP studies of TEMPO in acetic acid and in hydroxyl done by Müller-Warmuth et al., (Müller-Warmuth, Öztekin, Vilhjalmsson & Yalciner, 1970). In a similar study, Frank et al. (Franck, Pavlova, Scott & Han, 2013) calculated the ξ to be 0.27 for TEMPO in water at room temperature. In addition, DNP enhancements in solutions such as water, toluene and chloroform with

different nitroxide polarizers were investigated by Höfer et al. (Höfer et al., 2008) and Leiven et al. (Levien, Hiller, Tkach, Bennati & Orlando, 2020).

In 4-fluorobenzylamine, -NH2 and -F are attached to the aromatic ring. The most reactive element is fluorine. Interestingly, an amine group (-NH2) strongly increases the reactivity of the aromatic ring to which it is attached, due to its electron donor property. In the end, the reason why we couldn't get a larger ξ value might be the reactivity of the 4FBA solvent.

CONCLUSIONS

In recent years, Dynamic nuclear polarization (DNP) has recently become one of the base research areas in magnetic resonance spectroscopy. In this study we have reviewed ^{1}H-DNP experiments were carried out to investigate solutions of TEMPO free radical in 4-fluorobenzylamine (4FBA) solvent at 1.53 mT. We observed a single Gaussian peak in TEMPO's EPR spectrum at 43 MHz. ODNP studies in liquid state and results obtained have been briefly summarized throughout this chapter

The unpaired electron spin density is usually localized in a NO-group in free radical molecules. In such a situation, DNP studies present a new and efficient process of obtaining information on the formation of different solvent complexes. The ξ value ranges from -1 to +0.5, depending on the type of interaction. That is, it varies from -1 in the pure scalar state to +0.5 in the pure dipolar state. The results of our studies and the calculated DNP parameters between the nuclear spin and the electron spin, indicate dipolar interactions occur for TEMPO/4FBA samples. Especially the coupling parameter ξ gives information about interactions and depends on the dynamics of the electron–nuclear spin system and supports the investigation of the effects of molecular dynamics on the DNP enhancement. This conclusion is also supported by the parameter K. TEMPO radicals appear to be a good polarizing agent for ^{1}HDNP studies and will remain popular for applications in other research branches in the future.

REFERENCES

Akay, C., Yalciner, A. (1995). Anew weak field double resonance NMR spectrometer. Z. Naturforsch, (50 a): 177-185.

Ardenkjaer-Larsen, J.H., Bowen, S., Petersen, J.R., Rybalko, O., Vinding, M.S., Ullisch, M., Nielsen, N.C. (2019). Cryogen-free dissolution dynamic nuclear polarization polarizer operating at 3.35 T, 6.70 T, and 10.1 T. Magnetic Resonance in Medicine, 81, 2184-2194.

Armstrong, B.D., Soto, P., Shea, J-E., Han, S. (2009). Overhauser dynamic nuclear polarization and molecular dynamics simulations using pyrroline and piperidine ring nitroxide radicals. Journal of Magnetic Resonance, 200, 137–141.

Atsarkin, A.V., Kockenberger, W. (2012). The different magnetic resonance communities join forces for progress in DNP. Applied Magnetic Resonance, 43, 1–2.

Banerjee, D., Shimon, D., Feintuch, A., Vega, S., Goldfarb, D. (2013). The interplay between the solid effect and the cross effect mechanisms in solid state ^{13}C DNP at 95 GHz using trityl radicals. Journal of Magnetic Resonance, 230, 212-219.

Biller, J.R., Stupic, K.F., Moreland, J. (2018). A table-top PXI based low-field spectrometer for solution dynamic nuclear polarization. Magnetic Resonance Chemistry. 56,153–163.

Biller, J.R., Barnes, R., Hanb, S, (2018). Perspective of Overhauser Dynamic Nuclear Polarization for the Study of Soft Materials. Current Opinion in Colloid and Interface Science, 33, 72-85.

Bunyatova, E.I. (2004). Free radicals and polarized targets. Nuclear Instruments and Methods in Physics Research A, 526, 22-27.

Corzilius, B. (2020). High-field dynamic nuclear polarization. Annual Review of Physical Chemistry, 71, 143–170.

Dai, D., Wang, X., Liu, Y., Yang, X-L., Glaubitz, C., Denysenkov, V., He, V., Prisner, T., Mao, J. (2021). Room-temperature dynamic nuclear polarization enhanced NMR spectroscopy of small biological molecules in water. Nature Communications, 12, 6880.

Doll, A., Bordignon, E., Joseph, B., Tschaggelar, R., Jeschke, G. (2012). Liquid state DNP for water accessibility measurements on spin-

labeled membrane proteins at physiological temperatures. Journal of Magnetic Resonance, 222, 34–43.

Franck, J.M., Han, S. (2019). Overhauser Dynamic Nuclear Polarization for the Study of Hydration Dynamics. Methods in Enzymology, Elsevier No: 615, pp. 131-175, Cambridge-United States.

Franck, J. M.; Pavlova, A.; Scott, J. A.; Han, S. (2013). Quantitative cw Overhauser effect dynamic nuclear polarization for the analysis of local water dynamics. Progress in Nuclear Magnetic Resonance Spectroscopy, 74, 33−56.

Gizatullin, B., Mattea, C., Stapf, S. (2019). X-nuclei hyperpolarization for studying molecular dynamics by DNP-FFC. Journal of Magnetic Resonance, 307, 106583.

Goertz, S., Meye,r W., Reicherz, G. (2002). Polarized H, D and ^{3}He Targets for Particle Physics Experiments. Progress in Particle and Nuclear Physics, 49, 403-489.

Hausser, K.H., Stehlik, D. (1968). Dynamic Nuclear Polarization in Liquids. Advances in Magnetic and Optical Resonance, 3, 79-139.

Höfer, P., Parigi, G., Luchinat, C., Carl, P., Guthausen, G., Reese, M., Carlomagno, T., Griesinger, C., Bennati, M., (2008). Field dependent dynamic nuclear polarization with radicals in aqueous solution. Journal of the American Chemical Society, 130, 3254.

Ionita, G., Madalan, A.M., Ariciu, A.M., Medvedovici, A., Ionita, P. (2015). Synthesis of novel TEMPO stable free (poly)radical derivatives and their host–guest interaction with cucurbit[6]uril. New Journal Chemistry, DOI: 10.1039/c5nj01518a.

Jaudzems, K., Polenova, T., Pintacuda, G., Oschkinat, H., Lesage, A. (2019). DNP NMR of biomolecular assemblies. Journal of Structural Biology, 206, 90-98.

Johansson, E., Mansson, S., Wirestam, R., Petersson, J., Golman, K., Stahlberg, F. (2004). Cerebral Perfusion Assessment by Bolus Tracking Using Hyperpolarized ^{13}C. Magnetic Resonance in Medicine, 51 (3), 464- 472.

Keller, T.J., Laut, A.J., Sirigiri, J., Maly, T. (2020). High-resolution Overhauser dynamic nuclear polarization enhanced proton NMR

spectroscopy at low magnetic fields. Journal of Magnetic Resonance, 313, 106719.

Keller, T.J., Maly, T. (2021). Overhauser Dynamic Nuclear Polarization Enhanced Two-Dimensional Proton NMR Spectroscopy at Low Magnetic Fields. Magnetic Resonance, 2 (1), 117–128.

Kirimli, H.E. (2017). Determining the interaction and characterization of asphaltene in alkylbenzene solvents using nuclear-electron double resonance. Journal of Dispersion Science and Technology, 38(4), 498–505.

Kirimli, H.E., Peksoz, A. (2011). A low field proton-electron double resonance study for paramagnetic solutions. Molecular Physics, 109 (3), 337-350.

Küçük, S.E., Neugebauer, P., Prisner, T.F., Sezer, D. (2015). Molecular simulations for dynamic nuclear polarization in liquids: a case study of TEMPOL in acetone and DMSO. Physical Chemistry Chemical Physics, 17, 6618–6628.

Levien, M., Hiller, M., Tkach, I., Bennati, M., Orlando, T. (2020). Nitroxide Derivatives for Dynamic Nuclear Polarization in Liquids: The Role of Rotational Diffusion. Journal of Physical Chemistry Letters, 11, 1629-1635.

Marko, A., Sojka, A., Laguta, O., Neugebauer, P. (2021). Simulation of nitrogen nuclear spin magnetization of liquid solved nitroxides. Physical Chemistry Chemical Physics, 23, 17310–17322.

McCoy, K.M., Rogawski, R., Stovicek, O., McDermott, A.E. (2019). Stability of nitroxide biradical TOTAPOL in biological sample. Journal of Magnetic Resonance, 303, 115–120.

Müller-Warmuth W, Öztekin E, Vilhjalmsson R, Yalciner A, 1970. Dynamic Polarization, Molecular Motion and Solvent Effects in Several Organic Solutions as Studied by Proton-Electron Double Resonance. Z. Naturforsch, (25 a), 1688-1695.

Müller-Warmuth, W., Meise-Gresch, K. (1983). Molecular Motions and Interactions as Studied by Dynamic Nuclear Polarization (DNP) in Free Radical Solutions. Advances in Magnetic and Optical Resonance, 11, 1-45.

Nelson, S.J., Vigneron, D., Kurhanewicz, J., Chen, A., Bok, R., Hurd, R. (2008). DNP-Hyperpolarized ^{13}C magnetic resonance metabolic imaging for cancer applications. Applied Magnetic Resonance, 34 (3-4), 533-544.

Nevzorov, A.A., Marek, A., Milikisiyants, S., Smirnov, A.I. (2021). Characterization of photonic band resonators for DNP NMR of thin film samples at 7 T magnetic field. Journal of Magnetic Resonance, 323, 106893.

Nicholson, I., Lurie, D.J., Robb, F.J.L. (1994). The Application of Proton-Electron Double-Resonance Imaging Techniques to Proton Mobility Studies. Journal of Magnetic Resonance, 104: 3, 250-255.

Niinikoski, T.O. (2020). The Physics of Polarized Targets. Cambridge University Press, Cambridge.

Overhauser, A.W. (1953). Polarization of nuclei in metals. Physical Review, 92(2), 411–415.

Prisner, T., Denysenkov, V., Sezer, D. (2016). Liquid state DNP at high magnetic fields: Instrumentation, experimental results and atomistic modelling by molecular dynamics simulations. Journal of Magnetic Resonance, 264, 68-77.

Ravera, E., Luchinat, C., Parigi, G. (2016). Basic facts and perspectives of Overhauser DNP. Journal of Magnetic Resonance, 264, 78–87.

Sezer, D. (2013). Computation of DNP coupling factors of a nitroxide radical in toluene: seamless combination of MD simulations and analytical calculations, Physical Chemistry Chemical Physics, 15, 526–540.

Steiner, J.M., Hautle, P., Wenckebach, W.T. (2021). Relaxation of nuclear dipolar energy. Journal of Magnetic Resonance, 333, 107099.

Wenckebach. W.Th. (2021). Electron Spin–Spin Interactions in DNP: Thermal Mixing vs. the Cross Effect. Applied Magnetic Resonance, DOI: 10.1007/s00723-021-01335-0.

CHAPTER 6

VAJDA THEOREMS OF JACOBSTHAL AND JACOBSTHAL-LUCAS OCTONIONS

Assist. Prof. Dr. Ümit TOKEŞER[1]

[1] Kastamonu University, Faculty of Science and Arts, Department of Mathematics, Kastamonu, Turkey. E-mail : utokeser@kastamonu.edu.tr, ORCID ID : https://orcid.org/0000-0003-4773-8291

INTRODUCTION

Quaternions and octonions were first defined by Sir William R. Hamilton in 1843 and Cayley Dickson in 1845. After these definitions, many authors have studied the types of quaternions and octonions. Akyiğit et. al. (Akyiğit.2013, Akyiğit.2014) gave split Fibonacci quaternions and generalized Fibonacci quaternions, Kecilioglu and Akkus (Keçilioğlu.2015, Akkus.2015) also gave Fibonacci octonions and split Fibonacci and Lucas octonions with their Binet's formulas. Halici (Halici.2015) worked on dual Fibonacci octonions and obtained the Binet's formula with their generator function. Bilgici at. al. introduced generalized Fibonacci and Lucas octonions and gave many identities related to them (Bilgici.2018).

Horadam (Horadam.1963) introduced Fibonacci and Lucas quaternions as follows;

$$Q_n = F_n + F_{n+1}e_1 + F_{n+2}e_2 + F_{n+3}e_3$$

and

$$P_n = L_n + L_{n+1}e_1 + L_{n+2}e_2 + L_{n+3}e_3$$

where F_n and L_n are n-th Fibonacci and n-th Lucas numbers, respectively.

Akkus and Kecilioglu (Keçilioğlu.2015) also defined Fibonacci and Lucas octonions as follows;

$$Q_n = \sum_{s=0}^{7} F_{n+s}e_s$$

and

$$T_n = \sum_{s=0}^{7} L_{n+s}e_s$$

where F_n is the n-th Fibonacci and L_n is the n-th Lucas numbers.

The octonions constitute the largest normed division algebra over the real numbers and it is shown with the letter O. The octonions have eight dimensions and they are alternative, flexible, power-associative, non-commutative and non-associative. If we take $a = b = c = 1$ in the generalized

octonion multiplication table in (Bilgici.2018), we get the following octonion table.

Table 1: Multiplication Table of Octonions

•	e_0	e_1	e_2	e_3	e_4	e_5	e_6	e_7
e_0	e_0	e_1	e_2	e_3	e_4	e_5	e_6	e_7
e_1	e_1	-1	e_3	$-e_2$	e_5	$-e_4$	$-e_7$	e_6
e_2	e_2	$-e_3$	-1	e_1	e_6	e_7	$-e_4$	$-e_5$
e_3	e_3	e_2	$-e_1$	-1	e_7	$-e_6$	e_5	$-e_4$
e_4	e_4	$-e_5$	$-e_6$	$-e_7$	-1	e_1	e_2	e_3
e_5	e_5	e_4	$-e_7$	e_6	$-e_1$	-1	$-e_3$	e_2
e_6	e_6	e_7	e_4	$-e_5$	$-e_2$	e_3	-1	$-e_1$
e_7	e_7	$-e_6$	e_5	e_4	$-e_3$	$-e_2$	e_1	-1

Many researchers studied on generalizations of Fibonacci and Lucas quaternions and octonions (Flaut.2013, Halici.2012, Iakin.1977, Swamy.1973, Savin.2015).

Szynal-Liana and Wloch (Szynal-Liana.2016) defined JQ_n Jacobsthal and JLQ_n Jacobsthal-Lucas quaternions and gave them as follows, respectively;

$$JQ_n = J_n + J_{n+1}e_1 + J_{n+2}e_2 + J_{n+3}e_3$$

and

$$JLQ_n = j_n + j_{n+1}e_1 + j_{n+2}e_2 + j_{n+3}e_3$$

where $\{e_0 \cong 1, e_1 \cong i, e_2 \cong j, e_3 \cong k\}$ is a basis of 4-dimensional IR vector space, J_n is the *n*-th Jacobsthal and j_n is the *n*-th Jacobsthal-Lucas numbers.

Aydin and Yüce (Aydin.2017) gave many properties of Jacobsthal quaternions with a new approach and obtained Binet's formulas and Cassini's identities for these quaternions. Also, Aydin (Aydin.2018) investigated generalized Jacobsthal, complex Jacobsthal and dual Jacobsthal sequences

using Jacobsthal numbers. Yasarsoy (Yasarsoy.2018) derived new and interesting properties for the Jacobsthal quaternion and Jacobsthal-Lucas quaternion and for these octonions. In addition, they introduced *k*-Jacobsthal and *k*-Jacobsthal-Lucas octonions. Tasci (Tasci.2017) generalized Jacobsthal and Jacobsthal-Lucas quaternions to *k*-Jacobsthal and *k*-Jacobsthal-Lucas quaternions.

Cimen and İpek (Cimen.2017) defined Jacobsthal and Jacobsthal-Lucas octonions with J_n and j_n are *n*-th Jacobsthal and *n*-th Jacobsthal-Lucas numbers, respectively, as follows;

$$\hat{J}_n = \sum_{s=0}^{7} J_{n+s} e_s$$

and

$$\hat{j}_n = \sum_{s=0}^{7} j_{n+s} e_s \,.$$

They also gave conjugate, norm, some basic identities and Binet formulas for these octonions.

In this paper, based on works of Horadam, Kecilioglu and Akkus, Bilgici at. al., and Cimen and İpek, we study the Jacobsthal and Jacobsthal-Lucas octonions over the algebra $\mathrm{O}(a,b,c)$. Furthermore, we give Catalan's identitiy, Cassini's identity, d'Ocagne's identity, some properties and Vajda theorems for Jacobsthal and Jacobsthal-Lucas octonions.

1. BINET FORMULAS FOR JACOBSTHAL AND JACOBSTHAL-LUCAS OCTONIONS

In this part, we give Binet formulas for the *n*-th Jacobsthal octonion JO_n and the *n*-th Jacobsthal-Lucas octonion JLO_n. We obtain Catalan's, Cassini's and d'Ocagne's identities for Jacobsthal and Jacobsthal-Lucas octonions using the Binet formulas.

Theorem 1. Let $n \geq 0$ be integer, *n*-th Jacobsthal octonion is

$$JO_n = \frac{\gamma'\gamma^n - \delta'\delta^n}{\gamma - \delta} \tag{1}$$

and *n*-th Jacobsthal-Lucas octonion is

$$JLO_n = \gamma'\gamma^n + \delta'\delta^n \tag{2}$$

where $\gamma = 2,\ \delta = -1, \gamma' = \sum_{s=0}^{7} \gamma^s e_s$ and $\delta' = \sum_{s=0}^{7} \delta^s e_s$.

Proof. The *n*-th Jacobsthal octonion JO_n is

$$JO_n = \sum_{s=0}^{7} J_{n+s} e_s \tag{3}$$

and the *n*-th Jacobsthal-Lucas octonion JLO_n is

$$JLO_n = \sum_{s=0}^{7} JL_{n+s} e_s \tag{4}$$

where J_n is the *n*-th Jacobsthal number and JL_n is the *n*-th Jacobsthal-Lucas number. Considering the following for equation (3)

$$\gamma JO_n + JO_{n-1} = \sum_{s=0}^{7} \left(\gamma J_{n+s} + J_{n+s-1}\right) e_s .$$

With the help of the identity $\gamma^n = \gamma J_n + J_{n-1}$, we get

$$\gamma JO_n + JO_{n-1} = \gamma'\gamma^n . \tag{5}$$

Similarly, using the identity $\delta^n = \delta J_n + J_{n-1}$, we have

$$\delta JO_n + JO_{n-1} = \delta'\delta^n . \tag{6}$$

From the equations (5) and (6)

$$JO_n = \frac{\gamma'\gamma^n - \delta'\delta^n}{\gamma - \delta}$$

is obtained. By using similar method, we get equation (2).

Now we give some useful identities that we require and play very important roles in this paper for calculations.

Lemma 2. We have following

$$\gamma'^2 = \zeta_1 + JLO_0 + 3\left(\zeta_2 + JO_0\right), \tag{7}$$

$$\delta'^2 = \zeta_1 + JLO_0 - 3\left(\zeta_2 + JO_0\right), \tag{8}$$

$$\gamma'\delta' = 85 + JLO_0 + 6\kappa, \tag{9}$$

$$\delta'\gamma' = 85 + JLO_0 - 6\kappa \tag{10}$$

where

$\zeta_1 = -\frac{21853}{2},$

$\zeta_2 = -\frac{7277}{2},$

$\kappa = 22e_1 + 7e_2 - 39e_3 - 15e_4 + 37e_5 + 15e_6 - 13e_7.$

Proof. Using the multiplication table for the basis of $\mathrm{O}(a,b,c)$ and when we take $a = b = c = 1$ in the generalized octonion multiplication table in (Bilgici.2018), we get

$$\gamma'^2 = \left(\sum_{s=0}^{7} \gamma^s e_s\right)\left(\sum_{s=0}^{7} \gamma^s e_s\right)$$

$$= -1 - \frac{5}{2}a - \frac{17}{2}b - \frac{65}{2}ab - \frac{257}{2}c - \frac{1025}{2}ac - \frac{4097}{2}bc - \frac{16385}{2}abc$$
$$+ JLO_0 + 3\left(\frac{1}{2}a - \frac{5}{2}b - \frac{21}{2}ab - \frac{85}{2}c - \frac{341}{2}ac - \frac{1365}{2}bc - \frac{5461}{2}abc\right.$$
$$\left. + JO_0\right)$$
$$= \zeta_1 + JLO_0 + 3\left(\zeta_2 + JO_0\right)$$

and similarly

$$\gamma'\delta' = \left(\sum_{s=0}^{7}\gamma^s e_s\right)\left(\sum_{s=0}^{7}\delta^s e_s\right)$$
$$= 128abc + 8ab + 32ac - 64c + 2a - 4b - 16c - 1 + JLO_0$$
$$+ 6\left[2\left(16bc - b - 4c\right)e_1 + \left(16ac - a - 8c\right)e_2 - 39ce_3\right.$$
$$\left. + 5\left(-4ab - a + 2b\right)e_4 + 37be_5 + 15ae_6 - 13abce_7\right]$$
$$= 85 + JLO_0 + 6\kappa$$

are obtained. The others can be proved similary.

Now, in the following theorem, we give Catalan's identities for these octonions.

Theorem 3. For every integers *n* and *r*, we have

$$JO_{n+r}JO_{n-r} - JO_n^2 = -\left(-2\right)^{n-r}\left[\frac{1}{9}\left(85 + JLO_0\right)\left(JL_{2r} - 2\left(-2\right)^r\right) + 2\kappa J_{2r}\right]$$

and

$$JLO_{n+r}JLO_{n-r} - JLO_n^2 = \left(-2\right)^{n-r}\left[\left(85 + JLO_0\right)\left(JL_{2r} - 2\left(-2\right)^r\right) + 18\kappa J_{2r}\right].$$

Proof. By using the Binet's formula for the Jacobsthal octonion, we get

$$JO_{n+r}JO_{n-r} - JO_n^2 = \frac{1}{9}\left[\left(\gamma'\gamma^{n+r} - \delta'\delta^{n+r}\right)\left(\gamma'\gamma^{n-r} - \delta'\delta^{n-r}\right) - \left(\gamma'\gamma^n - \delta'\delta^n\right)^2\right]$$

$$= \frac{1}{9}\left[-\gamma'\delta'\gamma^{n+r}\delta^{n-r} - \delta'\gamma'\delta^{n+r}\gamma^{n-r} + \gamma'\delta'\gamma^n\delta^n + \delta'\gamma'\delta^n\gamma^n\right]$$

$$= \frac{1}{9}\left[-\gamma^{n-r}\delta^{n-r}\left(\gamma'\delta'\gamma^{2r} + \delta'\gamma'\delta^{2r}\right) + 2(-2)^n\left(85 + JLO_0\right)\right]$$

$$= \frac{1}{9}\left[-(-2)^{n-r}\left(\left(85 + JLO_0\right)\left(\gamma^{2r} + \delta^{2r}\right) + 6\kappa\left(\gamma^{2r} - \delta^{2r}\right)\right)\right.$$

$$\left. +2(-2)^n\left(85 + JLO_0\right)\right]$$

$$= -(-2)^{n-r}\left[\frac{1}{9}\left(85 + JLO_0\right)\left(JL_{2r} - 2(-2)^r\right) + 2\kappa J_{2r}\right].$$

The second identity can be obtained similarly.

For $r = 1$ in Catalan's identities give Cassini's identities for these octonions which are in the following.

Corollary 4. For every integer *n*, we have

$$JO_{n+1}JO_{n-1} - JO_n^2 = -(-2)^{n-1}\left[85 + JLO_0 + 2\kappa\right]$$

and

$$JLO_{n+1}JLO_{n-1} - JLO_n^2 = (-2)^{n-1}\left[9\left(85 + JLO_0\right) + 18\kappa\right].$$

In the next theorem, we present d'Ocagne's identities for Jacobsthal and Jacobsthal-Lucas octonions.

Theorem 5. For every integers *n* and *m*, we have

$$JO_{m+1}JO_n - JO_mJO_{n+1} = (-2)^m\left[\left(85 + JLO_0\right)J_{n-m} - 2\kappa JL_{n-m}\right]$$

and

$$JLO_{m+1}JLO_n - JLO_mJLO_{n+1} = (-2)^m\left[-9\left(85 + JLO_0\right)J_{n-m} + 18\kappa JL_{n-m}\right].$$

Proof. Using the Binet's formula for Jacobsthal octonion, we obtain

$$JO_{m+1}JO_n - JO_mJO_{n+1} = \frac{1}{9}\Big[\left(\gamma'\gamma^{m+1} - \delta'\delta^{m+1}\right)\left(\gamma'\gamma^n - \delta'\delta^n\right) - \left(\gamma'\gamma^m - \delta'\delta^m\right)\left(\gamma'\gamma^{n+1} - \delta'\delta^{n+1}\right)\Big]$$

$$= \frac{1}{3}(-2)^m\left(\delta'\gamma'\gamma^{n-m} - \gamma'\delta'\delta^{n-m}\right)$$

$$= \frac{1}{3}(-2)^m\left[3\left(85 + JLO_0\right)J_{n-m} - 6\kappa JL_{n-m}\right]$$

$$= (-2)^m\left[\left(85 + JLO_0\right)J_{n-m} - 2\kappa JL_{n-m}\right].$$

Jacobsthal-Lucas octonion can be done similarly.

2. SOME PROPERTIES FOR JACOBSTHAL AND JACOBSTHAL-LUCAS OCTONIONS

In this part, after deriving Catalan's, Cassini's and d'Ocagne's identities, we present other identities and Vajda theorems for Jacobsthal and Jacobsthal-Lucas octonions.

Theorem 6. Jacobsthal and Jacobsthal-Lucas octonions satisfy the following identities;

i) $$JO_n^2 + JLO_n^2 = \frac{10}{9}\left[\left(\zeta_1 + JLO_0\right)JL_{2n} + 9\left(\zeta_2 + JLO_0\right)J_{2n}\right] + \frac{16}{9}(-2)^n\left(85 + JLO_0\right),$$

ii) $$JO_n^2 - JLO_n^2 = -\frac{8}{9}\left[\left(\zeta_1 + JLO_0\right)JL_{2n} + 9\left(\zeta_2 + JLO_0\right)J_{2n}\right] - \frac{20}{9}(-2)^n\left(85 + JLO_0\right),$$

iii) $$JLO_mJO_n - JO_mJLO_n = (-2)^{m+1}\left[2\kappa JL_{n-m} - \left(85 + JLO_0\right)J_{n-m}\right],$$

iv) $JO_nJO_m - JO_mJO_n = 2(-2)^{m+1}\kappa J_{n-m}$,

v) $JLO_nJLO_m - JLO_mJLO_n = 36(-2)^m \kappa J_{n-m}$.

Proof. We prove the first and fifth identities and use Binet formulas for these octonions for calculations.

i) $$JO_n^2 + JLO_n^2 = \frac{1}{9}\left[\left(\gamma'\gamma^n - \delta'\delta^n\right)\left(\gamma'\gamma^n - \delta'\delta^n\right) + \left(\gamma'\gamma^n + \delta'\delta^n\right)\left(\gamma'\gamma^n + \delta'\delta^n\right)\right]$$

$$= \frac{10}{9}\left(\gamma'^2\gamma^{2r} + \delta'^2\delta^{2r}\right) + \frac{8}{9}(-2)^n\left(\gamma'\delta' + \delta'\gamma'\right)$$

$$= \frac{10}{9}\left[\left(\zeta_1 + JLO_0\right)\left(\gamma^{2r} + \delta^{2r}\right) + 3\left(\zeta_2 + JLO_0\right)\left(\gamma^{2r} - \delta^{2r}\right) + \frac{16}{9}(-2)^n\left(85 + JLO_0\right)\right]$$

$$= \frac{10}{9}\left[\left(\zeta_1 + JLO_0\right)JL_{2n} + 9\left(\zeta_2 + JLO_0\right)J_{2n} + \frac{16}{9}(-2)^n\left(85 + JLO_0\right)\right].$$

Similarly, using Binet formulas again, we have

v) $$JLO_nJLO_m - JLO_mJLO_n = \left(\gamma'\gamma^n + \delta'\delta^n\right)\left(\gamma'\gamma^m + \delta'\delta^m\right) - \left(\gamma'\gamma^m + \delta'\delta^m\right)\left(\gamma'\gamma^n + \delta'\delta^n\right)$$

$$= \gamma'\delta'\gamma^n\delta^m + \delta'\gamma'\gamma^m\delta^n - \gamma'\delta'\gamma^m\delta^n - \delta'\gamma'\gamma^n\delta^m$$
$$= -\left(\delta'\gamma' - \gamma'\delta'\right)\left(\gamma^n\delta^m - \gamma^m\delta^n\right)$$
$$= -\left(-12\kappa\right)\gamma^m\delta^m\left(\gamma^{n-m} - \delta^{n-m}\right)$$
$$= 36(-2)^m\kappa J_{n-m}.$$

In this theorem, the other identities can be obtained similary.

Finally, we give Vajda theorems for Jacobsthal and Jacobsthal-Lucas octonions.

Theorem 7. For every integers *n*, *r* and *s*, we have

$$JO_{n+r}JO_{n+s} - JO_nJO_{n+r+s} = (-2)^n J_r\left[\left(85 + JLO_0\right)J_s - 2\kappa JL_s\right]$$

and

$$JLO_{n+r}JLO_{n+s} - JLO_nJLO_{n+r+s} = (-2)^n J_r\left[-9(85+JLO_0)J_s + 18\kappa JL_s\right].$$

Proof. We show the proof of Vajda theorem for Jacobsthal octonion.

$$\begin{aligned}
JO_{n+r}JO_{n+s} - JO_nJO_{n+r+s} &= \frac{1}{9}\left(\gamma'\gamma^{n+r} - \delta'\delta^{n+r}\right)\left(\gamma'\gamma^{n+s} - \delta'\delta^{n+s}\right) \\
&\quad -\frac{1}{9}\left(\gamma'\gamma^{n} - \delta'\delta^{n}\right)\left(\gamma'\gamma^{n+r+s} - \delta'\delta^{n+r+s}\right) \\
&= \frac{1}{9}\Big[\gamma'\delta'\left(-\gamma^{n+r}\delta^{n+s} - \gamma^{n}\delta^{n+r+s}\right) \\
&\quad -\delta'\gamma'\left(-\gamma^{n+s}\delta^{n+r} + \gamma^{n+r+s}\delta^{n}\right)\Big] \\
&= \frac{(-2)^n}{9}\left[-\gamma'\delta'\delta^r\left(\gamma^r - \delta^r\right) + \delta'\gamma'\gamma^s\left(\gamma^r - \delta^r\right)\right] \\
&= \frac{(-2)^n}{3}J_r\Big[(85+JLO_0)\left(\gamma^s - \delta^s\right) \\
&\quad -6\kappa\left(\gamma^s + \delta^s\right)\Big] \\
&= (-2)^n J_r\left[(85+JLO_0)J_s - 2\kappa JL_s\right].
\end{aligned}$$

We can observe the Vajda theorem for Jacobsthal-Lucas octonion, similarly.

Corollary 8. In the Vajda theorem for Jacobsthal and Jacobsthal-Lucas octonions, if we take $-r$ instead of s, Catalan's identity is obtained.

Corollary 9. In the Vajda theorem for Jacobsthal and Jacobsthal-Lucas octonions, if we take $-r$ instead of s and then 1 instead of r, Cassini's identity is obtained.

Corollary 10. In the Vajda theorem for Jacobsthal and Jacobsthal-Lucas octonions, if we take m instead of n, n-m instead of s and then 1 instead of r, d'Ocagne's identity is obtained.

REFERENCES

Akyiğit, M., Köksal, H.H., Tosun, M. (2013). Split Fibonacci Quaternions, Advances in Applied Clifford Algebras, Vol. 25, No. 3, pp 535-545.

Akyiğit, M., Köksal, H.H., Tosun, M. (2014). Fibonacci Generalized Quaternions, Advances in Applied Clifford Algebras, Vol. 24, No. 3, pp 631-641.

Keçilioğlu, O., Akkus, I. (2015). The Fibonacci Octonions, Advances in Applied Clifford Algebras, Vol. 25, No. 1, pp 151-158.

Akkus, I., Keçilioğlu, O. (2015). Split Fibonacci and Lucas Octonions, Advances in Applied Clifford Algebras, Vol. 25, No. 3, pp 517-525.

Halici, S. (2015). On Dual Fibonacci Octonions, Advances in Applied Clifford Algebras, Vol. 25, No. 4, pp 905-914.

Bilgici, G., Ünal, Z., Tokeşer, Ü., Mert, T. (2018). On Fibonacci and Lucas Generalized Octonions, Ars Combinatoria, Vol. 138, pp 35-44.

Horadam, A.F. (1963). Complex Fibonacci Numbers and Fibonacci Quaternions, The American Mathematical Monthly, Vol. 70, No. 3, pp 289-291.

Flaut, C., Shpakivskyi, V. (2013). On Generalized Fibonacci Quaternions and Fibonacci-Narayan Quaternions, Advances in Applied Clifford Algebras, Vol. 23, No. 3, pp 673-688.

Halici, S. (2012). On Fibonacci Quaternions, Advances in Applied Clifford Algebras, Vol. 22, No. 2, pp 321-327.

Iakin, I.L. (1977). Generalized Quaternions of Higher Order, The Fibonacci Quaterly, Vol. 15, No. 4, pp 343-346.

Swamy, M.N.S. (1973). On Generalized Fibonacci Quaternions, The Fibonacci Quaterly, Vol. 11, No. 5, pp 547-549.

Savin, D. (2015). Some Properties of Fibonacci Numbers, Fibonacci Octonions, and Generalized Fibonacci-Lucas Octonions, Advances in Difference Equations, Vol. 2015:298, pp 1-10.

Szynal-Liana, A., Wloch, I. (2016). A Note on Jacobsthal Quaternions, Advances in Applied Clifford Algebras, Vol. 26, pp 441-447.

Aydin, F.T., Yüce, S. (2017). A New Approach to Jacobsthal Quaternions, Filomat, Vol. 31, No. 18, pp 5567-5579.

Aydin, F.T. (2018). On Generalizations of the Jacobsthal Sequence, Notes on Number Theory and Discrete Mathematics, Vol. 24, No. 1, pp 120-135.

Yasarsoy, S., Acikgoz, M., Duran, U. (2018). A Study on the *k*-Jacobsthal and *k*-Jacobsthal-Lucas Quaternions and Octonions, Journal of Analysis and Number Theory, Vol. 6, No. 2, pp 1-7.

Tasci, D. (2017). On *k*-Jacobsthal and *k*-Jacobsthal-Lucas Quaternions, Journal of Science and Arts, Vol. 3, No. 40, pp 469-476.

Cimen, C.B., İpek, A. (2017). On Jacobsthal and Jacobsthal-Lucas Octonions, Mediterranean Journal of Mathematics, Vol. 14, No. 37, pp 1-13.

CHAPTER 7

PHYSICOCHEMICAL PROPERTIES OF ZEOLITE AND MODIFIED ZEOLITE CLAY, NANOCATALYST AND NANOADSORBENT SUPPORTED APPLICATIONS

Assist. Prof. Dr. Murat KIRANŞAN[1*]

[1]*University of Gumushane, Vocational School of Gumushane, Department of Chemistry and Chemical Processing Technologies, 29100-Gümüşhane, TURKEY.
*murat.kiransan@gumushane.edu.tr (*Corresponding Author), ORCID ID: 0000-0002-8520-6563

INTRODUCTION

Zeolites are microstructures containing aluminum, silica and oxygen in their lattice structures porous clay group. Zeolite clay has cations and water in its pores (Weckhuysen and Yu 2015). Silica and aluminum atoms are tetrahedral bonded to each other by a common oxygen atom. There are wide gaps forming channels in the zeolite structure (Armaroli et al. 2006; Obaid et al. 2018). These gaps allow ions and molecules to easily pass through the zeolite. Zeolites are known as molecular sieves because of these properties (Hashimoto, 2003). Zeolites are generally seen in the geological environments such as low temperature marine residues, lake residues, alkaline deserts. Clinoptilolite, a natural zeolite mineral has properties such as tetrahedral structure, typical formula, high ion exchange, catalytic structure and high adsorption capacity (Alpat et al. 2008; Armağan et al. 2004). In addition, it is one of the natural adsorbents that are very suitable for adsorption, which has been used for years due to its low cost and environmental friendliness, together with its rich resources in the nature (Bekkum et al., 2001). Zeolites are crystalline, aqueous aluminum silicates containing alkali and alkaline soil elements (Tsujiguchi et al. 2014b). Aluminasilicates are known as zeolites and are crystalline structures occuring of a three-dimensional SiO_4 tetrahedral complex structure with a lattice structure (Dehghani et al. 2017; Tsujiguchi et al. 2014a). Zeolites are classified as synthetic or naturally occurring alumina silicate minerals. Natural zeolites are preferred because they are cheaper than synthetic ones (Ansari et al. 2014; Benito et al. 1996). Zeolites are hydrated aluminosilicates belonging to the class of tetra silicates (Gao et al. 2016; Missengue et al. 2018). The complex network structure consists of tetrahedrons consisting of $[SiO_4]^{4-}$ and $[AlO_4]^{5-}$ formed by the addition of general oxygen atoms (Ahmadpour and Taghizadeh 2015; Jiang et al. 2011). The exchange of some structurally isomorphic Al^{3+} atoms with Si^{4+} atoms formed a negatively charged structure in the zeolites (Charkhia et al. 2012; Masoudian et al. 2013). The tetrahedral lattice systems of zeolite clay have a stable structure. This stable structure gives zeolites different properties from minerals under aqueous conditions (Shah et al. 2013). It has been observed that as the SiO_4/AlO_4 ratio increases the resistance of zeolites to acids and temperature increases (Wang et al. 2012). Since the cations in the zeolite structure are weakly bonded to each other ion exchange can occur easily (Jin

et al. 2008; Kragovic et al. 2013). Liquid that can easily enter and displace the spaces in the zeolite and gas molecules and alkaline soil ions are present (Han et al. 2009; Nibou et al., 2010). Due to its high BET surface area, special channel structure, acid zones, thermal and hydrothermal stability properties, it is widely applied in the petrochemistry, environmental protection and adsorption (Henry et al. 2017; Mirzaei et al. 2013). The catalytic degradation of hydrocarbon is the important for industrial production because of the advantages of high decomposition conversion efficiency, alkene selectivity and low carbon accumulation compared to thermal decomposition (Marcilla et al. 2009; Wong et al. 2016). Natural zeolites are an important alternative as adsorbent and catalyst due to their high ion exchange, adsorption capacity, thermal and mechanical stability (Baybaş and Ulusoy 2011; Tavasoli et al. 2014).

1. PROPERTIES OF ZEOLITE CLAY

1.1. Chemical Properties of Zeolite Clay

Zeolites are microporous crystalline solids containing aluminum, silica and oxygen in their lattice structures and cation and water in their pores (Zhang et al. 2008). Silica and aluminum atoms are connected to each other tetrahedrally by a common oxygen atom support (Yonli et al. 2012). Zeolite literally means boiling stone. It was given this name because it explodes when heated (Sun et al. 2010; Tsai et al. 2006). Zeolite clay has many advantageous properties. These features are regular structure, large specific surface area, uniform sized pores, good thermal stability (Neppolian et al. 2016; Rakic et al. 2010). In addition, zeolites are clean, inert and non-toxic materials suitable for many industrial, agricultural, environmental applications (Liu et al. 2014; Martucci et al. 2012).

Some tetrahedrons of the zeolites have Si^{4+} valence and Al^{3+} structures. For this reason, a lack of positive charge occurs (Yu et al. 2015). The lack of positive charge is the balanced by alkaline and alkaline soil cations such as Na^{+}, K^{+}, Ca^{2+}, Mg^{2+}, Sr^{2+} entering the zeolite cavities (Ikhlaq et al. 2014; Wittayakun et al. 2008). The size and shape of the pores of the zeolites change according to the temperature and the added substance (Ghanavati et al. 2020; Wahono et al. 2020). For this reason, the structure of zeolites should be investigations under different conditions (Hung et al. 2005).

The pore sizes of zeolite clay change depending on their crystal structure and the cations they include (Guvenc and Ahunbay 2012). The crystal structure of many zeolites consists of pores intertwined with rings formed by Si-O-Al atoms (Chica et al. 2005). The nanostructure brought together by these rings is named the window. The window size changes proportionally to the amount of atoms in the rings (Foster et al. 2006; Lee and Shantz 2005). In industrially important zeolites, the windows consist of rings with 8, 10, 12 units (Zhou et al. 2014). Due to the chemical and physical properties of zeolite clay, it is used in different industrial areas (Ebadi Amooghin et al. 2016; Zorpas et al. 2002). The types of zeolites used in different industrial areas and their properties are given in Table 1.

Table 1: The types of zeolites used in different industrial areas and their properties (Bekkum et al. 2001; Gulen et al. 2012).

Types of zeolites	Size of Pore (A^0)	SiO_2/AlO_3 (Mole Ratio)
Natural Zeolites		
Mordenite	6.7x7.0	8.2-10.0
Shabazit	3.6x3.7	3.2-6.0
Erionite	3.6x5.2	5.8-7.4
Clinoptilolite	(4.4x7.2)(4.1x4.7)	8.5-10.5
Synthetic Zeolites		
KA	3	2.0
NaA	4	2.0
CaA	5	2.0
ZSM	(5.4x5.6)	30

The adsorptive capacity of the zeolite clay is not adsorption to the surface, but filling the crystal holes (Dejaco et al. 2016). One of the important properties of zeolites is their high adsorption capacity at low partial pressures (Burton et al. 2005; Kaengsilalai et al. 2007). The use of zeolite clay as an adsorbent has increased in the removal of low concentration impurities in different liquids and gases (Damjanovic et al. 2010; Ennaert et al. 2016).

Despite the differences in the Si/Al ratios and the cation types and amounts they contain, in the zeolite molecule structure it is generally (M^+, M^{2+})$O.Al_2O_3.9SiO_2.nH_2O$ it has the formula (Wu et al. 2008). M^+ is an alkaline cation, usually Na^+ or K^+ (Elwakeel et al. 2017). M^{2+} is an alkaline soil metal, usually Mg^{2+}, Ca^{2+}, Fe^{2+} is the cation (Rad et al. 2014).

1.2. Physical Properties of Zeolite Clay

Crystal structure geometries of zeolites, such as blank structures and hole connections, provides important physical properties to zeolites (Dragan and Dinu 2015). The zeolite molecule is formed by the combination of two crystals. Some zeolites appear as cross linked molecules (Jin et al. 2006; Weitkamp, 2000). This molecular structure is generally seen in chabazite crystals. Natrolite group minerals such as erionite are in the form of the needles and thorns consists of aggregates (Li et al. 2011). Zeolites have low refractive indices. Although zeolite clay is usually colorless or white, it can sometimes be yellow, brown or red depending on the presence of impurities such as iron hydroxides (Sarıoglu, 2005; Valdes et al. 2006).

The color of ion exchanged zeolites depends on the degree of compounding of the sample with water (Panayotova and Velikov 2003; Payne and Abdel-Fattah 2004). Since natural zeolites tendency to absorb significant moisture, they can easily absorb water (Rehan et al. 2017; Wu et al. 2009). During the heating of the water molecules in the pores of the zeolite clay it can quickly leave the zeolitic structure and be adsorbed again (Turkman et al. 2004). In addition, due to their crystal structures and moisture absorbing properties, they can return the water they have absorbed without any degradation (Saltalı et al. 2007). Due to these properties, activated natural zeolites are effectively used as desiccants (Simon et al. 2015; Taffarel and Rubio 2009). Zeolite clay is found in the abundance and in very pure reserves in nature. The formation of zeolites in nature can be up to 15-20 cm (Roque-Malherbe, 2000). Synthetic zeolites are produced by using chemical processes (Nagrockiene and Girskas 2016). Compared to natural zeolites, more pure and symmetrical forms are obtained (Wang and Peng 2010). In the production of synthetic zeolites, chemicals containing rich silica and alumina are used as raw materials (Georgiev et al. 2009). As a result of the limited number of natural zeolites of industrial importance, approximately 150 types of zeolites used in industry are obtained synthetic (Rajos-Valencia et al. 2014).

Properties such as ion exchange, adsorption, molecular sieve, silica-rich chemical composition, crystal structure are common in natural and synthetic zeolites (Andac et al. 2005; Wang and Yan 2010). However, cheaper raw materials such as clay minerals, natural zeolites, coal ash and industrial clinkers are used as starting materials for zeolite synthesis (Su et al. 2016; Wittayakun et al. 2008). Zeolites are preferred to be used in different chemical and physical processes due to their crystalline geometry such as pore size, structure and channel connections (Taheri et al. 2019; Venglovsky et al. 2005). The physical characteristics of the zeolite clay are as given in Table 2.

Table 2: Different physical properties of zeolite clay (Guisnet and Gilson, 2002; Payra and Dutta, 2003)

Properties	Values and Units
Appearance	Chalky, Slightly Soft Layered
Pore Sizes	2.2-8.0 A^0
Pore Volume	15-50%
Intensity	2.0-2.4 g/cm^3
Hardness	3.5-5.5
Colour	Yellowish Brown, Light Green
Structure	Needle-Like and Fibrous
Surface Area	900 m^2/g
Water Affinity	Hydrophilic-Hydrophobic
Thermal Stability	500- 1.000 ^0C

1.3. Application and Usage Areas of the Zeolite Clay

Zeolites are used in the industrial areas for many reasons such as adsorption, ion exchange, high selectivity, light color in sedimentary zeolites, silica content, acidic medium durability, molecular sieve, low costs and pore structure of crystals (Panic and Velickovic 2014; Rhodes, 2010; Shi et al. 2017). Zeolite clay is the used in various sectors such as energy, agriculture and livestock, mining and metallurgy, construction, detergent, paper industry (Villasenor et al. 2011; Zorpas et al. 2008). Due to the high ion exchange and adsorption capacity of zeolite clay, it is used in environmental pollution

control. It is used to remove undesirable metals in the wastewater (Shirani et al. 2016; Wingenfelder et al. 2005). The use of zeolite molecule in the environmental pollution control is increasing in areas such as radioactive waste separation, cleaning of wastewater, cleaning of flue gases, cleaning of petroleum spills and oxygen production (Wibowo et al. 2017; Zeng et al. 2010). Zeolites are known as environmental molecules (Prasad and Kumar 2016). The reason for this is that nitrogen fertilizers are prevented from being washed away due to excessive fertilization or incorrect irrigation in the soil (Hermassi et al. 2016; Lin et al. 2015). Therefore, it prevents the pollution of our underground and surface waters which directly affects the health of the humans and other living things (Kuwahara et al. 2010).

Due to the high moisture absorption and desorption properties of zeolite, it is preferred because it increases afforestation efficiency in the sloping lands and arid regions (Kazemian et al. 2009). Due to the high ion exchange and adsorption capacity of natural zeolites, they can be used as a drug carrier material in agricultural applications (Dassanayake et al. 2015; Nakhli et al. 2017). Natural and synthetic zeolites are used to convertion natural resources into energy (Galadima and Muraza 2015). Natural and synthetic zeolites are used as catalysts in coal gasification, hydrocarbon cleaning, solar energy and petroleum production (Richardeau et al. 2004; Tawfik et al. 2016; Yi et al. 2014). The usage and application areas of zeolite mineral are as shown in Figure 1.

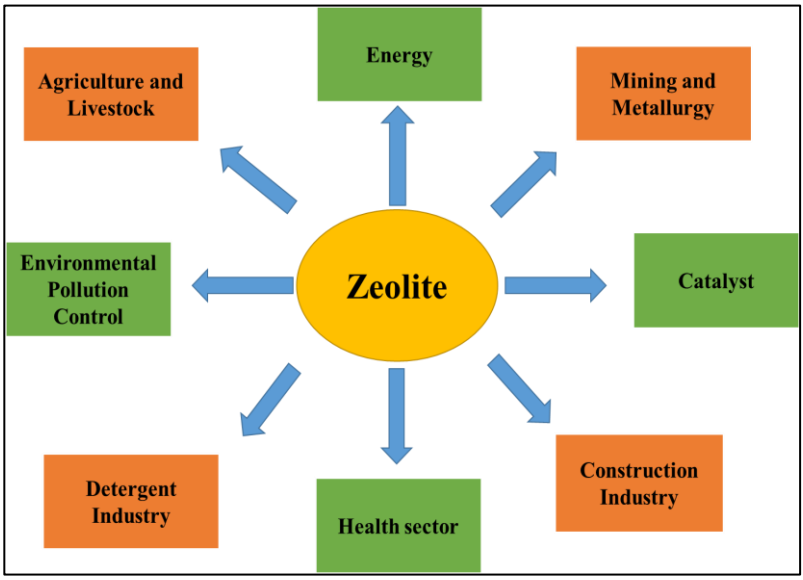

Figure 1: Different application and usage areas of the zeolite clay (Bukhari et al. 2016; Julbe et al. 2000; Katsuki et al. 2005; Reeve and Fallowfield 2018).

In addition, natural zeolites are used as animal feed additives in raising soil pH, fertilizers and livestock (Beler-Baykal et al. 2011). Zeolite clay is used in mining, detection mineral deposits and removal some heavy metals (Choi et al. 2016; Wen et al. 2016). Other uses of zeolite clay are in the construction, as a cement additive, as an additive in paper production, in medicine and toothpaste production in the health sector and instead of phosphates in the detergent sector (Huang et al. 2015; Zhao et al. 2009). Natural zeolites are a type of clay with high selectivity for some radioactive substances (Ibrahim et al. 2008; Malekpour et al. 2008; Munthali et al. 2015). On the adsorbing of radioactive materials by zeolites in studies, it has been reported that the absorbing by plants of radioactive materials emitted as a result of nuclear accidents is the decreased by using clinoptilolite clay (Mustafa and Zaiter 2011; Olguin et al. 1999). Natural zeolite is a new and very good natural filter medium that can be used for water filtration (Gibb et al. 2017; Guo et al. 2013). By providing more pure water and higher efficiency that requires less maintenance, it offers superior performance compared to sand and carbon filters (Henao-Sierra et al. 2018). Zeolites have three basic properties in the industrial areas. These properties are adsorption,

catalyst and ion exchange (Moshoeshoe et al. 2017). Especially the molecular sieve properties of zeolites are widely used in the industry (Byrappa and Yoshimura 2001). Zeolites are preferred for use in the degradation of straight chain hydrocarbons, chemical sensors, industrial process control, environmental and air quality, waste and automatic exhaust control (Bento Ribeiro et al. 2015; Fischer, 2015; Maretto et al. 2015).

2. PREPARATION OF MODIFIED ZEOLITES

The pore widths of the zeolites are determined by the cations that can be added from the outside the structures formed by changing are named to modified zeolites (Salminen et al. 2013; Suzuki et al. 2009). Modified zeolites are synthesized as a result of chemical processes. The pore structure of the modified zeolites is more uniform than natural zeolites in terms of size (Lin et al. 2013; Perez-Perez et al. 2018). The raw materials generally used for the synthesis of modified zeolites can be pure chemicals rich in silica and aluminum, and substances produced by industries (Jung et al. 2004; Qin et al. 2011). In the modification of zeolites, it is aimed to decrease the surface pH and expanded the pore size (Xie et al. 2012). As a result, while the cation exchange capacity of the zeolite is increased, its molecular sieve properties becomes more effective (Fei et al. 2006; Vidal et al. 2011). By modified zeolites a microporous natural substance with superior properties, effective different properties are gained (Long et al. 2013; Schick et al. 2010; Sun et al. 2011). These properties are selectivity against metals, sorption of certain gases, adsorption of radioactive elements and heavy metals and use as a catalyst in different reactions (Nascimento et al. 2009; Peng et al. 2015). Fly ashes are inexpensive industrial products, rich in molecules containing silica and aluminum and are alternative materials for the preparation of the modified zeolites (Han et al. 2016; Montalvo et al. 2012; Taheri Soudejani et al. 2018).

The type of modified zeolites preparation, temperature, pressure, the concentration of reactive solutions, pH, SiO_2 and Al_2O_3 varies according to the properties of materials containing (Jafari et al. 2020; Taheri Soudejani et al. 2019). As a result of the substitution of Si^{4+} and Al^{3+} ions, the zeolite molecule has great blanks containing negatively charged areas with its three-dimensional structure (Ates et al. 2011; Cordoves et al. 2008). Positively charged ions such as sodium, potassium, calcium, magnesium can be

substitution by heavy metals by settling in the spaces in the zeolite (Abu-Zied et al. 2008; Altare et al. 2007; El-Kamash, 2008). Zeolite in the crystal structure and different zeolite molecules are as shown in Figure 2.

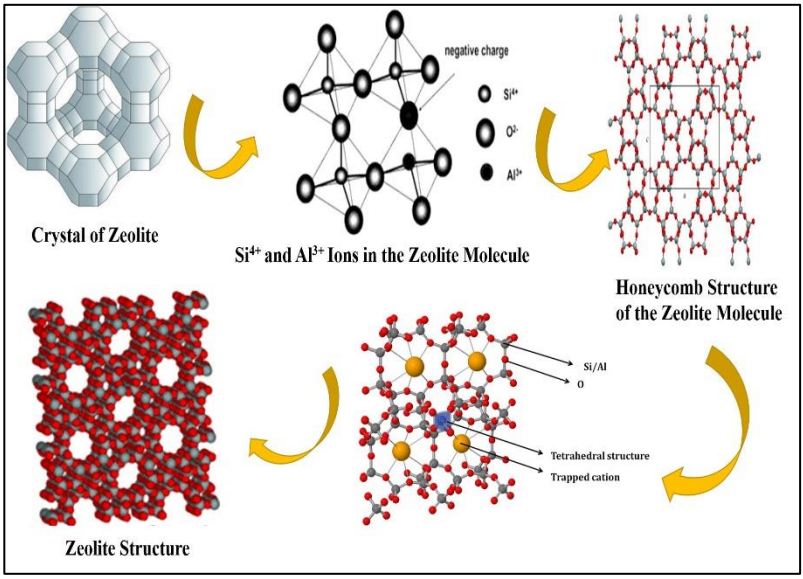

Figure 2: Zeolite crystal structure and different zeolite molecules (Johnson and Worrall 2007; Moshoeshoe et al. 2017; Pirc and Stare 2008; Watanabe et al. 2003).

As a result of the modification of zeolite clay with acid, the thermal stability of the modified structures increases and their surface areas increase causes (Tran et al. 2018; Zhang et al. 2016). The substitution of H^+ ions and exchangeable cations between the layers as a result of the modification of zeolite like clays with acid is expressed as the removal of Al^{3+} and Mg^{2+} ions out of the octahedral centers (Song et al. 2015; Zhang et al. 2018). The modification process at high acid concentration causes degradation in the structure of the zeolite (Runtti et al. 2017). Zeolite molecule undergoes deformation by transforming into gel form in the acidic medium (Ayodele et al. 2012; Lee and Tiwari 2012). The silicates in the zeolite structure transformation into different structures as a result of acid degradation (Saka et al. 2021; Stacey et al. 2020). These formed structures form an insoluble silica structure without gel formation and a gelatinous structure with acid application (Krajisnik et al. 2013; Lin and Zhan 2012). As a result of the thermal effect, the physically adsorbed surface water and zeolitic water are

removed in the structure of the zeolite clay (Bakhtiari et al. 2016; Gong et al. 2009). When heat treatment up to 500 °C is applied to zeolite like clays, surface water, zeolitic water, adsorbed water and crystalline water attached to the structure are completely removal respectively (King and Li 2006; Salehi et al. 2020). This condition is named to dehydration. As a result of the dehydration of zeolite like clays, the hydroxyl groups attached to the crystal structure are also removal until the temperature reaches 900 °C (Jing and Huai 2009; Unaldı et al. 2009; Wajima et al. 2006). The thermal activation process is based on keeping a certain amount of zeolite minerals in the furnace at certain temperatures and times (Korkuna et al. 2006; Li et al. 2000). Zeolite that undergoes dehydration as a result of the thermal activation process Lewis acid structure is formed in its molecules (Triantafyllidis et al. 2001). The acidity of zeolites is due to the presence of Bronsted acid sites in the structure (Alipour et al. 2014; Busca, 2014; Zheng et al. 2002).

3. NANOCATALYST AND NANOADSORBENT SUPPORTED APPLICATIONS OF ZEOLITE AND MODIFIED ZEOLITE CLAY

Modified catalysts with higher catalytic activities are preparation by addition different metal atoms and metal oxides to the structure of the zeolite clay (Lakiss et al. 2020; Melian-Cabrera et al. 2006). Fe, Ni, Zn, Ti, and Cu metals are examples of these adding metal oxides, while TiO_2, PdO, SrO, Fe_2O_3, ZnO and MoO_3 are examples (Htay and Oo 2008; Kianfar, 2019; Kuwahara et al. 2008). These metals and metal oxides are used either alone or in the combinations of zeolite clay (Abello et al. 2009; Dong et al. 2011). Adsorption and catalytic properties of metal oxide/montmorillonite nanocomposites preparation by addition different metal oxides to structures such as montmorillonite clay are more effective (Khataee et al. 2016; Kıranşan et al. 2014; Kıranşan et al. 2015a). Nanocomposites obtained with metal oxides immobilized on the structures of clays such as zeolite and montmorillonite show nanocatalyst and nanoadsorbent properties (Hassani et al. 2016; Khataee et al. 2017; Özyürek et al. 2021).

Synthesized metal oxide/clay nanocomposites are used as nanocatalysts and nanoadsorbent in different applications, especially in the environmental technologies (Gurses et al. 2014; Karaca et al. 2013). Different

methods applied in environmental technologies are the removal of organic pollutants in industrial wastewater by photocatalytic, photocatalytic-ozonation, adsorption, sonocatalytic, fenton-like processes (Hassani et al. 2015; Karaca et al. 2016; Kıranşan et al. 2015b). Metal and heavy metal removal by using zeolite clay usually increases with high temperature (Terbouche et al. 2011; Yuna et al. 2016; Zhang et al. 2014). In general, due to the endothermic nature of the adsorption process, it is expected that the adsorption processes in zeolites increase the activation of the adsorption surfaces with increasing temperature (Gonzalez-Olmos et al. 2013; Reungoat et al. 2007; Zaitan et al. 2016). Higher diffusion coefficients result in the faster movements of cations and consequently increase metal removal at higher temperatures (Koubaissy et al. 2008; Kwakye-Awuah et al. 2014; Yoldi et al. 2019). This process can be accounts by the appearance of powerless electrostatic interactions and smaller ion diameters with increasing temperature(Grieco and Ramarao, 2013; Khalid et al. 2004). Classical zeolite clays are easily deactivated by carbon accumulation due to their simple microporous structure, high diffusion capacity and strong acid regions (Guo et al. 2009; Kusic et al. 2005; Zhijian et al. 2014). Although strong acid regions are important in the catalytic reactions, especially in hydrocarbon accumulation, reactants reaction in acid regions and turn into aromatic hydrocarbons (Bleken et al. 2013; Conte et al. 2012; Daza et al. 2011; Hwang et al. 2001; Rungsirisakun et al. 2006). Also, the reactants are converted to carbon accumulation, if too many acid regions are present resulting in the deactivation of the catalyst (Erichsen et al. 2013; Eskandari et al. 2019; Lanzafame et al. 2018). In addition, since the classical zeolite clay has only a microporous structure, the diffusion efficiency of the molecule is low (Ji et al. 2017; Ma et al. 2017; Vicente et al. 2017). Great molecules are difficult to disperse in micropores. Therefore, they turn into carbon accumulation by blocking the pore gap (Forni et al. 2004; Primo and Garcia 2014). Zeolite clay is the widely used in adsorption and separation applications (Ren et al. 2020; Ruenngam et al. 2009). It has features such as moisture absorption, storage of various gases, separation of substances as the molecular sieves (Pahlavanzadeh and Motamedi 2020; Rashed and Palanisamy 2018). Adsorption applications include drying of natural gas, removal of carbon dioxide and sulfur components, separation of oxygen and nitrogen from the

air can be given as examples (Verrecchia et al. 2020; Zhang et al. 2019; Zhu et al. 2019). Clinoptilolite is a natural zeolite with multifunctional properties (Zaidun et al. 2019). Clinoptilolite is used as a chemical sieve, gas absorber, feed additive, deodorant and water filter in drinking and aquarium waters (Gedik and Imamoglu, 2008; Rahmani et al. 2004; Wang et al. 2007). Clinoptilolite has very effective adsorption and catalyst properties due to its great pore volume, resistance to high temperatures and being chemically neutral (Latifah et al. 2017; Ugrina et al. 2020). Clinoptilolite easily adsorption ammonia and other toxic gases from water and air (Bhardwaj et al. 2012).

4. CONCLUSION

Zeolite is the most preferred with its catalyst and dehydration capacities, high adsorption capacity and cation exchange properties. Approximately 4 million tons of zeolite is used every year on earth. Zeolite, a highly acid resistant mineral, is treated with acid in the preparation of molecular sieves. Zeolite clay, gas and odor adsorbent, feed and food additive has such uses. In addition, zeolite mineral is used in the purification of radioactive wastes, the removal of wastewater, the removal of metal ions, nitrogen compounds and dyes in wastewater, the cleaning of flue gases, the purification of polluting gases such as CO, SO_2, CO_2, the purification of oil spills, the production of oxygen, the waste storage areas it is used to purify harmful ions in leaks. Zeolites are used extensively in agriculture and livestock sectors for purposes such as removing the irritating odors emitted by fertilizers and adjusting the pH of the soil.

ACKNOWLEDGEMENTS

The authors would like to express special thanks to the University of Gumushane for supports.

REFERENCES

Abello, S., Bonilla, A. and Perez-Ramirez, J. (2009). Mesoporous ZSM-5 zeolite catalysts prepared by desilication with organic hydroxides and comparison with NaOH leaching. *Applied Catalysis A: General*, Vol. 364, pp 191-198.

Abu-Zied, B. M., Schwieger, W. and Unger, A. (2008). Nitrous oxide decomposition over transition metal exchanged ZSM-5 zeolites prepared by the solid-state ion-exchange method. *Applied Catalysis B: Environmental,* Vol. 84, pp 277-288.

Ahmadpour, J. and Taghizadeh, M. (2015). Catalytic conversion of methanol to propylene over high-silica mesoporous ZSM-5 zeolites prepared by different combinations of mesogenous templates. *Journal of Natural Gas Science and Engineering,* Vol. 23, pp 184-194.

Alipour, Z., Rezaei, M. and Meshkani, F. (2014). Effect of Ni loadings on the activity and coke formation of MgO-modified Ni/Al_2O_3 nanocatalyst in dry reforming of methane. *Journal of Energy Chemistry,* Vol. 23, pp 633-638.

Alpat, S. K., Özbayrak, Ö., Alpat, Ş. and Akçay, H. (2008). The adsorption kinetics and removal of cationic dye, Toluidine Blue O from aqueous solution with Turkish zeolite. *Journal of Hazardous Materials,* Vol. 151 No. 1, pp 213-220.

Altare, C. R., Bowman, R. S., Katz, L. E., Kinney, K. A. and Sullivan, E. J. (2007). Regeneration and long-term stability of surfactant-modified zeolite for removal of volatile organic compounds from produced water. *Microporous and Mesoporous Materials,* Vol. 105, pp 305-316.

Andac, O., Tatlier, M., Sirkecioglu, A., Ece, I. and Erdemsenatalar, A. (2005). Effects of ultrasound on zeolite A synthesis. *Microporous and Mesoporous Materials,* Vol. 7, No. 9, pp 225-233.

Ansari, M., Aroujalian, A., Raisi, A., Dabir, B. and Fathizadeh, M. (2014). Preparation and characterization of nano-NaX zeolite by microwave assisted hydrothermal method. *Advanced Powder Technology,* Vol. 25, pp 722-727.

Armağan, B., Turan, M. and Çelik, M. S. (2004). Equilibrium studies on the adsorption of reactive azo dyes into zeolite. *Desalination,* Vol. 170, pp 33-39.

Armaroli, T, Simon, L. J., Digne, M., Montanari, T., Bevilacqua, M., Valtchev, V., Patarin, J. and Busca, G. (2006). Effects of crystal size and Si/Al ratio on the surface properties of H-ZSM-5 zeolites. *Applied Catalysis A: General,* Vol. 306, pp 78-84.

Ates, A., Reitzmann, A., Hardacre, C. and Yalcin, H. (2011). Abatement of nitrous oxide over natural and iron modified natural zeolites. *Applied Catalysis A: General,* Vol. 407, pp 67-75.

Ayodele, O. B., Lim, J. K. and Hameed, B. H. (2012). Degradation of phenol in photo-fenton process by phosphoric acid modified kaolin supported ferric-oxalate catalyst: optimization and kinetic modeling. *Chemical Engineering Journal,* Vol. 197, pp 181-192.

Bakhtiari, G., Abdouss, M., Bazmi, M. and Royaee, S. (2016). Optimization of sulfur adsorption over Ag-zeolite nanoadsorbent by experimental design method. *International Journal of Environmental Science and Technology,* Vol. 13 pp 803-812.

Baybaş, D. and Ulusoy, U. (2011). Polyacrylamide-clinoptilolite/Y-zeolite composites: Characterization and adsorptive features for terbium. *Journal of Hazardous Materials,* Vol. 187, No. 1-3, pp 241-249.

Bekkum, H., Flanigen, E. M., Jacobs, P. A. and Jansen, J. C. (2001). Introduction to zeolite science and practice. 2. Edition. *Elsevier,* pp 11-45.

Beler-Baykal, B., Allar, A. D. and Bayram, S. (2011). Nitrogen recovery from source-separated human urine using clinoptilolite and preliminary results of its use as fertilizer. *Water Science and Technology,* Vol. 63, pp 811-817.

Benito, P. L., Gayubo, A. G., Aguayo, A. T., Olazar, M. and Bilbao, J. (1996). Effect of Si/Al ratio and of acidity of H-ZSM5 zeolites on the primary products of methanol to gasoline conversion. *Journal of Chemical Technology & Biotechnology,* Vol. 66, pp 183-191.

Bento Ribeiro, L. E., Alcantara, G. P., Gonçalves Andrade, C. M. and Fruett, F. (2015). Analysis of the planar electrode morphology applied to

Zeolite based chemical sensors. *Sensors & Transducers Journal*, Vol. 193, pp 80-85.

Bhardwaj, D., Sharma, M., Sharma, P. and Tomar, R. (2012). Synthesis and surfactant modification of clinoptilolite and montmorillonite for the removal of nitrate and preparation of slow release nitrogen fertilizer. *Journal of Hazardous Materials*, Vol. 227-228, pp 292-300.

Bleken, F. L. et al. (2013). Catalyst deactivation by coke formation in microporous and desilicated zeolite H-ZSM-5 during the conversion of methanol to hydrocarbons. *Journal of Catalysis*, Vol. 307, pp 62-73.

Bukhari, S. S., Rohani, S. and Kazemian, H. (2016). Effect of ultrasound energy on the zeolitization of chemical extracts from fused coal fly ash. *Ultrasonics Sonochemistry*, Vol. 28, pp 47-53.

Burton, A. W., Zones, S. I. and Elomari, S. (2005). The chemistry of phase selectivity in the synthesis of high-silica zeolites. *Current Opinion in Colloid & Interface Science*, Vol. 10, pp 211-219.

Busca, G. (2014). Zeolites and other structurally microporous solids as acid-base materials, in: G. Busca (Ed.), Heterog. Catal. Mater. *Elsevier*, Amsterdam, pp 197-249.

Byrappa, K. and Yoshimura, M. (2001). Hydrothermal synthesis and growth of zeolites (Advanced structure studies) in Handbook of Hydrothermal Technology. pp 315-414.

Charkhia, A., Kazemeinia, M., Ahmadib, S. J. and Kazemian H. (2012). Fabrication of granulated NaY zeolite nanoparticles using a new method and study the adsorption properties. *Powder Technology*, Vol. 231, pp 1-6.

Chica, A., Strohmaier, K. G. and Iglesia, E. (2005). Effects of zeolite structure and aluminum content on thiophene adsorption, desorption and surface reactions. *Applied Catalysis B: Environmental*, Vol. 60, pp 223-232.

Choi, H. J., Yu, S. W. and Kim, K. H. (2016). Efficient use of Mg-modified zeolite in the treatment of aqueous solution contaminated with heavy metal toxic ions. *Journal of the Taiwan Institute of Chemical Engineers*, Vol. 63, pp 482-489.

Conte, M., Lopez-Sanchez, J. A., He, Q., Morgan, D. J., Ryabenkova, Y., Bartley, J. K., Carley, A. F., Taylor, S. H., Kiely, C. J., Khalid, K. and Hutchings, G. J. (2012). Modified zeolite ZSM-5 for the methanol to aromatics reaction. *Catalysis Science & Technology,* Vol. 2, pp 105-112.

Cordoves, A. P., Valdes, M. G., Fernandez, J. T., Luis, G. P., Garcia-Calzon, J. and Garcia, M. D. (2008). Characterization of the binding site affinity distribution of a surfactant-modified clinoptilolite. *Microporous and Mesoporous Materials,* Vol. 109, pp 38-48.

Damjanovic, L., Rakic, V., Rac, V., Stosic, D. and Auroux, A. (2010). The investigation of phenol removal from aqueous solutions by zeolites as solid adsorbents. *Journal of Hazardous Materials,* Vol. 184, pp 477-484.

Dassanayake, K. B., Jayasinghe, G. Y., Surapaneni, A. and Hetherington, C. (2015). A review on alum sludge reuse with special reference to agricultural applications and future challenges. *Waste Management,* Vol. 38, pp 321-335.

Daza, C. E., Gamba, O. A., Hernandez, Y., Centeno, M. A., Mondragon, F., Moreno, S., et al. (2011). High-stable mesoporous Ni-Ce/clay catalysts for syngas production. *Catalysis Letters,* Vol. 141, pp 1037-1046.

Dehghani, M. H., Dehghan, A. and Najafpoor, A. (2017). Removing Reactive Red 120 and 196 using chitosan/zeolite composite from aqueous solutions: Kinetics, isotherms, and process optimization. *Journal of Industrial and Engineering Chemistry,* Vol. 51, pp 185-195.

Dejaco, R. F., Bai, P., Tsapatsis, M. and Siepmann, J. I. (2016). Adsorptive separation of 1-Butanol from aqueous solutions using MFI- and FER-type zeolite frameworks: a Monte Carlo study. *Langmuir,* Vol. 32, pp 2093-2101.

Dong, Y., Niu, X., Zhu, Y., Yuan, F. and Fu, H. (2011). One-pot synthesis and characterization of Cu-SBA-16 mesoporous molecular sieves as an excellent catalyst for phenol hydroxylation. *Catalysis Letters,* Vol. 141, pp 242-250.

Dragan, E. and Dinu, M. (2015). Progress in polysaccharide/zeolites and polysaccharide hydrogel composite sorbents and their applications in

removal of heavy metal ions and dyes. *Current Green Chemistry*, Vol. 2, pp 342-353.

Ebadi Amooghin, A., Omidkhah, M., Sanaeepur, H. and Kargari, A. (2016). Preparation and characterization of Ag^{+} ion-exchanged zeolite-Matrimid®5218 mixed matrix membrane for CO_2/CH_4 separation. *Journal of Energy Chemistry*, Vol. 25, pp 450-462.

El-Kamash, A. M. (2008). Evaluation of zeolite A for the sorptive removal of Cs^{+} and Sr^{2+} ions from aqueous solutions using batch and fixed bed column operations. *Journal of Hazardous Materials*, Vol. 151, pp 432-445.

Elwakeel, K. Z., El-Bindary, A. A. and Kouta, E. Y. (2017). Retention of copper, cadmium and lead from water by Na-Y-Zeolite confined in methyl methacrylate shell. *Journal of Environmental Chemical Engineering*, Vol. 5, pp 3698-3710.

Ennaert, T., Van Aelst, J., Dijkmans, J., De Clercq, R., Schutyser, W., Dusselier, M., Verboekend, D. and Sels, B. F. (2016). Potential and challenges of zeolite chemistry in the catalytic conversion of biomass. *Chemical Society Reviews*, Vol. 45, pp 584-611.

Erichsen, M. W., Svelle, S. and Olsbye, U. (2013). H-SAPO-5 as methanol-to-olefins (MTO) model catalyst: towards elucidating the effects of acid strength. *Journal of Catalysis*, Vol. 298, pp 94-101.

Eskandari, P., Farhadian, M., Nazar, A. R. S. and Jeon, B. H. (2019). Adsorption and photodegradation efficiency of TiO_2/Fe_2O_3/PAC and TiO_2/Fe_2O_3/zeolite nanophotocatalysts for the removal of cyanide. *Industrial & Engineering Chemistry Research*, Vol. 58, pp 2099-2112.

Fei, J., Hou, Z., Zhu, B., Lou, H. and Zheng, X. (2006). Synthesis of dimethyl ether (DME) on modified HY zeolite and modified HY zeolite-supported Cu-Mn-Zn catalysts. *Applied Catalysis A: General*, Vol. 304, pp 49-54.

Fischer, M. (2015). Structure and bonding of water molecules in zeolite hosts: Benchmarking plane-wave DFT against crystal structure data. Zeitschrift für Kristallographie. *Crystalline Materials*, Vol. 230, pp 325-336.

Forni, L., Fornasari, G., Giordano, G., Lucarelli, C., Katovic, A., Trifiro, F., Perri, C. and Nagy, J. B. (2004). Vapor phase Beckmann rearrangement using high silica zeolite catalyst. *Physical Chemistry Chemical Physics,* Vol. 6, pp 1842-1847.

Foster, M. D., Rivin, I., Treacy, M. M. J. and Delgado Friedrichs, O. (2006). A geometric solution to the largest-free-sphere problem in zeolite frameworks. *Microporous and Mesoporous Materials,* Vol. 90, pp 32-38.

Galadima, A. and Muraza, O. (2015). In situ fast pyrolysis of biomass with zeolite catalysts for bioaromatics/gasoline production: A review. *Energy Conversion and Management,* Vol. 105, pp 338-354.

Gao, Y., Zheng, B., Wu, G., Ma, F. and Liu, C. (2016). Effect of the Si/Al ratio on the performance of hierarchical ZSM-5 zeolites for methanol aromatization. *RSC Advances,* Vol. 6, pp 83581-83588.

Gedik, K. and Imamoglu, I. (2008). Affinity of clinoptilolite-based zeolites towards removal of Cd from aqueous solutions. *Separation Science and Technology,* Vol. 43, pp 1191-1207.

Georgiev, D., Bogdanov, B., Angelova, K., Markovska, I. and Hristov, Y. (2009). Synthetic zeolite-structure, clasification, current trends in zeolite synthesis review. *International Science conference,* Stara Zagora, Bulgaria, pp 4-5.

Ghanavati, L., Hekmati, A. H., Rashidi, A. and Shafiekhani, A. (2020). Application of electrospun polyamide-6/modified zeolite nanofibrous composite to remove acid blue 74 dye from textile dyeing wastewater. *Journal of the Textile Institute,* pp 1-13, https:// doi.org/10.1080/00405000.2020.1840691.

Gibb, N. P., Dynes, J. J. and Chang, W. (2017). Synergistic desalination of potash brine-impacted groundwater using a dual adsorbent. *Science of the Total Environment,* Vol. 593-594, pp 99-108.

Gong, Y., Dou, T., Kang, S., Li, Q. and Hu, Y. (2009). Deep desulfurization of gasoline using ion exchange zeolites: Cu(I)- and Ag(I)-beta. *Fuel Processing Technology,* Vol. 90, pp 122-129.

Gonzalez-Olmos, R., Kopinke, F. D., Mackenzie, K. and Georgi, A. (2013). Hydrophobic Fe-zeolites for removal of MTBE from water by

combination of adsorption and oxidation. *Environmental Science & Technology,* Vol. 47, pp 2353-2360.

Grieco, S. A. and Ramarao, B. V. (2013). Removal of TCEP from aqueous solutions by adsorption with zeolites. *Colloids and Surfaces A: Physicochemical and Engineering Aspects,* Vol. 434, pp 329-338.

Guisnet, M. and Gilson, J. P. (2002). Zeolites for cleaner technologies. *Imperial College Press,* London.

Gulen, J., Zorbay, F. and Arslan, S. (2012). Zeolitler ve kullanım alanları. *Karaelmas Fen ve Mühendislik Dergisi,* Vol. 2, No. 1, pp 63-68.

Guo, P., Wang, X. and Guo, H. (2009). TiO_2/Na-HZSM-5 nano-composite photocatalyst: reversible adsorption by acid sites promotes photocatalytic decomposition of methyl orange. *Applied Catalysis B: Environmental,* Vol. 90, pp 677-687.

Guo, X., Zeng, L. and Jin, X. (2013). Advanced regeneration and fixed-bed study of ammonium and potassium removal from anaerobic digested wastewater by natural zeolite. *Journal of Environmental Sciences-China,* Vol. 25, pp 954-961.

Gurses, A., Hassani, A., Kıranşan, M., Açışlı, Ö. and Karaca, S. (2014). Removal of methylene blue from aqueous solution using by untreated lignite as potential low-cost adsorbent: Kinetic, thermodynamic and equilibrium approach. *Journal of Water Process Engineering,* Vol. 2, pp 10-21.

Guvenc, E. and Ahunbay, M. G. (2012). Adsorption of methyl tertiary butyl ether and trichloroethylene in MFI-type zeolites. *The Journal of Physical Chemistry C,* Vol. 116, pp 21836-21843.

Han, R., Zhang, S., Liu, C., Wang, Y. and Jian X. (2009). Effect of NaA zeolite particle addition on poly(phthalazinone ether sulfone ketone) composite ultrafilitration (UF) membrane performance. *Journal of Membrane Science,* Vol. 345, pp 5-12.

Han, X., Li, H., Huang, H., Zhao, L., Cao, L., Wang, Y., Gao, J. and Xu, C. (2016). Effect of olefin and aromatics on thiophene adsorption desulfurization over modified NiY zeolites by metal Pd. *RSC Advances,* Vol. 6, pp 75006-75013.

Hashimoto, S. (2003). Zeolite photochemistry: impact of zeolites on photochemistry and feedback from photochemistry to zeolite science.

Journal of Photochemistry and Photobiology C: Photochemistry Reviews, Vol. 4, pp 19-49.

Hassani, A., Khataee, A. R., Karaca, S., Karaca, M. and Kıranşan, M. (2015). Adsorption of two cationic textile dyes from water with modified nanoclay: A comparative study by using central composite design. *Journal of Environmental Chemical Engineering,* Vol. 3, No. 4, pp 2738-2749.

Hassani, A., Soltani, R. D. C., Kıranşan, M., Karaca, S., Karaca, C. and Khataee, A. R. (2016). Ultrasound-assisted adsorption of textile dyes using modified nanoclay: Central composite design optimization. *Korean Journal of Chemical Engineering,* Vol. 33, No. 1, pp 178-188.

Henao-Sierra, W., Romero-Saez, M., Gracia, F., Cacua, K. and Buitrago-Sierra, R. (2018). Water vapor adsorption performance of Ag and Ni modified 5A zeolite. *Microporous and Mesoporous Materials,* Vol. 265, pp 250-257.

Henry, E. M., Ikenna, C. E. and Ganiyu, I. L. (2017). Paper zeolite synthesis, characterization and application areas: A review. *International Research Journal,* Vol. 6, No. 10, pp 45-59.

Hermassi, M., Valderrama, C., Moreno, N., Font, O., Querol, X., Batis, N. and Cortina, J. L. (2016). Powdered Ca-activated zeolite for phosphate removal from treated waste-water. *Journal of Chemical Technology & Biotechnology,* Vol. 91, pp 1962-1971.

Htay, M. M. and Oo, M. M. (2008). Engineering, technology, preparation of Zeolite Y catalyst for petroleum cracking. *World Academy of Science, Engineering and Technology,* Vol. 48, pp 114-120.

Huang, H., Yang, L., Xue, Q., Liu, J., Hou, L. and Ding, L. (2015). Removal of ammonium from swine wastewater by zeolite combined with chlorination for regeneration. *Journal of Environmental Management,* Vol. 160, pp 333-341.

Hung, H. W., Lin, T. F., Baus, C., Sacher, F. and Brauch, H. J. (2005). Competitive and hindering effects of natural organic matter on the adsorption of MTBE onto activated carbons and zeolites. *Environmental Technology,* Vol. 26, pp 1371-1382.

Hwang, K. S., Zhu, H. Y. and Lu, G. Q. (2001). New nickel catalysts supported on highly porous alumina intercalated laponite for methane reforming with CO_2. *Catalysis Today*, Vol. 68, pp 183-190.

Ibrahim, H. A., El-Kamash, A. M., Hanafy, M. and Abdel-Monem, N. M. (2008). Examination of the use of synthetic Zeolite NaA-X blend as backfill material in a radioactive waste disposal facility: thermodynamic approach. *Chemical Engineering Journal*, Vol. 144, pp 67-74.

Ikhlaq, A., Brown, D. R. and Kasprzyk-Hordern, B. (2014). Catalytic ozonation for the removal of organic contaminants in water on ZSM-5 zeolites. *Applied Catalysis B: Environmental*, Vol. 154-155, pp 110-122.

Jafari, M., Zendehdel, R., Rafieepour, A., Pour, M. N., Irvani, H. and Khodakarim, S. (2020). Comparison of Y and ZSM-5 zeolite modified with magnetite nanoparticles in removal of hydrogen sulfide from air. *International Journal of Environmental Science and Technology*, Vol. 17, pp 187-194.

Ji, Y., Yang, H. and W, Yan. (2017). Strategies to enhance the catalytic performance of ZSM-5 zeolite in hydrocarbon cracking: A review. *Catalysts*, No. 7, pp 367.

Jiang, N., Yang, G., Zhang, X., Wang, L., Shi, C. and Tsubaki, N. (2011). A novel silicalite-1 zeolite shell encapsulated iron-based catalyst for controlling synthesis of light alkenes from syngas. *Catalysis Communications*, Vol. 12, pp 951-954.

Jin, L., Fang, Y. and Hu, H. (2006). Selective synthesis of 2,6-dimethylnaphthalene by methylation of 2-methylnaphthalene with methanol on Zr/(Al)ZSM-5. *Catalysis Communications*, Vol. 7, pp 255-259.

Jin, L., Zhou, X., Hu, H. and Ma, B. (2008). Synthesis of 2,6-dimethylnaphthalene by methylation of 2-methylnaphthalene on mesoporous ZSM-5 by desilication. *Catalysis Communications*, Vol. 10, pp 336-340.

Jing, Y. and Huai, S. (2009). A theoretical study of hydrothermal stability of P-modified ZSM-5 zeolites. *Science in China Series B: Chemistry,* Vol. 52, No. 3, pp 282-287.

Johnson, C. D. and Worrall, F. (2007). Novel granular materials with microcrystalline active surfaces-waste water treatment applications of zeolite/vermiculite composites. *Water Research,* Vol. 41, pp 2229-2235.

Julbe, A., Farrusseng, D., Jalibert, J. C., Mirodatos, C. and Guizard, C. (2000). Characteristics and performance in the oxidative dehydrogenation of propane of MFI and V-MFI zeolite membranes. *Catalysis Today,* Vol. 56, No. 1-3, pp 199-209.

Jung, J. Y., Chung, Y. C., Shin, H. S. and Son, D. H. (2004). Enhanced ammonia nitrogen removal using consistent biological regeneration and ammonium exchange of zeolite in modified SBR process. *Water Research,* Vol. 38, No. 2, pp 347-354.

Kaengsilalai, A., Luengnaruemitchai, A., Jitkarnka, S. and Wongkasemjit, S. (2007). Potential of Ni supported on KH zeolite catalysts for carbon dioxide reforming of methane. *Journal of Power Sources,* Vol. 165, pp 347-352.

Karaca, S., Gürses, A., Açışlı, Ö., Hassani, A., Kıranşan, M. and Yıkılmaz, K. (2013). Modeling of adsorption isotherms and kinetics of remazol red RB adsorption from aqueous solution by modified clay. *Desalination and Water Treatment,* Vol. 51, No. 13, pp 2726-2739.

Karaca, M., Kıranşan, M., Karaca, S., Khataee, A. R. and Karimi, A. (2016). Sonocatalytic removal of naproxen by synthesized zinc oxide nanoparticles on montmorillonite. *Ultrasonic Sonochemistry,* Vol. 31, pp 250-256.

Katsuki, H., Furuta, S., Watari, T. and Komarneni, S. (2005). ZSM-5 zeolite/porous carbon composite: Conventional-and microwave-hydrothermal synthesis from carbonized rice husk. *Microporous and Mesoporous Materials,* Vol. 86, No. 1-3, pp 145-151.

Kazemian, H., Modarress, H., Kazemi, M. and Farhadi, F. (2009). Synthesis of submicron zeolite LTA particles from natural clinoptilolite and industrial grade chemicals using one stage procedure. *Powder Technology,* Vol. 196, pp 22-25.

Khalid, M., Joly, G., Renaud, A. and Magnoux, P. (2004). Removal of phenol from water by adsorption using zeolites. *Industrial & Engineering Chemistry Research,* Vol. 43, pp 5275-5280.

Khataee A. R., Kıranşan, M., Karaca, S. and Arefi-Oskoui, S. (2016). Preparation and characterization of ZnO/MMT nanocomposite for photocatalytic ozonation of a disperse dye. *Turkish Journal of Chemistry,* Vol. 40, pp 546-564.

Khataee, A. R., Kıranşan, M., Karaca, S. and Sheydaei, M. (2017). Photocatalytic ozonation of metronidazole by synthesized zinc oxide nanoparticles immobilized on montmorillonite. *Journal of the Taiwan Institute of Chemical Engineers,* Vol. 74, pp 196-204.

Kianfar, E. (2019). Ethylene to propylene over zeolite ZSM-5: improved catalyst performance by treatment with CuO. *Russian Journal of Applied Chemistry,* Vol. 92, No. 7, pp 933-939.

King, D. L. and Li, L. (2006). Removal of sulfur components from low sulfur gasoline using copper exchanged zeolite Y at ambient temperature. *Catalysis Today,* Vol. 116, pp 526-529.

Kıranşan, M., Khataee A. R., Karaca, S. and Sheydaei, M. (2015a). Artificial neural network modeling of photocatalytic removal of a disperse dye using synthesized of ZnO nanoparticles on montmorillonite. *Spectrochimica Acta Part A: Molecular and Biomolecular Spectroscopy,* Vol. 140, pp 465-473.

Kıranşan, M., Khataee A. R., Karaca, S. and Sheydaei, M. (2015b). Synthesis of zinc oxide nanoparticles on montmorillonite for photocatalytic degradation of basic yellow 28: Effect of parameters and neural network modeling. *Current Nanoscience,* Vol. 11, No. 3, pp 343-353.

Kıranşan, M., Soltani, R. D. C., Hassani, A., Karaca, S. and Khataee, A. R. (2014). Preparation of cetyltrimethylammonium bromide modified montmorillonite nanomaterial for adsorption of a textile dye. *Journal of the Taiwan Institute of Chemical Engineers,* Vol. 45, No. 5, pp 2565-2577.

Korkuna, O., Leboda, R., Skubiszewska-Zieba, J., Vrublevska, T., Gunko, V. M. and Ryczkowski, J. (2006). Structural ve physicochemical properties of natural zeolites: clinoptilolite ve mordenite. *Microporous ve Mesoporous Materials,* Vol. 87, pp 243-254.

Koubaissy, B., Joly, G. and Magnoux, P. (2008). Adsorption and competitive adsorption on zeolites of nitrophenol compounds present in wastewater. *Industrial & Engineering Chemistry Research,* Vol. 47, pp 9558-9565.

Kragovic, M., Dakovic, A., Markovic, M., Krstic, J., Gattac, G.D. and Rotirotic N. (2013). Characterization of lead sorption by the natural and Fe(III)-modified zeolite. *Applied Surface Science,* Vol. 283, pp 764-774.

Krajisnik, D., Dakovic, A., Malenovic, A., Milojevic-Rakic, M., Dondur, V., Radulovic, Z., Milic, D. J. (2013). Investigation of adsorption and release of diclofenac sodium by modified zeolites composites. *Applied Clay Science,* Vol. 83, pp 322-326.

Kusic, H., Koprivanac, N. and Locke, B. R. (2005). Decomposition of phenol by hybrid gas/liquid electrical discharge reactors with zeolite catalysts. *Journal of Hazardous Materials,* Vol. 125, pp 190-200.

Kuwahara, Y., Ohmichi, T., Kamegawa, T., Mori, K. and Yamashita, H. J. (2010). A novel conversion process for waste slag: synthesis of a hydrotalcite-like compound and zeolite from blast furnace slag and evaluation of adsorption capacities. *Journal of Materials Chemistry,* Vol. 20, pp 5052-5062.

Kuwahara, Y., Ohmichi, T., Mori, K., Katayama, I. and Yamashita, H. J. (2008). Synthesis of zeolite from steel slag and its application as a support of nano-sized TiO_2 photocatalyst. *Journal of Materials Science,* Vol. 43, pp 2407-2410.

Kwakye-Awuah, B., Labik, L. K., Nkrumah, I. and Williams, C. (2014). Removal of ammonium ions by laboratory-synthesized zeolite linde type A adsorption from water samples affected by mining activities in Ghana. *Journal of Water and Health,* Vol. 12, pp 151-160.

Lakiss, L., Gilson, J. P., Valtchev, V., Mintova, S., Vicente, A., Vimont, A., Bedard, R., Abdo, S. and Bricker, J. (2020). Zeolites in a good shape: catalyst forming by extrusion modifies their performances. *Microporous and Mesoporous Materials,* Vol. 299, pp 110114.

Lanzafame, P., Barbera, K., Papanikolaou, G., Perathoner, S., Centi, G., Migliori, M., Catizzone, E. and Giordano, G. (2018). Comparison of

H^+ and NH_4^+ forms of zeolites as acid catalysts for HMF etherification. *Catalysis Today,* Vol. 304, pp 97-102.

Latifah, O., Ahmed, O. H. and Majid, N. M. A. (2017). Enhancing nitrogen availability from urea using clinoptilolite zeolite. *Geoderma,* Vol. 306, pp 152-159.

Lee, S. and Shantz, D. F. (2005). Zeolite growth in nonionic microemulsions: Synthesis of hierarchically structured zeolite particles. *Chemistry of Materials*, Vol. 17, pp 409-417.

Lee, S. M. and Tiwari, D. (2012). Organo and inorgano-organo-modified clays in the remediation of aqueous solutions: an overview. *Applied Clay Science,* Vol. 59-60, pp 84-102.

Li, Z., Burt, T. and Bowman, R. S. (2000). Sorption of ionizable organic solutes by surfactant-modified zeolite. *Environmental Science and Technology,* Vol. 34, pp 3756-3760.

Li, C., Li, L., Wu, W., Wang, D., Tokratev, A. V., Kikhtyanin, O. V. and Echevskii, G. V. (2011). Highly selective synthesis of 2,6-dimethylnaphthalene over alkaline treated ZSM-12 zeolite. *Procedia Engineering*, Vol. 18, pp 200-205.

Lin, J. and Zhan, Y. (2012). Adsorption of humic acid from aqueous solution onto unmodified and surfactant-modified chitosan/zeolite composites. *Chemical Engineering Journal,* 200, pp 202-213.

Lin, L., Lei, Z. F., Wang, L., Liu, X., Zhang, Y., Wan, C. L., Lee, D. J. and Tay, J. H. (2013). Adsorption mechanisms of high-levels of ammonium onto natural and NaCl-modified zeolites. *Separation and Purification Technology*, Vol. 103, pp 15-20.

Lin, G., Zhuang, Q., Cui, Q., Wang, H. and Yao, H. (2015). Synthesis and adsorption property of zeolite FAU/LTA from lithium slag with utilization of mother liquid. *Chinese Journal of Chemical Engineering*, Vol. 23, pp 1768-1773.

Liu, S., Lim, M. and Amal, R. (2014). TiO_2-coated natural zeolite: rapid humic acid adsorption and effective photocatalytic regeneration. *Chemical Engineering Science,* Vol. 105, pp 46-52.

Long, H., Wu, P. and Zhu, N. (2013). Evaluation of Cs^+ removal from aqueous solution by adsorption on ethylamine-modified

montmorillonite. *Chemical Engineering Journal,* Vol. 225, pp 237-244.

Ma, Z., Hu, H., Sun, Z., Fang, W., Zhang, J., Yang, L., Zhang, Y. and Wang, L. (2017). Acidic zeolite-L as a highly efficient catalyst for dehydration of fructose to 5- hydroxymethylfurfural in ionic liquid. *ChemSusChem,* Vol. 10, pp 1669-1674.

Malekpour, A., Millani, M. and Kheirkhah, M. (2008). Synthesis and characterization of a NaA zeolite membrane and its applications for desalination of radioactive solutions. *Desalination,* Vol. 225, pp 199-208.

Marcilla, A., Beltran, M. I. and Navarro, R. (2009). Thermal and catalytic pyrolysis of polyetilen over HZSM-5 and HUSY zeolites in a batch reactor under dynamic conditions. *Applied Catalysis B: Environmental,* Vol. 86, pp 78-86.

Maretto, M., Vignola, R., Williams, C. D., Bagatin, R., Latini, A. and Papini, M. P. (2015). Adsorption of hydrocarbons from industrial wastewater onto a silica mesoporous material: Structural and thermal study. *Microporous and Mesoporous Materials,* Vol. 203, pp 139-150.

Martucci, A., Pasti, L., Marchetti, N., Cavazzini, A., Dondi, F. and Alberti, A. (2012). Adsorption of pharmaceuticals from aqueous solutions on synthetic zeolites. *Microporous and Mesoporous Materials,* Vol. 148, pp 174-183.

Masoudian, S. K., Sadighi, S. and Abbasi, A. (2013). Synthesis and characterization of high aluminum zeolite X from technical grade materials. *Bulletin of Chemical Reaction Engineering & Catalysis,* 8(1), 54-60.

Melian-Cabrera, I., Espinosa, S., Mentruit, C., Kapteijn, F. and Moulijn, J. A. (2006). Alkaline leaching for synthesis of improved Fe-ZSM5 catalysts. *Catalysis Communications,* Vol. 7, pp 100-103.

Mirzaei, S. M. J., Heidarpour, M., Tabatabaei, S. H., Najafi, P. and Hashemi, S. E. (2013). Immobilization of leachate's heavy metals using soil-zeolite column. *International Journal of Recycling of Organic Waste in Agriculture,* Vol. 2, No. 1, pp 20.

Missengue, R. N. M., Losch, P., Musyoka, N. M., Louis, B., Pale, P. and Petrik, L. F. (2018). Conversion of south african coal fly ash into

high-purity ZSM-5 zeolite without additional source of silica or alumina and its application as a methanol-to-olefins catalyst. *Catalysts,* Vol. 8, pp 124.

Montalvo, S., Guerrero, L., Borja, R., Sanchez, E., Milan, Z., Cortes, I. and Angeles, R. M. (2012). Application of natural zeolites in anaerobic digestion processes: A review. *Applied Clay Science,* Vol. 58, pp 125-133.

Moshoeshoe, M., Tabbiruka, M. S. N. and Obuseng, V. (2017). A review of the chemistry, structure, properties and applications of zeolites. *American Journal of Materials Science,* Vol. 7, No. 5, pp 196-221.

Munthali, M. W., Johan, E., Aono, H. and Matsue, N. (2015). Cs^{+} and Sr^{2+} adsorption selectivity of zeolites in relation to radioactive decontamination. *Journal of Asian Ceramic Societies,* Vol. 3, pp 245-250.

Mustafa, Y. A. and Zaiter, M. J. (2011). Treatment of radioactive liquid waste (Co-60) by sorption on Zeolite Na-A prepared from Iraqi kaolin. *Journal of Hazardous Materials,* Vol. 196, pp 228-233.

Nagrockiene, D. and Girskas, G. (2016). Research into the properties of concrete modified with natural zeolite, Addition, Department of Building Materials, Vilnius Gediminas Technical University, Lithuania, Research Institute of Buildings Materials and Products, Vilnius Gediminas Technical University. *Construction and Building Materials,* Vol. 113, pp 964-969.

Nakhli, S. A. A., Delkash, M., Bakhshayesh, B. E. and Kazemian H. (2017). Application of zeolites for sustainable agriculture: A review on water and nutrient retention. *Water Air Soil Pollution,* Vol. 228, No. 12, DOI:10.1007/s11270-017-3649-1.

Nascimento, M., Soares, P. S. M. and Souza, V. P. D. (2009). Adsorption of heavy metal cations using coal fly ash modified by hydrothermal method. *Fuel,* Vol. 88, pp 1714-1719.

Neppolian, B., Mine, S., Horiuchi, Y., Bianchi, C. L., Matsuoka, M., Dionysiou, D. D. and Anpo, M. (2016). Efficient photocatalytic degradation of organics present in gas and liquid phases using Pt-TiO_2/Zeolite (H-ZSM). *Chemosphere,* Vol. 153, pp 237-243.

Nibou, D., Mekatel, H., Amokrane, S., Barkat, M., Trari, M. (2010). Adsorption of Zn^{2+} ions onto NaA and NaX zeolites: Kinetic, equilibrium and thermodynamic studies. *Journal of Hazardous Materials*, Vol. 173, pp 637-646.

Obaid, S. S., Gaikwad, D. K., Sayyed, M. I., Khader, A. R. and Pawar, P. P. (2018). Heavy metal ions removal from waste water by the natural zeolites. *Materials Today: Proceedings,* Vol. 5, No. 9, pp 17930-17934.

Olguin, M. T., Solache-Rios, M., Acosta, D., Bosch, P. and Bulbulian, S. (1999). Uranium sorption in zeolite X: the valence effect. *Microporous and Mesoporous Materials,* Vol. 28, pp 377-385.

Özyürek, I. N., Kıranşan, M. and Karaca, S. (2021). Investigation of the removal of sulfamethoxazole drug waste from aqueous solutions under the effect of zinc oxide/montmorillonite nanocomposite by photocatalytic ozonation process. *Desalination and Water Treatment,* Vol. 242, pp 144-161. Doi: 10.5004/dwt.2021.27847.

Pahlavanzadeh, H. and Motamedi, M. (2020). Adsorption of nickel, Ni(II), in aqueous solution by modified zeolite as a cation-exchange adsorbent. *Journal of Chemical & Engineering Data,* Vol. 65, pp 185-197.

Panayotova, M. and Velikov, B. (2003). Influence of zeolite transformation in a homoionic form on the removal of some heavy metal ions from wastewater. *Journal of Environmental Science and Health Part A,* Vol. 38, No. 3, pp 545-554.

Panic, V. V. and Velickovic, S. J. (2014). Removal of model cationic dye by adsorption onto poly (methacrylic acid)/zeolite hydrogel composites: kinetics, equilibrium study and image analysis. *Separation and Purification Technology,* Vol. 122, pp 384-394.

Payne, K. B. and Abdel-Fattah, T. M. (2004). Adsorption of divalent lead ions by zeolites and activated carbon: Effects of pH, temperature, and ionic strength. *Journal of Environmental Science and Health Part A,* Vol. 39, No. 9, pp 2275-2291.

Payra, P. and Dutta, P. K. (2003). Zeolites: A Primer. In S.M. Auerbach, K. Carrado, P.K. Dutta, eds. Handbook of zeolite science and technology. New York: Marcel Dekker Inc. Ch.1.

Peng, S., Hao, K., Han, F., Tang, Z., Niu, B., Zhang, X., Wang, Z. and Hong, S. (2015). Enhanced removal of bisphenol-AF onto chitosan-modified zeolite by sodium cholate in aqueous solutions. *Carbohydrate Polymers,* Vol. 130, pp 364-371

Perez-Perez, T., Pereda-Reyes, I., Pozzi, E., Oliva-Merencio, D. and Zaiat, M. (2018). Performance and stability of an expanded granular sludge bed reactor modified with zeolite addition subjected to step increases of organic loading rate (OLR) and to organic shock load (OSL). *Water Science and Technology,* Vol. 77, No. 1, pp 39-50.

Pirc, G. and Stare J. (2008). Titanium site preference problem in the TS-1 zeolite catalyst: A periodic hartree-fock study. *Acta Chimica Slovenica,* Vol. 55, pp 951-959.

Prasad, B. and Kumar, H. (2016). Treatment of acid mine drainage using a fly ash zeolite column. *Mine Water and the Environment,* Vol. 35, pp 553-557.

Primo, A. and Garcia, H. (2014). Zeolites as catalysts in oil refining. *Chemical Society Reviews,* Vol. 43, pp 7548-7561.

Qin, B., Zhang W. X , Zhang Z. Z., Ling X. F. and Sun F. W. (2011). Synthesis, characterization and catalytic properties of Y-beta zeolite composites. *Petroleum Science,* Vol. 8, No. 2, pp 224-228.

Rad, L. R., Momeni, A., Ghazani, B. F., Irani, M., Mahmoudi, M. and Noghreh, B. (2014). Removal of Ni^{2+} and Cd^{2+} ions from aqueous solutions using electrospun PVA/zeolite nanofibrous adsorbent. *Chemical Engineering Journal,* Vol. 256, pp 119-127.

Rahmani, A. R., Mahvi, A. H., Mesdaghinia, A. R. and Nasseri, S. (2004). Investigation of ammonia removal from polluted waters by Clinoptilolite zeolite. International. *Journal of Environmental Science and Technology,* Vol. 1, pp 125-133.

Rajos-Valencia, M. N., Espejel-Ayala, F., Marin, S. and Ramirez-Zamora, R. J. (2014). Technology synthesis of zeolite using paper industry sludge as raw material, *J. Res. Sci. Technol.,* Vol. 11, pp 21-27.

Rakic, V., Damjanovic, L., Rac, V., Stosic, D., Dondur, V. and Auroux, A. (2010). The adsorption of nicotine from aqueous solutions on different zeolite structures. *Water Research,* Vol. 44, pp 2047-2057.

Rashed, M. N. and Palanisamy, P. N. (2018). Introductory chapter: Adsorption and ion exchange properties of zeolites for treatment of polluted water. In: Zeolites and Their Applications. *IntechOpen*, pp 3-10.

Reeve, P. J. and Fallowfield, H. J. (2018). Natural and surfactant modified zeolites: A review of their applications for water remediation with a focus on surfactant desorption and toxicity towards microorganisms. *Journal of Environmental Management*, Vol. 205, pp 253-261.

Rehan, M., Miandad, R. and Barakat, M. A. (2017). Effect of zeolite catalysts on pyrolysis liquid oil. *International Biodeterioration and Biodegradation*, Vol. 119, pp 162-175.

Ren, X., Liu, S., Qu, R., Xiao, L., Hu, P., Song, H., Wu, W., Zheng, C., Wu, X. and Gao, X. (2020). Synthesis and characterization of single-phase submicron zeolite Y from coal fly ash and its potential application for acetone adsorption. *Microporous and Mesoporous Materials*, Vol. 295, pp 109940.

Reungoat, J., Pic, J. S., Manero, M. H. and Debellefontaine, H. (2007). Adsorption of nitrobenzene from water onto high silica zeolites and regeneration by ozone. *Separation Science and Technology*, Vol. 42, pp 1447-1463

Rhodes, C. J. (2010). Properties and applications of zeolites. *Science Progress*, Vol. 93, pp 223-284.

Richardeau, D., Joly, G., Canaff, C., Magnoux, P., Guisnet, M., Thomas, M. and Nicolaos, A. (2004). Adsorption and reaction over HFAU zeolites of thiophene in liquid hydrocarbon solutions. *Applied Catalysis A: General*, Vol. 263, pp 49-61.

Roque-Malherbe, R. (2000). Complementary approach to the volume filling theory of adsorption in zeolites. *Microporous and Mesoporous Materials*, Vol. 41, pp 227-240.

Ruenngam, D., Rungsuk, D., Apiratikul, R. and Pavasant, P. (2009). Zeolite formation from coal fly ash and its adsorption potential. *Journal of the Air & Waste Management Association*, Vol. 59, pp 1140-1147.

Rungsirisakun, R., Nanok, T., Probst, M. and Limtrakul, J. (2006). Adsorption and diffusion of benzene in the nanoporous catalysts FAU, ZSM-5

and MCM-22: a molecular dynamics study. *Journal of Molecular Graphics and Modelling,* Vol. 24, pp 373-382.

Runtti, H., Tynjala, P., Tuomikoski, S., Kangas, T., Hu, T., Ramo, J. and Lassi, U. (2017). Utilisation of barium-modified analcime in sulphate removal: isotherms, kinetics and thermodynamics studies. *Journal of Water Process Engineering,* Vol. 16, pp 319-328.

Saka, C., Eygi, M. S. and Balbay, A. (2021). Cobalt loaded organic acid modified kaolin clay for the enhanced catalytic activity of hydrogen release via hydrolysis of sodium borohydride. *International Journal of Hydrogen Energy,* Vol. 46, pp 3876-3886.

Salehi, S., Alijani, S. and Anbia, M. (2020). Enhanced adsorption properties of zirconium modified chitosan-zeolite nanocomposites for vanadium ion removal. *International Journal of Biological Macromolecules,* Vol. 164, pp 105-120.

Salminen, E., Kumar, N., Virtanen, P., Tenho, M., Maki-Arvela, P. and Mikkola, J. P. (2013). Etherification of 5-hydroxymethylfurfural to a biodiesel component over ionic liquid modified zeolites. *Topics in Catalysis,* Vol. 56, pp 765-769.

Saltalı, K., Sarı, A. and Aydın, M. (2007). Removal of ammonium ion from aqueous solution by natural Turkish (Yıldızeli) zeolite for environmental quality. *Journal of Hazardous Materials,* Vol. 141, No. 1, pp 258-263.

Sarıoglu, M. (2005). Removal of ammonium from municipal wastewater using Turkish (Dogantepe) zeolite. *Separation and Purification Technology,* Vol. 41, pp 1-11.

Schick, J., Caullet, P., Paillaud, J. L., Patarin, J. and Mangold-Callarec, C. (2010). Batch-wise nitrate removal from water on a surfactant-modified zeolite. *Microporous and Mesoporous Materials,* Vol. 132, pp 395-400.

Shah, B. A., Mistry, C. B. and Shah, A. V. (2013). Sequestration of Cu(II) ve Ni(II) from wastewater by synthesized zeolitic materials: Equilibrium, kinetics ve column Dynamics. *Chemical Engineering Journal,* Vol. 220, pp 172-184.

Shi, Y. C., Xing, E. H., Wu, K. J., Wang, J. L., Yang, M. D. and Wu, Y. L. (2017). Recent progress on upgrading of bio-oil to hydrocarbons over metal/zeolite bifunctional catalysts. *Catalysis Science and Technology,* Vol. 7, pp 2385-2415.

Shirani, M., Semnani, A., Habibollahi, S., Haddadi, H. and Narimani, M. (2016). Synthesis and application of magnetic NaY zeolite composite immobilized with ionic liquid for adsorption desulfurization of fuel using response surface methodology. *Journal of Porous Materials,* Vol. 23, pp 701-712.

Simon, V., Thuret, A., Candy, L., Bassil, S., Duthen, S., Raynaud, C. and Masseron, A. (2015). Recovery of hydroxycinnamic acids from renewable resources by adsorption on zeolites. *Chemical Engineering Journal,* Vol. 280, pp 748-754.

Song, W., Shi, T., Yang, D., Ye, J., Zhou, Y. and Feng, Y. (2015). Pretreatment effects on the sorption of Cr(VI) onto surfactant-modified zeolite: mechanism analysis. *Journal of Environmental Management,* Vol. 162, pp 96-101.

Stacey, Z. I., Christopher, L. M., Dan, X., Tracy, D. M., Joel, S. E. and Robert S. J. (2020). Studies on the use of faujasite as a reagent to deliver silica and alumina in building new zeolite structures with organo-cations. *Microporous and Mesoporous Materials,* Vol. 300, pp 110162.

Su, S., Ma, H. and Chuan, X. (2016). Hydrothermal synthesis of zeolite A from K-feldspar and its crystallization mechanism. *Advances Powder Technology,* Vol. 27, No. 1, pp 139-144.

Sun, Z., Li, C. and Wu, D. (2010). Removal of methylene blue from aqueous solution by adsorption onto zeolite synthesized from coal fly ash and its thermal regeneration. *Journal of Chemical Technology & Biotechnology,* Vol. 85, pp 845-850.

Sun, S., Wang, L., Huang, S., Tu, T. and Sun, H. (2011). The effect of capping with natural and modified zeolites on the release of phosphorus and organic contaminants from river sediment. *Frontiers of Chemical Science and Engineering,* Vol. 5, pp 308-313.

Suzuki, K., Noda, T., Sastre, G., Katada, N. and Niwa, M. (2009). Periodic density functional calculation on the bronsted acidity of modified Y-

type zeolite. *The Journal of Physical Chemistry C,* Vol. 113, pp 5672-5680.

Taffarel, S. R. and Rubio, J. (2009). On the removal of Mn^{2+} ions by adsorption onto natural and activated Chilean zeolites. *Minerals Engineering,* Vol. 22, No. 4, pp 336-343.

Taheri, S. H., Heidarpour, M., Shayannejad, M., Shariatmadari, H., Kazemian, H. and Afyuni, M. (2019). Composts containing natural and Mg-modified zeolite: the effect on nitrate leaching, drainage water and yield. *Clean-Soil Air Water,* Vol. 47, No. 8, pp 1800257.

Taheri Soudejani, H., Heidarpour, M., Shayannejad, M. and George, P. (2018). Incorporation of Mg-modified zeolite in municipal solid waste compost reduces heavy metal concentration in soil and corn plant. *Journal of Biodiversity and Environmental Sciences (JBES),* Vol. 12, pp 361-369.

Taheri Soudejani, H., Heidarpour, M., Shayannejad, M., Kazemian, H., Shariatmadari, H. and Afyuni, M. (2019). Improving quality of municipal solid waste compost through Mg-modified zeolite. *Journal of Agricultural Science and Technology,* Vol. 21, pp 747-760.

Tavasoli, M., Kazemian, H., Sadjadi, S. and Tamizifar, M. (2014). Synthesis and characterization of zeolite NaY using kaolin with different synthesis methods. *Clay Minerals,* Vol. 62, pp 508-518.

Tawfik, A. S., Gaddafi, I. D. and Taye Damola, S. (2016). Nanocomposites and hybrid materials for adsorptive desulfurization, in: A.S. Tawfik (Ed.), Applying Nanotechnology to the Desulfurization Process in Petroleum Engineering. *IGI Global, Hershey, PA, USA 2016,* pp 129-153.

Terbouche, A., Ramdane-Terbouche, C. A., Hauchard, D. and Djebbar, S. (2011). Evaluation of adsorption capacities of humic acids extracted from Algerian soil on polyaniline for application to remove pollutants such as Cd(II), Zn(II) and Ni(II) and characterization with cavity microelectrode. *Journal of Environmental Sciences (China),* Vol. 23, pp 1095-1103.

Tran, H. N., Viet, P. V. and Chao, H. P. (2018). Surfactant modified zeolite as amphiphilic and dual-electronic adsorbent for removal of cationic and

oxyanionic metal ions and organic compounds. *Ecotoxicology and Environmental Safety,* Vol. 147, pp 55-63.

Triantafyllidis, K. S., Vlessidis, A. G., Nalbandian, L. and Evmiridis, N. P. (2001). Effect of the degree and type of the dealumination method on the structural, compositional and acidic characteristics of H-ZSM-5 zeolites. *Microporous and Mesoporous Materials,* Vol. 47, pp 369-388.

Tsai, W. T., Hsu, H. C., Su, T. Y., Lin, K. Y. and Lin, C. M. (2006). Adsorption characteristics of bisphenol-A in aqueous solutions onto hydrophobic zeolite. *Journal of Colloid and Interface Science,* Vol. 299, pp 513-519.

Tsujiguchi, M., Kobashi, T., Oki, M., Utsumi, Y., Kakimori, N. and Nakahira, A. (2014a). Synthesis and characterization of zeolite a from crushed particles of aluminoborosilicate glass used in LCD panels. *Journal of Asian Ceramic Societies,* Vol. 2, pp 27-32.

Tsujiguchi, M., Kobashi, T., Utsumi, Y., Kakimori, N. and Nakahira, A. (2014b). Synthesis of zeolite A from aluminoborosilicate glass used in glass substrates of liquid crystal display panels and evaluation of its cation exchange capacity. *Journal of the American Ceramic Society,* Vol. 97, pp 114-119.

Turkman, A., Aslan, S. and Ege, I. (2004). Treatment of metal containing wastewaters by natural zeolites. *Fresenius Environmental Bulletin,* Vol. 13, pp 574-579.

Ugrina, M., Ceru, T., Nuic, I. and Trgo, M. (2020). Comparative study of mercury(Ii) removal from aqueous solutions onto natural and iron-modified clinoptilolite rich zeolite. *Processes,* Vol. 8, pp 1-21.

Unaldı, T., Orhun, O. and Kadir, S. (2009). Physicochemical characterization of natural ve Na^+ -, K^+ -, Ca^{2+} - ve Mg^{2+} -modified clinoptilolite from Gördes (Manisa, Turkey). *Adsorption Science & Technology,* Vol. 27, No. 6, pp 615-631.

Valdes, M. G., Cordoves, A. I. P. and Garcia, M. E. D. (2006). Zeolites and zeolite based materials in analytical chemistry. *Trends in Analytical Chemistry,* Vol. 25, No. 1, pp 24-30.

Venglovsky, J., Sasakova, N., Vargova, M., Pacajova, Z., Placha, I., Petrovsky, M. and Harichova, D. (2005). Evolution of temperature

and chemical parameters during composting of the pig slurry solid fraction amended with natural zeolite. *Bioresource Technology*, Vol. 96, No. 2, 181-189.

Verrecchia, G., Cafiero, L., Caprariis, B. D., Dell, A., Pettiti, I., Tuffi, R., Scarsella, M., Casaccia, E., Anguillarese, V. and Galeria, S. M. (2020). Study of the parameters of zeolites synthesis from coal fly ash in order to optimize their CO_2 adsorption. *Fuel*, Vol. 276, pp 118041.

Vicente, J. G. P., Lima, P. M. and Cardoso, D. (2017). Nanosized particles of X zeolite containing ammonium cations as basic catalysts. *Catalysis Letters*, Vol. 147, pp 880-892,

Vidal, C. B., Barros, A. L., Moura, C. P., De Lima, A. C., Dias, F. S., Vasconcellos, L. C., Fechine, P. B. and Nascimento, R. F. (2011). Adsorption of polycyclic aromatic hydrocarbons from aqueous solutions by modified periodic mesoporous organosilica. *Colloid Interface Science*, Vol. 357, pp 466-473.

Villasenor, J., Rodriguez, L. and Fernandez, F. J. (2011). Composting domestic sewage sludge with natural zeolites in a rotary drum reactor. *Bioresource Technology*, Vol. 102, pp 1447-1454.

Wahono, S. K., Stalin, J., Addai-Mensah, J., Skinner, W., Vinu, A. and Vasilev, K. (2020). Physico-chemical modification of natural mordenite-clinoptilolite zeolites and their enhanced CO_2 adsorption capacity. *Microporous and Mesoporous Materials*, Vol. 294, pp 109871.

Wajima, T., Haga, M., Kuzawa, K., Ishimoto, H., Tamada, O., Ito, K., Nishiyama, T., Downs, R. T. and Rakovan, J. F. (2006). Zeolite synthesis from paper sludge ash at low temperature (90°C) with addition of diatomite. *Journal of Hazardous Materials*, Vol. 132, pp 244-252.

Wang, Y. F., Lin, F. and Pang, W. Q. (2007). Ammonium exchange in aqueous solution using Chinese natural clinoptilolite and modified zeolite. *Journal of Hazardous Materials*, Vol. 142, pp 160-164.

Wang, S. and Peng, Y. (2010). Natural zeolites as effective adsorbents in water and wastewater treatment, Department of Chemical Engineering, Curtin University of Technology, Australia, College of

Environmental and Energy Engineering, Beijing University of Technology. *Chemical Engineering Journal,* p 11-24.

Wang, X. and Yan, C. (2010). Synthesis of nano-sized NaY zeolite composite from metakaolin by ionothermal with microwave assisted. *Inorganic Materials,* Vol. 46, pp 517-521.

Wang, X., Özdemir, O., Hampton, M. A., Nguyen, A. V. and Do, D. D. (2012). The effect of zeolite treatment by acids on sodium adsorption ration of coal seam gas water. *Water Research,* Vol. 46, pp 5247-5254.

Watanabe, Y., Yamada, H., Kokusen, H., Tanaka, J., Moriyoshi, Y. and Komatsu, Y. (2003). Ion exchange behavior of natural zeolites in distilled water, hydrochloric acid and ammonium chloride solution. *Separation Science and Technology,* Vol. 38, pp 1519-1532.

Weckhuysen, B. M. and Yu, J. (2015). Recent advances in zeolite chemistry and catalysis. *Chemical Society Reviews,* Vol. 44, pp 7022-7024.

Weitkamp, J. (2000). Zeolites and Catalysis. Solid State Ionics, 131, 175-188.

Wen, J., Yi, Y. and Zeng, G. (2016). Effects of modified zeolite on the removal and stabilization of heavy metals in contaminated lake sediment using BCR sequential extraction. *Journal of Environmental Management,* Vol. 178, pp 63-69.

Wibowo, E., Sutisna Rokhmat, M., Murniati, R., Khairurrijal and Abdullah, M. (2017). Utilization of natural zeolite as sorbent material for seawater desalination. *Process Engineering,* Vol. 170, pp 8-13.

Wingenfelder, U., Hansen, C., Furrer, G. and Schulin, R. (2005). Removal of heavy metals from mine waters by natural zeolites. *Environmental Science & Technology,* Vol. 39, pp 4606-4613.

Wittayakun, J., Khemthong, P. and Prayoonpokararch. S. (2008). Synthesis of characterization of zeolite NaY from rice husk silica. *Korean Journal of Chemical Engineering,* Vol. 25, pp 861-864.

Wong, S. L., Tuan Abdullah, T. A., Ngadi, N., Ahmad, A. and Inuwa, I. M. (2016). Parametric study on catalytic of LDPE to liquid fuel over ZSM-5 zeolite. *Energy Conversion and Management,* Vol. 122, pp 428-438.

Wu, Z. C., An, Y., Wang, Z. W., Yang, S., Chen, H. Q., Zhou, Z. and Mai, S. H. (2008). Study on zeolite enhanced contact-adsorption regeneration-

stabilization process for nitrogen removal. *Journal of Hazardous Materials,* Vol. 156, No. 1-3, pp 317-326.

Wu, Y., Ren, X. and Wang, J. (2009). Facile synthesis and morphology control of zeolite MCM-22 via a two-step sol-gel route with tetraethyl orthosilicate as silica source. *Materials Chemistry and Physics,* Vol. 113, pp 773-779.

Xie, J., Meng, W., Wu, D., Zhang, Z. and Kong, H. (2012). Removal of organic pollutants by surfactant modified zeolite: Comparison between ionizable phenolic compounds and non-ionizable organic compounds. *Journal of Hazardous Materials,* Vol. 231, pp 57-63.

Yi, D., Huang, H., Meng, X. and Shi, L. (2014). Adsorption-desorption behavior and mechanism of dimethyl disulfide in liquid hydrocarbon streams on modified Y zeolites. *Applied Catalysis B: Environmental,* Vol. 148-149, pp 377-386.

Yoldi, M., Fuentes-Ordonez, E. G., Korili, S. A. and Gil, A. (2019). Zeolite synthesis from industrial wastes. *Microporous and Mesoporous Materials,* Vol. 287, pp 183-191.

Yonli, A. H., Batonneau-Gener, I. and Koulidiati, J. (2012). Adsorptive removal of alpha-endosulfan from water by hydrophobic zeolites. An isothermal study. *Journal of Hazardous Materials,* Vol. 203, pp 357-362.

Yu, W. B., Deng, L. L., Yuan, P., Liu, D., Yuan, W. W. and Chen. F. R. (2015). Preparation of hierarchically porous diatomite/MFI-Type zeolite composites and their performance for benzene adsorption: The effects of desilication. *Chemical Engineering Journal,* Vol. 270, pp 450-458.

Yuna, Z. (2016). Review of the natural, modified, and synthetic zeolites for heavy metals removal from wastewater. *Environmental Engineering Science,* Vol. 33, pp 443-454.

Zaidun, S. W., Jalloh, M. B., Awang, A., Sam, L. M., Besar, N. A., Musta, B., Ahmed, O. H. and Omar, L. (2019). Biochar and clinoptilolite zeolite on selected chemical properties of soil cultivated with maize (Zea mays L.). *Eurasian Journal of Soil Science,* Vol. 8, pp 1-10.

Zaitan, H., Manero, M. H. and Valdes, H. (2016). Application of high silica zeolite ZSM-5 in a hybrid treatment process based on sequential

adsorption and ozonation for VOCs elimination. *Journal of Environmental Science,* Vol. 41, pp 59-68.

Zeng, Y., Woo, H., Lee, G. and Park, J. (2010). Adsorption of Cr (VI) on hexadecylpyridinium bromide (HDPB) modified natural zeolites. *Microporous and Mesoporous Materials,* Vol. 130, pp 83-91.

Zhang, H., Li, A., Zhang, W. and Shuang, C. (2016). Combination of Na-modified zeolite and anion exchange resin for advanced treatment of a high ammonia-nitrogen content municipal effluent. *Journal of Colloid Interface Science,* Vol. 468, pp 128-135.

Zhang, X., Li, X., Zhang, F., Peng, S., Tumrani, S. H. and Ji, X. (2019). Adsorption of Se(IV) in aqueous solution by zeolites synthesized from fly ashes with different compositions. *Journal of Water Reuse and Desalination,* Vol. 9, pp 506-519.

Zhang, Y., Mancke, R. G., Sabelfeld, M. and Geissen, S. U. (2014). Adsorption of trichlorophenol on zeolite and adsorbent regeneration with ozone. *Journal of Hazardous Materials,* Vol. 271, pp 178-184.

Zhang, Z. Y., Shi, T. B., Jia, C. Z., Ji, W. J., Chen, Y. and He, M. Y. (2008). Adsorptive removal of aromatic organosulfur compounds over the modified Na-Y zeolites. *Applied Catalysis B Environmental,* Vol. 82, pp 1-10.

Zhang, G. X., Song, A. K., Duan, Y. W. and Zheng, S. L. (2018). Enhanced photocatalytic activity of TiO_2/zeolite composite for abatement of pollutants. *Microporous and Mesoporous Materials,* Vol. 255, pp 61-68.

Zhao, H. T., Vance, G. F., Urynowicz, M. A. and Gregory, R. W. (2009). Integrated treatment process using a natural Wyoming clinoptilolite for remediating produced waters from coalbed natural gas operation. *Applied Clay Science,* Vol. 42, pp 379-385.

Zheng, S., Heydenrych, H. R., Jentys, A. and Lercher, J. A. (2002). Influence of surface modification on the acid site distribution of HZSM-5. *The Journal of Physical Chemistry B,* Vol. 106, pp 9552-9558.

Zhijian, W., Wei, W. U., Wan, C., Hong, Y. and Dongke, Z. (2014). Direct synthesis of hierarchical ZSM-5 zeolite and its performance in catalyzing methanol to gasoline conversion. *Industrial & Engineering Chemistry Research,* Vol. 53, No. 50, pp 19471-19478.

Zhou, Z., Jin, G., Liu, H., Wu, J. and Mei, J. (2014). Crystallization mechanism of zeolite A from coal kaolin using a two-step method. *Applied Clay Science,* Vol. 97-98, pp 110-114.

Zhu, T., Zhang, X., Han, Y., Liu, T., Wang, B. and Zhang, Z. (2019). Preparation of zeolite X by the aluminum residue from coal fly ash for the adsorption of volatile organic compounds. *Frontiers in Chemistry,* Vol. 7, pp 1-8.

Zorpas, A. A., Inglezakis, V., Loizidou, M. and Grigoropoulou, H. (2002). Particle size effects on uptake of heavy metals from sewage sludge compost using natural zeolite clinoptilolite. *Journal of Colloid Interface Science,* Vol. 250, No. 1, pp 1-4.

Zorpas, A. A., Inglezakis, V. J. and Loizidou, M. (2008). Heavy metals fractionation before, during and after composting of sewage sludge with natural zeolite. *Waste Management,* Vol. 28, pp 2054-2060.

CHAPTER 8

BIONANOCOMPOSITES AS FUNGICIDE AGAINST PHYTOPATHOGENIC FUNGI

Assoc. Prof. Hilal ACAY[1], Assist. Prof. Dr. Ayfer YILDIRIM[2]

[1] Department of Nutrition and Dietetics, Faculty of Health Science, Mardin/Turkey
hilalacay@gmail.com, ORCID ID: https://orcid.org/0000-0002-7732-106X
[2] Mardin Artuklu University, Vocational School of Health Services, Mardin/Turkey
ayferyildirim@artuklu.edu.tr ORCID ID: https://orcid.org/0000-0002-2079-4587

INTRODUCTION

Over the past decades, the amount of plastic continues to increase as it is used in many different applications. The main plastics derived from non-renewable resources such as polyvinylchloride, polypropylene, polyethylene, polystyrene are unfortunately not biodegradable, and their enzymatic degradation requires a very long process. As a result, ecological pollution and global warming are threatened all over the planet due to the difficulties in both disposal and recycling of this large amount of plastic waste produced (Díez-Pascual, 2021). Thus, current research focuses on developing biodegradable biopolymers as potential candidates to replace petroleum-synthetic polymers to overcome these disadvantages.

Nowadays, nanomaterials synthesis is becoming popular when considering materials science. The introduction of biological approaches helps transform basic science into nanomaterials and tools. This creates better sustainability by developing new materials and improving existing materials (Kozielski et al., 2013) Indeed, many of these nano-materials particularly bionanocomposites, are manufactured at a large scale and currently used in various application fields involving biomedical, packaging, agriculture, automotive, etc. (Yildirim and Acay, H. 2021.)

Friedrich (2015) states that the expected population density in the next 30 years will be 9.2 billion and global food production will be approximately 70%. This can only be achieved through the application of sustainable, nutritious food supply and safe innovative techniques.

The literature study, it is stated that nanomaterials synthesized by chemical, physical and biological methods can be an important tool in the protection of the product such as filtration of irrigation water, improvement of harmful phytopathogenic pesticides, development of new degradable pesticides, plant disease control, the effective introduction of fertilizers and other agricultural chemicals to the use of organic agriculture (Barık et al., 2008; Prasad et al., 2014).

Although nanomaterials synthesized by physical and chemical means are used quite frequently, the presence of toxic chemicals limits their applications in agriculture, and interest in biological production is increasing (Yildirim, and Acay, 2021).

In this chapter, the antifungal applications of green synthesis composites, which is an important area of nanotechnology, against plant

pathogens, which are important issues in the agricultural sector, were evaluated.

1. BIONANOCOMPOSITES

Nanocomposites are a class of nanostructured hybrid materials formed by the combination of a matrix that can be a biodegradable polymer (bionanocomposites) or a synthetic polymer (nanocomposite) that also has a charge that can be an inorganic/organic solid with at least one of its nanoscale dimensions (Garrido-Miranda, Rivas, Perez-Rivera, Sanfuentes, Pena-Fartal, 2018; Basavegowda, and Baek, 2021).

In the recent past, the concept of bionanocomposites has been widely used in research areas. These materials are emerging as a group of emerging nanostructured bio-hybrid materials containing a biopolymer (naturally occurring polymer) in combination with reinforcements, obtained from the combination of biopolymers such as polysaccharides, nucleic acid, proteins, and essential oils showing at least one dimension on the nanometer scale. In addition to the natural properties of biopolymers, these new composite materials are being developed very well in terms of their physical, structural, and functional properties and synergistic activities with the help of nano-reinforcements and may produce a synergistic antifungal effect for many applications. Bionanocomposites exhibit improved biological, thermal, mechanical, magnetic, optical, photoelectronic properties (Karimi-Maleh et al., 2021).

In the literature, definitions such as biocomposites, nano-sized biopolymers, nanocomposites, nanobiocomposites, green composites, biohybrids, or bio-based plastics, and similar approaches have been encountered to define an emerging class of biohybrid materials that show dimensions in the nanometer range. In this context, the definition of bionanocomposites would be very appropriate because they are both nano-structured and obtained from combinations of biologically origin materials such as polysaccharides, proteins, and nucleic acids with inorganic solids at the nanometric scale. Green and environmentally friendly bionanocomposites replace traditional materials within the framework of the promotion of research that reduces environmental damage and are preferred in various fields including food packaging biomedical materials, drug delivery systems, agriculture sector, sensing, and electronic materials to create a forward-looking process that does not harm the environment (Darder et al., 2011).

Thanks to their multidimensional properties such as biocompatibility, antimicrobial activity, and biodegradability, bionanocomposites can be widely used in various fields and show good properties (mechanical, optical, etc.) compared to both micro and macro composites (Amina et al., 2011).

2. FUNGAL PATHOGENS

Plant pathogens are of two types, biotic factors involving microorganisms and parasitic plants, and abiotic factors including all environmental factors. Plant pathology has common fields of study with sciences such as entomology, bacteriology, mycology, virology, and herbology due to its relationship in insects, bacteria, fungi, viruses/viroids, and weeds as plant pests (Bruehl, 1991).

The modern approach of plant disease control, which is environmentally friendly and suitable for human and animal health, depends on the production of antimicrobial agents that can be developed with new green synthesis methods, the production of genetically improved plant strains that are resistant to plant diseases by biotechnological methods, and the discovery of new biological control agents (Cramer, 1967).

It is stated that fungal pathogens, which have approximately 1.5 million species in the mushroom kingdom, and also phytopathogenic fungi comprise an important group of plant pathogens that cause approximately $45 billion in crop losses every year all over the (Pimentel, 2009).

These fungal pathogens, either parasitic or saprophytic, cause different diseases in agricultural products. While fungal pathogens such as Rhizoctonia solani, Fusarium spp., Phythophora spp infect the aerial and soil parts of plants, Botrytis cinerea can cause disease in the green and fruit tissues of more than 200 plant varieties. However, some plant pathogens may be responsible for fruit damage during distribution and storage. (Fernández-Acero, Carbú, Garrido, Inmaculada, Jesus Manuel, 2007)

As seen above, plant pathogens that can contaminate any plant tissue at different stages of crop growth can result in a significant loss of income. For example, Pimentel 2009 states that B. cinerea alone is responsible for 10% of the world fungicide market and this represents more than approximately 500 million Euros.

Since fungicides have positive advantages such as rapid action and high availability, disease control depends on the use of agricultural chemicals such as fungicides. However, adverse effects on non-target living organisms

due to their toxicity, systemic effects, resistance in target microorganisms, and revival of pest population are undesirable effects (Zaller, and Brühl, 2019; Stephenson, 2003). However, considering that approximately 80-90% of the fungicides are lost in the environment after or during application procedures (Stephenson, 2003). There is an urgent need to provide cost-effective, high-performance fungicides that can minimize the negative impact on the environment.

The applications of nanotechnology for innovative research in plant pathology represent a second revolution after biotechnology. Although the use of nanotechnology in agriculture was mostly theoretical until a few years ago, nanoformulation developments in the agricultural industry have started to increase in importance (Thul, and Sarangi, 2015).

Effective disease control is provided by nanofungicides, as they have different mechanisms compared to chemical fungicides, pose less risk compared to others with a very small amount of active substance in their structure, and allow the active substance to be released in a controlled manner. Also, to protect plants from pathogen attacks, soil, seed, or leaf The simplest application method is the direct application of nanoparticles to plant parts such as (Khan et al., 2014). Considering these features, the use and applicability of nanotechnology in the fight against diseases are quite remarkable. For all these reasons, new, environmentally friendly, inexpensive, sustainable alternatives in the fight against plant pathogens constitute a wide research area. Although studies on this subject are still in their infancy, they are quite interesting. This study examines the studies on nanocomposites with antifungal properties developed by the green synthesis method against fungal pathogens.

3. BIONANOCOMPOSITES AGAINST PHYTOPATHOGENIC FUNGI

Bionanocomposites, which are stable under difficult process conditions and have superior antimicrobial properties, have great potential in the management of different diseases. Bio-based materials such as chitosan show very rapid and significant development in recent years. Chitosan is a linear polysaccharide composed of randomly distributed β-(1–4)-linked D-glucosamine (deacetylated unit) and N-acetyl-D-glucosamine (acetylated unit). Chitosan is currently being extensively researched for the biomedical, pharmaceutical, agricultural, cosmetic, food, biotechnological, paper, water

treatment, and textile industries (Dananjaya et al., 2017; Shende, Oza and Gaud, 2018). Chitosan shows antitumoral, antifungal and antimicrobial activitiy. However, the very high molecular weight of Chitosan and therefore very high viscosity makes it insoluble in most solvents, narrowing many of its biological applications. For this reason, chitosan will be combined with other materials by chemical modification, thus maintaining the original physicochemical, biochemical properties without changing the basic skeleton of the biopolymer, with the modifications obtained, new properties will be gained depending on the nature of the added group, and as a result, a wider usage area will be obtained thanks to the superior properties of bionanocomposites.

Metal oxides are widely used due to their non-toxicity, high biocompatibility, and simple preparation processes. The antifungal activities of these materials are known. With the bionanocomposites that metal oxides will form in combination with other materials, they can become more altered and effective materials by changing their thermal, mechanical, photocatalytic, and chemical activities. Thus, thanks to the high surface-to-volume ratio of nanomaterials, the metal bionanocomposites formed in combination increase their contact with fungi and further improve their antifungal effects.

3.1. Chitosan-Based Bionanocomposites against Phytopathogenic Fungi

Due to the chemical properties of chitosan, the richness of its antifungal properties is known. In addition, an alternative to make biocomposite molecules is essential oils, which have antifungal, antibacterial, and antiviral biological properties. These oils are biomolecules and secondary metabolites synthesized by medicinal and aromatic plants with superior bioactivity. However, since these oils have properties that limit their usabilities, such as low water solubility, high volatility, and susceptibility to light, heat, and oxygen degradation, especially their volatility, superior biocomposites have been synthesized by combining them with other materials such as essential oil (Mohammadi et al., 2015, Zhaveh et al., 2015), polyvinyl alcohol (Perumal et al., 2022), Cellulose (Perumal et al., 2022), montmorillonite (Pankaj Jha, (2020b)) (Pola et al., 2019). When the studies in the literature are examined, it has been proven that the antifungal activity of essential oils with chitosan-based bionanocomposites is quite good (Mohammadi, Hashemi, & Hosseini, 2015; Zhaveh et al., 2015).

According to **Table 1,** it is seen that the bionanocomposite obtained by preparing chitosan with Thymol, the main antimicrobial agent of the aromatic plant thyme (Thymus vulgaris), showed very good (100%) antifungal inhibition against *Botrytis cinerea* (Medina et al., 2019). It is emphasized that the synergistic combination of both chitosan and essential oil creates a very good antifungal compound.

Table 1. Chitosan-Based Bionanocomposites for phytopathogenic fungi

Chitosan-based bionanocomposites	**Fungal Pathogens**	**Inhibition % / Inhibition zone(mm)**	**References**
Corn starch/ chitosan/ nanoclay/ sorbitol/ grapefruit seed extract	*Aspergillus niger*	25.59 ± 0.64 mm	Jha, (2020a)
Zataria multiflora (essential oil)/chitosan	*Botrytis cinerea*	50%	Mohammadi et al. (2015)
T. vulgaris (essential oil) / chitosan / benzoic acid	*Aspergillus flavus*		Khalili et al., (2015)
Chitosan/thymol	*Botrytis cinerea*	100%	Medina et al., (2019)
Cuminum cyminum (essential oil)/ chitosan / caffeic acid	*Aspergillus flavus*		Zhaveh et al., 2015
Cellulose/polyvinyl alcohol /chitosan	*C. gloeosporioide,L. theobromae*	67-69/40-41 %	Perumal et al., 2022
Grapefruit seed extract/chito-san/ montmorillonite	*Aspergillus niger*	22.29 ± 0.7 0.4 mm	Pankaj Jha, (2020b)
Chitosan/zinc	*Aspergillus flavus*	93%	Kaur et al. (2015)
Chitosan/carboxymethyl cellulose/zinc oxide	*Aspergillus niger*	40%	Noshirvani, Ghanbarzadeh,

			Mokarram, Hashemi, Coma, (2017)
Chitosan/*Schinus molle* (pepper tree) essential oil	*Aspergillus parasiticus*		Luque-Alcaraz et al. (2016)

ND: No Data

3.2. Metaloxide-Based Bionanocomposites Against Phytopathogenic Fungi

Metal oxide nanoparticles, which form an important class of materials in electrochemistry, magnetism, biology, and environmental science, have a stable structure and are considered safe for humans, are a very good alternative material as antifungal and antibacterial agents and have been recognized as an excellent agent for the control of pathogenic microbes. (Li et al., 2019; Safaei, & Taran, 2017).

In the literature, it has been proven that metal oxides strengthened with bio nanoparticles prepared by combining materials such as gelatin (Sahraee, Ghanbarzadeh, Milani, & Hamishehkar, 2017), alginate (Safaei, Taran, & Imani, 2019), cellulose (Guo, Wu, Li, & Sun, 2020), chitin (Sahraee et al. 2017), alginic acid (Zare, Lakouraj, Mohseni, & Motahari, 2015) and Pullulan (Pinto et al., 2013) show much more excellent antifungal properties against pathogenic fungi (**Table 2**).

Table 2. Metaloxide-Based Bionanocomposites for phytopathogenic fungi

Metaloxide-Based Bionanocomposites	**Fungal Pathogens**	**Inhibition % / Inhibition zone(mm)**	**References**
Carboxymethylcellulose-with plant-sourced cinnamaldehyde/zinc oxide nanoparticles	*Aspergillus niger*	ND	Guo et al. (2020)
Soybean protein isolate / plant-sourced	*Aspergillus niger*	ND	Li et al. (2019)

cinnamaldehyde/zinc oxide			
Alginate-copper oxide	*Aspergillus niger*	83.17%	Safaei et al. (2019)
Sodium hyaluronate/titanium dioxide	*Aspergillus niger*	13.3 mm	Safaei, and Taran (2017)
Gelatin/zinc oxide /chitin nanocomposite	*Aspergillus niger*	27.138±0.218 mm	Sahraee et al. (2017)
Pullulan/silver nanoparticles	*Aspergillus niger*	76%	Pinto et al. (2013)
Silver ions/ polyvinyl chloride	*Aspergillus niger*, *Fusarium solani*	13.5 mm	Braga, Rangel, Suarez, and Machado (2018)

ND: No data

3.3. Other Bionanocomposites Against Phytopathogenic Fungi

New alternative-bionanomaterials that are effective against microorganisms, diseases and do not harm the environment and the health of living things should be developed. In addition, in studies against fungal pathogens, montmorillonite clay (Garrido-Miranda et al., 2018), lysozyme (Feng et al., 2017), gum kondagogu (Malkapur, Devi, Rupula, and Sashidhar, 2017), cellulose (Ahmad et al., 2017; Zhou et al., 2018), protein isolate (Wu et al., 2019), solid lipid (Nasseri, Golmohammadzadeh, Arouiee, Jaafari, and Neamati, 2016), chitin (Sahraee, Ghanbarzadeh, Milani, Hamishehkar, 2017) based bionanocomposites have shown superior antifungal activity (**Table 3**).

In recent years, it has been proven that plant-derived essential oils and active ingredients have a very good antiseptic activity against bacteria and fungi. Among the tested plant-sourced essential oils, cinnamaldehyde is the most effective antifungal agent (Arezoo, Mohammadreza, Maryam, & Abdorreza, 2020).

More recently, the preparation of silver composites with biopolymer matrix has gained great importance due to their renewable nature, biocompatibility, and biodegradability. Recently, it has been proven that silver nanoparticles can be used as an excellent and very effective antimicrobial agent (Malkapur, Devi, Rupula, Sashidhar, 2017).

Garrido-Miranda et al. (2018) investigated the influence of eugenol on the Eugenol/poly(3-hydroxybutyrate)/thermoplastic starch/montmorillonite bionanocomposite with antifungal activity against *Botritys cinerea*. The antifungal activity was determined by calculating the area of inhibition of the bionanocomposites. The bionanocomposite after 7 days of contact with *Botritys cinerea*. As expected, this finding reflects the absence of antifungal activity of these components. Significant growth reductions against *Botrytis cinerea* were obtained with increasing eugenol concentrations in the bionanocomposites, where the greater area of inhibition was seen 6.4 ± 2.5 cm^2 (**Table 3**).

Table 3. Other Bionanocomposites for phytopathogenic fungi

Other Bionanocomposites	**Fungal Pathogens**	**Inhibition % / Inhibition zone**	**References**
Eugenol(essential oil)/ poly(3-hydroxybutyrate)/thermoplastic starch/ montmorillonite	*Botritys cinerea*	ND	Garrido-Miranda et al. (2018)
Polivinylalcohol/cyclodextrin/ cinnamon essential oil/ lysozyme	*Aspergillus niger, Penicillium*	**ND**	Feng et al. (2017)
Silver nanoparticles/gum kondagogu (*Cochlospermum gossypium*)	*Aspergillus parasiticus, Aspergillus flavus*	3.5-6.5 µg/ml	Malkapur et al. (2017)
Nickel doped polyaniline/cellulose	*Rhizoctonia solani,*	25-35 %	Ahmad et al. (2019)

	Alternaria alternate		
Soy protein isolate/plant-sourced cinnamaldehyde	*Aspergillus niger*	2.5 mm	Wu et al. (2019)
Z. multiflora (essential oil)/ Glyceryl monostearate (solid lipid)	*Aspergillus ochraceus, Aspergillus niger, Aspergillus flavus, Alternaria solani, Rhizoctonia solani, and Rhizopus stolonifer*	37-87 %	Nasseri et al. (2016)
Gelatin/chitin	*Aspergillus niger*	15.72 mm	Sahraee et al.(2017)
Methyl cellulose/plant essential oil(oregano: thyme)	*Aspergillus niger, A. flavus, A. Parasiticus, P. chrysogenum*	35-40 mm	Hossain et al. (2018)
Polylactic acid/chitin/glycerol triacetate	*Aspergillus niger*	70%	Herrera et al. (2016)

ND: No data

CONCLUSION

Although it is still in its infancy in the agriculture and food sector, it is seen that nanotechnology will offer much more application areas in the coming years. Nanoparticles, which form an excellent platform for various biological applications, are attracting more researchers' attention for future developments. More research is still needed to make agriculture environmentally friendly, avoid potential economic losses, make agrochemicals more effective through composite materials, formulate high-yield carrier composites, and find the best materials that are cost-effective, easily degradable, and can be incorporated into the soil after use. Also, considering the negative aspect of prolonged contact or exposure to some metal NPs such as AgNPs and AuNPs, some research has indicated, studies on green nanoparticles synthesized from natural products should be increased to make the environment safe and to protect humans and other plants, microorganisms and animals from risk. Given that the subject is new, materials researchers and biologists need to work to gain a deeper understanding of the main interactions and mechanisms in a bionanotechnology system.

REFERENCES

Ahmad, N. Sultana, S. Kumar, G. Zuhaib, M. Sabir, S. Khan, M. Z. (2019). Polyaniline based hybrid bionanocomposites with enhanced visible light photocatalytic activity and antifungal activity. *Journal of Environmental Chemical Engineering, 7(1),* 102804.

Amina, M. Al Musayeib, N. M. Al-Hamoud, G. A. Al-Dbass, A. El-Ansary, A. Ali, M.A. (2021). Prospective of biosynthesized L.satiVum oil/PEG/Ag-MgO bionanocomposite film for its antibacterial and anticancer potential. *Saudi Journal of Biological Sciences, 28,* 5971–5985.

Arezoo, E. Mohammadreza, E. Maryam, M. Abdorreza, M. N. (2020). The synergistic effects of cinnamon essential oil and nano TiO_2 on antimicrobial and functional properties of sago starch films. *International Journal of Biological Macromolecules, 157,* 743-751.

Barik, T. K. Sahu B. and Swain, V. (2008). Nanosilica-From medicine to pest control. *Parasitol. Res., 103,* 253-258.

Basavegowda, N.and Baek, K. H. (2021). Advances in Functional Biopolymer-Based Nanocomposites for Active Food Packaging Application. *Polymers., 13(23),* 4198.

Braga, L. R. Rangel, E. T. Suarez, P.A. Z. Machado, F. (2018). Simple synthesis of active films based on PVC incorporated with silver nanoparticles: Evaluation of the thermal, structural and antimicrobial properties. *Food Packaging and Shelf Life, 15,* 122-129.

Bruehl, G. W. (1991). Plant pathology, a changing profession in a changing world. *Annu Rev Phytopathol., 29,* 1–12.

characterization of active emulsified films based on chitosan-carboxymethyl cellulose containing zinc oxide nano particles. *Int. J. Biol. Macromol., 99,* 530-538.

chitosan-PVA film for synergistic antimicrobial activity, *Int. J. Polym. Mater. Polym., 67(18),* 1080-1086.

Cramer, H. H. (1967). Plant protection and crop production. 5th ed. Farbenfabriken Bayer AG; Leverkusen.

Dananjaya, S.H.S. Udayangani, R.M.C. Oh, C. Nikapitiya, C. Lee, J. Zoysa, M. D. (2017). Green synthesis, physio-chemical characterization and

anti-candidal function of a biocompatible chitosan gold nanocomposite as a promising antifungal therapeutic agent. *RSC Adv. 7(15),* 9182-9193.

Darder, M. Aranda, P. Ferrer, M. L. Guti´errez, M. C. Del Monte, F. Ruiz-Hitzky, E. (2011). Progress in bionanocomposite and bioinspired foams. *Adv. Mater., 23,* 5262–5267.

Díez-Pascual, A. M. (2021). Poly(3-hydroxybutyrate-co-3-hydroxyhexanoate) with zinc oxide nanoparticles for food packaging, *J. Food Process. Eng.*, e13814.

Feng, K. Wen, P. Yang, H. Li, N. Lou, W. Y. Zong, M. H. Wu, H. (2017). Enhancement of the antimicrobial activity of cinnamon essential oil-loaded electrospun nanofilm by the incorporation of lysozyme. *RSC Advances, 7(3),* 1572-1580.

Fernández-Acero, F. J. Carbú, M. Garrido, C. Inmaculada, V. Jesus Manuel, C. (2007). Proteomic advances in phytopathogenic fungi. *Curr Proteomics,* 4(2), 79-88.

Friedrich, T. (2015). A new paradigm for feeding the world in 2050 the sustainable intensification of crop production. *Resour. Mag., 22,* 18-18.

Garrido-Miranda, K. A. Rivas, B. L. Pérez-Rivera, M. A. Sanfuentes, E. A. Peña-Farfal, C. (2018). Antioxidant and antifungal effects of eugenol incorporated in bionanocomposites of poly(3-hydroxybutyrate)-thermoplastic starch. *LWT - Food Science and Technolog, Volume 98*, 260-267.

Guo, X. Wu, B.C.X. Li, J. Sun, Q. (2020). Utilization of cinnamaldehyde and zinc oxide nanoparticles in a carboxymethylcellulose-based composite coating to improve the postharvest quality of cherry tomatoes. *International Journal of Biological Macromolecules, 157,* 743–751.

Herrera, N. Roch, H. Salaberria, A. M. Pino-Orellana, M. A. Labidi, J. Fernandes, S. C.M. Radic, D. Leiva, A. Oksman, K. (2016). Functionalized blown films of plasticized polylactic acid/chitin nanocomposite: Preparation and characterization. *Materials and Design, 92*, 846–852.

Hossain, F. Follett, P. Vu, K.D. Salmieri, S. Fraschini, C. Jamshidian, M. Lacroix, M. (2018). Antifungal activity of combined treatments of

active methylcellulose-based films containing encapsulated nanoemulsion of essential oils and γ–irradiation: in vitro and in situ evaluations. Cellulose, 26 (2),1335-1354.

Jha, P. (2020a). Effect of plasticizer and antimicrobial agents on functional properties of bionanocomposite films based on corn starch-chitosan for food packaging applications. *International Journal of Biological Macromolecules, 160,* 571–582.

Jha, P. (2020b). Effect of grapefruit seed extract ratios on functional properties of corn starch-chitosan bionanocomposite films for active packaging. *International Journal of Biological Macromolecules, 163,* 1546–1556.

Karimi-Maleh, H. Ayati, A. Davoodi, R. Tanhaei, B. Karimi, F. Malekmohammadi, S. Orooji, Y. Fu, L. Sillanpää, M. (2021). Recent advances in using of chitosan-based adsorbents for removal of pharmaceutical contaminants: a review. *J. Clean. Prod, 291,* 125880.

Kaur, P. Thakur, R. Barnela, M. Chopra, M. Manuja, A. Chaudhury, A. (2015). Synthesis, characterisation and in vitro evaluation of cytotoxicity and antimicrobial activity of chitosan-metal nanocomposites. *J. Chem. Technol. Biotechnol., 90 (5),* 867-873.

Khalili, S.T. Mohsenifar, A. Beyki, M. Zhaveh, S. Rahmani-Cherati, T. Abdollahi, A. Bayat, M. Tabatabaei M. (2015). Encapsulation of Thyme essential oils in chitosan-benzoic acid nanogel with enhanced antimicrobial activity against Aspergillus flavus. *LWT - Food Science and Technology, 60(1),* 502-508.

Khan, M.R. Haque, Z. and Kausar, N. (2014). Management of the root-knot nematode Meloidogyne graminicola infesting rice in the nursery and crop field by integrating seed priming and soil application treatments of pesticides. *Crop Protection, 63,* 15-25.

Kozielski, K.L. Tzeng, S.Y. Green, J.J. (2013). Bioengineered nanoparticles for siRNA delivery. *Wiley Interdiscip Rev Nanomed Nanobiotechnol, 5(5),* 449–468.

Li, J. Sun, Q. Sun, Y. Chen, B. Wu, X. Le, T. (2019). Improvement of banana postharvest quality using a novel soybean protein isolate/cinnamaldehyde/zinc oxide bionanocomposite coating strategy. *Scientia Horticulturae, 258,* 108786.

Luque-Alcaraz, A. G. Cortez-Rocha, M. O. Velázquez-Contreras, C. A. Acosta-Silva, A. L. Santacruz-Ortega, H.C. Burgos-Hernández, A. Argüelles-Monal, W. M. Plascencia-Jatomea, M. (2016). Enhanced antifungal effect of chitosan/pepper tree (*schinus molle*) essential oil bionanocomposites on the viability of *Aspergillus parasiticus* spores. *Journal of Nanomaterials, 2016*, 1-11.

Malkapur, D. Devi, M.S. Rupula, K. Sashidhar, R.B. (2017). Biogenic synthesis, characterisation and antifungal activity of gum kondagogu-silver nano bio composite construct: assessment of its mode of action. *IET Nanobiotechnol., 11(7),* 866-873.

Medina, E. Caro, N. Abugoch, L. Gamboa, A. Díaz-Dosque, M. Tapia, C. (2019). Chitosan thymol nanoparticles improve the antimicrobial effect and the water vapour barrier of chitosan-quinoa protein films. *Journal of Food Engineering, 240*, 191-198.

Mohammadi, A. Hashemi, M. Hosseini, S.M. (2015). Nanoencapsulation of Zataria multiflora essential oil preparation and characterization with enhanced antifungal activity for controlling Botrytis cinerea, the causal agent of gray mould disease. *Innovative Food Science & Emerging Technologies, 28*, 2015, 73-80.

Nasseri, M. Golmohammadzadeh, S. Arouiee, H. Jaafari, M. R. and Neamati, H. (2016). Antifungal activity of Zataria multiflora essential oil-loaded solid lipid nanoparticles in-vitro condition. *Iran J Basic Med Sci., 19(11),* 1231–1237.

Noshirvani, N. Ghanbarzadeh, B. Mokarram, R. R. Hashemi, M. Coma, V. (2017). Preparation and characterization of active emulsified films based on chitosan-carboxymethyl cellulose containing zinc oxide nano particles. Int. J. Biol. Macromol., 99, 530-538.

Perumal, A. B. Nambiar, R. B Sellamuthu, P. S. Sadiku, E. R. Li, X. He, Y. (2022). Extraction of cellulose nanocrystals from areca waste and its application in eco-friendly biocomposite film. *Chemosphere, 287*, 132084.

Pimentel, D. (2009). Pesticide and pest control. In: Peshin, P., Dhawan, A.K (eds) Integrated pest management: innovation-development process. *Springer, Dordrecht*, Netherlands pp 83-87.

Pinto, R.J.B. Almeida, A. Fernandes, S.C.M. Freire, C.S.R. Silvestre, A.J.D. Neto, C.P. Trindade, T. (2013). Antifungal activity of transparent nanocomposite thin films of pullulan and silver against Aspergillus niger. *Colloids Surfaces B Biointerfaces, 1(103),* 143-148.

Pola, C. C. Moraes, A.R.F. Medeirosa, E.A.A. Teófilo, R. F. Soares, N. F.F. Gomes, C.L. (2019). Development and optimization of pH-responsive PLGA-chitosan nanoparticles for triggered release of antimicrobials. *Food Chemistry, 295,* 671–679.

Prasad, R. Kumar, V. and Prasad, K.S. (2014). Nanotechnology in sustainable agriculture: Present concerns and future aspects. *Afr. J. Biotechnol., 13,* 705-713.

Safaei, M. Taran, Imani, M. M. M. (2019). Preparation, structural characterization, thermal properties and antifungal activity of alginate-CuO bionanocomposite. *Materials Science & Engineering C, 101,* 323–329.

Safaei, M. Taran, M. (2017). Fabrication, characterization, and antifungal activity of sodium hyaluronate-TiO_2 bionanocomposite against Aspergillus niger. *Materials Letters, 207,* 113–116.

Sahraee, S. Ghanbarzadeh B., Milani, J. M. Hamishehkar, H. (2017). Development of gelatin bionanocomposite films containing chitin and ZnO nanoparticles. *Food Bioprocess Technol., 10 (8,* 1441-1453.

Shende, P. Oza, B. Gaud, R.S. (2018). Silver-doped titanium dioxide nanoparticles encapsulated in

Stephenson, G. R. (2003). Pesticide Use and World Food Production: Risks and Benefits; *Environmental Fate and Effects of Pesticides (Chapter 15, pp 261-270,* ACS Publications: Washington, DC, USA.

Thul, S.T. and Sarangi, B.K. (2015). Implications of Nanotechnology on Plant Productivity and Its Rhizospheric Environment. In book: *Nanotechnology and Plant Sciences*: *Nanoparticles and Their Impact on* Plants (pp.37-53), Edition: Siddiqui, M. H. Al-Whaibi, M. H. Firoz. M. Publisher: Springer International Publishing, Switzerland Editors:

Wu, J. Sun, Q. Huang, H. Duan, Y. Xiao, G. Le, T. (2019). Enhanced physico-mechanical, barrier, and antifungal properties of soy protein isolate film by incorporating both plant-sourced cinnamaldehyde and

facile synthesized zinc oxide nanosheets. *Colloids and Surfaces B: Biointerfaces, 180*, 31–38.

Yildirim, A. And Acay, H. (2021). Applications of Biodegradable Green Composites. In Green Composites. Materials Horizons: From Nature to Nanomaterials., edited by Balakrishnan, P.; Thomas, *Singa-pore: Springer*, pp 373-392.

Zaller, J. Brühl, C. A. (2019). Editorial: Non-target Effects of Pesticides on Organisms Inhabiting Agroecosystems. *Front. Environ. Sci., 7*, 75.

Zhaveh, S. Mohsenifar, A. Beiki, M. Abdollahi, S. T. K. A. Rahmani-Cherati, T. Tabatabaei. M. (2015). Encapsulation of Cuminum cyminum essential oils in chitosan-caffeic acid nanogel with enhanced antimicrobial activity against *Aspergillus flavus. Industrial Crops and Products, 69*, 251–256.

Zhou, Y. Sun, S. Bei, W. Zahi, M. R. Yuan, Q. Liang, H. (2018). Preparation and antimicrobial activity of oregano essential oil Pickering emulsion stabilized by cellulose nanocrystals, *International Journal of Biological Macromolecules, 112*, 7-13.

ISBN: 978-625-8405-70-5